6 Results

6.1 Distributional analysis of hBCATc, hBCATm and hPDI proteins to the aged human brain

To define the cellular distribution of the BCAT proteins in the human brain, sections from 12 donated brains were labelled with antibodies specific to the hBCATc or hBCATm proteins. Previous work has focused on rodent model distribution, which demonstrated BCATc localisation to neurons, with recent work finally confirming the mapping of BCATm to the rat astrocytes (Bixel *et al.*, 2001; Bixel *et al.*, 1997; Cole *et al.*, 2012). However, BCATc has also been described at low levels in certain astrocyte populations in a human cell culture model that was not reported in rat models (Bixel *et al.*, 2001; Bixel *et al.*, 1997). Here, we investigated the distribution in the hippocampus, temporal, frontal, parietal and occipital lobe, cerebellum, mid brain, pons and medulla. A sub aim of this work was to investigate the localisation of hPDI to the temporal cortex and hippocampus as this protein i) has yet to be mapped to the human brain, ii) *in vitro* work has demonstrated association with hBCAT, iii) altered hPDI has been associated with AD.

6.1.1 Antibody specificity

Western blot analysis was utilised to assess the specificity of the rabbit raised antibodies to hBCATc and hBCATm. Purified overexpressed hBCATc and hBCATm protein, in addition to control homogenates demonstrated antibody specificity. No cross reactivity between isoforms was reported at the antibody concentrations utilised in these experiments (Figure 6.1), and distribution throughout the brain was identical when compared to
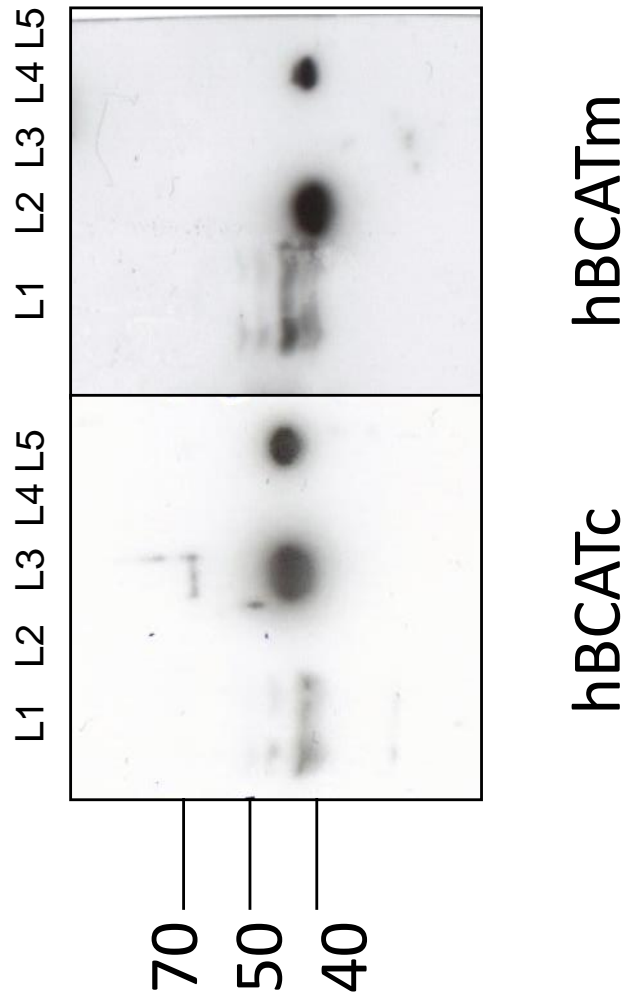
Figure 6. 1 Specificity of the antibodies raised to hBCATc and hBCATm. Western blot analysis of over-expressed hBCATm and hBCATc (5 and 10 ng respectively) using anti-hBCATc (1:1000) and re-probed with anti-hBCATm (1:1500). Lane 1, 20 µg of human control brain homogenate; Lane 2, 10 ng recombinant hBCATm; Lane 3, 10 ng recombinant hBCATc; Lane 4, 5 ng recombinant hBCATm; Lane 5, 5 ng recombinant hBCATc.

commercially available antibodies (Abcam, Cambridge, UK). For further confirmation, antigen absorption (at 200x molar excess) control was analysed during IHC (Figure 6.2 C, Figure 6.3 B, Figure 6.5 C, Figure 6.6 B, Figure 6.7 B, Figure 6.12 E+G, Figure 6.13 H, Figure 6.15 B+E, Figure 6.16 B+E).

6.1.2 Distribution of hBCATc within the human brain

Labelling of hBCATc was largely confined to neurons, and detected in all regions of the brain examined (Table 6.1). The cerebral cortex, hippocampal formation, subdivisions of the basal ganglia and diencephalon, the midbrain, cerebellum, pons and medulla all contained hBCATc-positive neurons. The antigen was largely confined to the neuronal soma and proximal dendrites but there was occasional focal labelling of axons and scanty weak labelling of oligodendrocytes.

The cerebral cortex is the outermost tissue of the human brain. It is divided into the left and right hemisphere and functions in attention, memory, thought, perceptual awareness and language. In the cerebral cortex, hBCATc positive neurons were predominantly small (Figure 6.2 A+D) but the antibody did label scattered larger pyramidal (Figure 6.2 B+D) and multipolar neurons (Figure 6.2 B). These pyramidal neurons are the primary excitatory neurons of the prefrontal cortex and function in cognition (Elston, 2003). Multipolar neurons possess a single axon and constitute the majority of neurons in the human brain. Both these neurons may use either glutamate or GABA as a neurotransmitter. Immunopositive neurons were numerous in

Table 6.1 An overview of hBCATc immunoreactivity throughout the human brain (n^i = 12, n^e = 35).

Area	¥Amount of staining in a cell population	§Intensity of stained cells
Temporal lobe		
-**Hippocampus:**		
○**GABAergic interneurons**	+++	+++
○**Pyramidal neurons**	+(+)	++++
○**Dentate gyrus (neurons)**	+	+
-**Cortex:**		
○**Neurons**	+++	++
○**Subiculum sub-population of neurons**	++	++
○**Lamina II neurons**	++	++
Cortex and white matter		
-**Cortical pyramidal cells**	+	+++
-**Cortical neurons**	++	++
-**Axonal staining**	-/+	++
Cerebellum		
-**Oligodendrocyte staining in the white matter.**	-/+	++
-**Purkinje cells**	+(+)	+
-**Stellate cells**	++	+++
-**Golgi cells**	++	++
-**Swollen axon terminals**	-/+	++
-**Interneurons**	++	+
-**Neurons in the dentate nucleus**	++	+
-**Inferior olivary nucleus**	++	++
Putamen and Basal ganglia		
-**Large neurons**	+	+++++
-**Small neurons**	+++	+
-**Insular cortex (small neurons)**	+(+)	++
-**Thalamus (neurons)**	+(+)	++
-**Caudate nucleus (neurons)**	+(+)	+
-**Lateral geniculate nucleus (neurons)**	+	+(+)
Medulla		
-**Hypoglossal nucleus (neurons)**	+(+)	++
-**Dorsal motor nucleus (neurons)**	+(+)	++
-**Supraoptic nucleus (neurons)**	+	+
-**Nucleus ambiguus (neurons)**	++	++
-**Gracile nucleus**	++	++
-**Inferior olivary nuclei (neurons)**	++	++
-**Inferior olivary nuclei neuropil**	++	++
Midbrain		
-**Widespread neuronal staining**	++++	+++
-**Periaqueductal grey matter (neurons)**	++	++
-**Neuropil staining**	++	+
-**Inferior colliculus (nerve cells)**	+(+)	+++
Pons		
-**Pontine nuclei (neurons)**	+(+)	++
-**Tegmental neurons**	+(+)	++
-**Neuronal processes (nigro striatal processes)**	++	+
-**Raphe nuclei (neurons)**	+	++
-**Nucleus basalis of Meynert (cholinergic neurons)**	+(+)	++++
-**Supraoptic nucleus of the hypothalamus**	+(+)	++++
-**Paraventricular neurons of the hypothalamus**	+(+)	++++

¥**Amount of staining**: (-), no staining observed; (-/+), staining observed but not consistent and not in the majority of subjects; (+), minimal staining; (++), low but convincing amount of neurons stained; (+++), moderate amount of neurons stained; (++++), Complete staining of neuron population.
§**Intensity of staining**: (+), minimal staining; (++), low but convincing amount of staining; (+++), moderate staining; (++++), strong staining; (+++++), very strong staining.
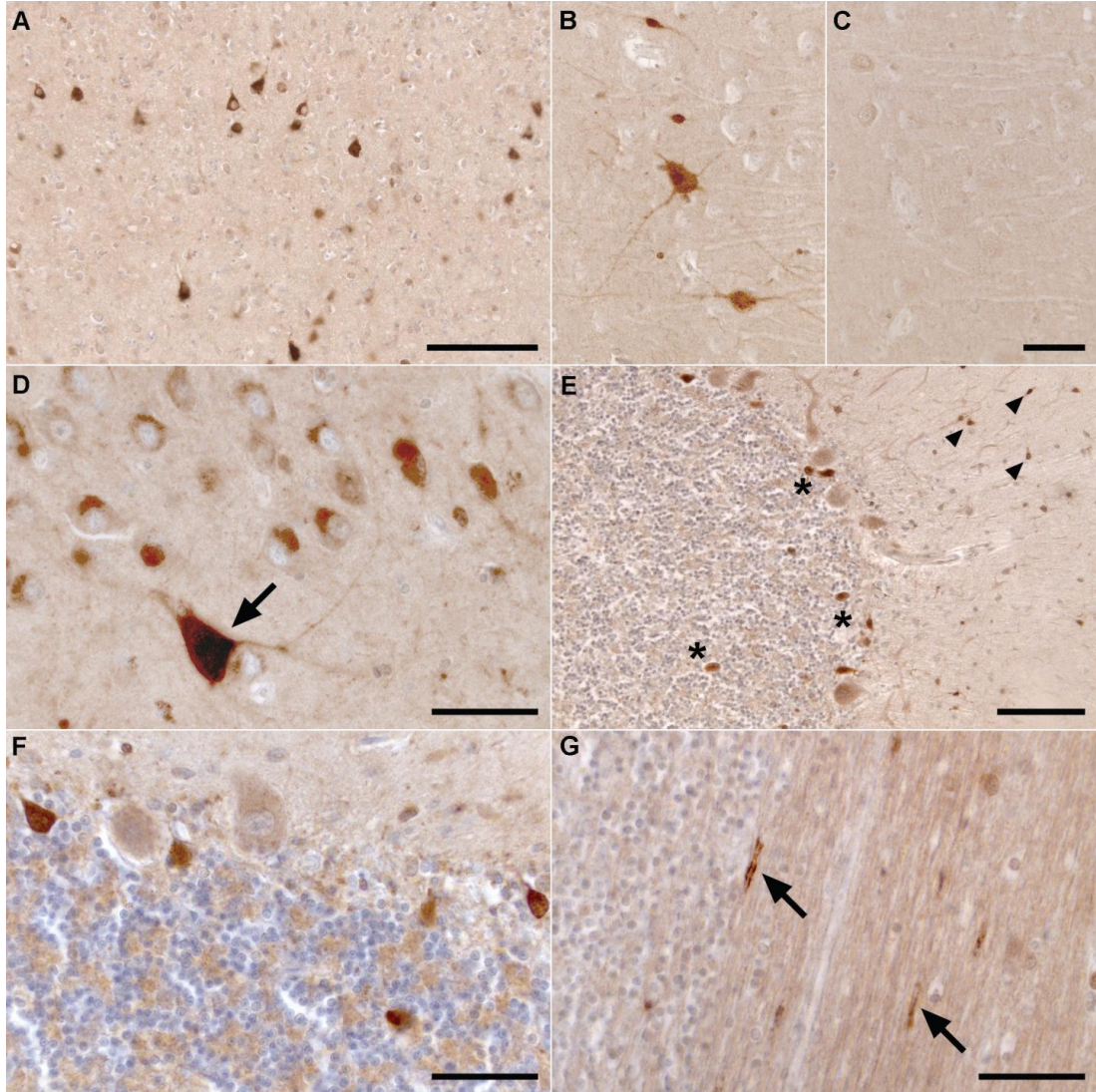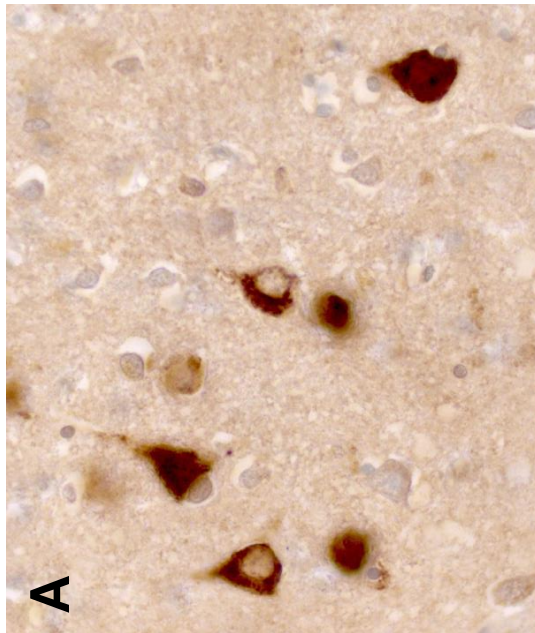
Figure 6. 2 Human cytosolic branched chain aminotransferase (hBCATc) staining in the temporal lobe and cerebellum (n^i = 12, n^e = 6). A: The temporal neocortex (inferior temporal gyrus) showing immunopositive neurons. B: Hippocampal region CA1 showing negative pyramidal cells and positive interneurons. C: Antigen incubation of serial section of B, at 200X molar excess. D: Small immunoreactive neurons and a large pyramidal neuron (large arrow) with visible processes. E: Granular cell layer with positive basket, golgi cells (*) and stellate cells (small arrows). F: Purkinje cell bodies shown to be weakly immunopositive with strongly labelled golgi cells. G: Intermittent staining of axons within the white matter (large arrows). Magnifications: A and E, X10; B, C, D, F and G, X40. Scale bars: A, 200 µm; E, 100 µm; B, C, D, F and G, 50 µm.

lamina 3 (the pyramidal layer) but were also present in lamina 2 (external granular layer) and the deeper layers (Figure 6.3 A). These layers (or lamina) of the cortex separate the cortex into 6 different segments with different populations of neurons.

The hippocampus is part of the cerebral cortex (specifically the limbic system) located within the temporal lobe. It is separated into Cornu Ammonis (CA) subdivisions and functions in memory and navigation. In the hippocampus there was variable labelling of pyramidal cells and strong labelling of multipolar interneurons (Figure 6.2 B+D, Figure 6.3 A). Strongest labelling occurred in the CA4 region and decreased towards the CA1 region (Figure 6.4). Throughout the cerebral cortex both large and small neurons were labelled for hBCATc (Figure 6.2 A-D, Figure 6.3 A, Figure 6.5, Figure 6.6, Figure 6.7 A+E). White matter labelling was almost completely absent however labelling of axons occurred in some individuals (Figure 6.2 G, Figure 6.7 C+D). Axons are the processes which extend from the neuron cell body (or soma). Presence of hBCATc labelling in the processes supports the role of glutamate production for neurotransmission, whereas hBCATc labelling within the soma supports the production of glutamate as a metabolite for the production of other neurotransmitters.

The putamen is one of the structures that make up the basal ganglia. The predominant function is to regulate movement and learning. Neurons of the putamen employ GABA, acetylcholine or encephalin neurotransmitters. In the putamen, large (aspiny) neurons were strongly labelled and there was

Temporal neocortex
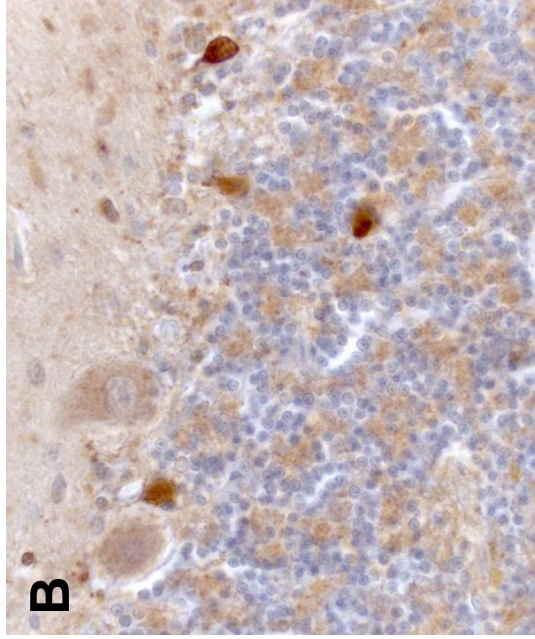
Cerebellum

Figure 6. 3 Human cytosolic branched chain aminotransferase (hBCATc) staining in the temporal neocortex and cerebellum (n^i = 12, n^e = 6). A: staining of hBCATc in the temporal neocortex (fusiform gyrus) in Lamina 5, some neurons are strongly labelled. B: Staining of hBCATc in the cerebellum, purkinje cells appear weakly stained while golgi cells are more immunopositive. Magnification: A and B, 50X.
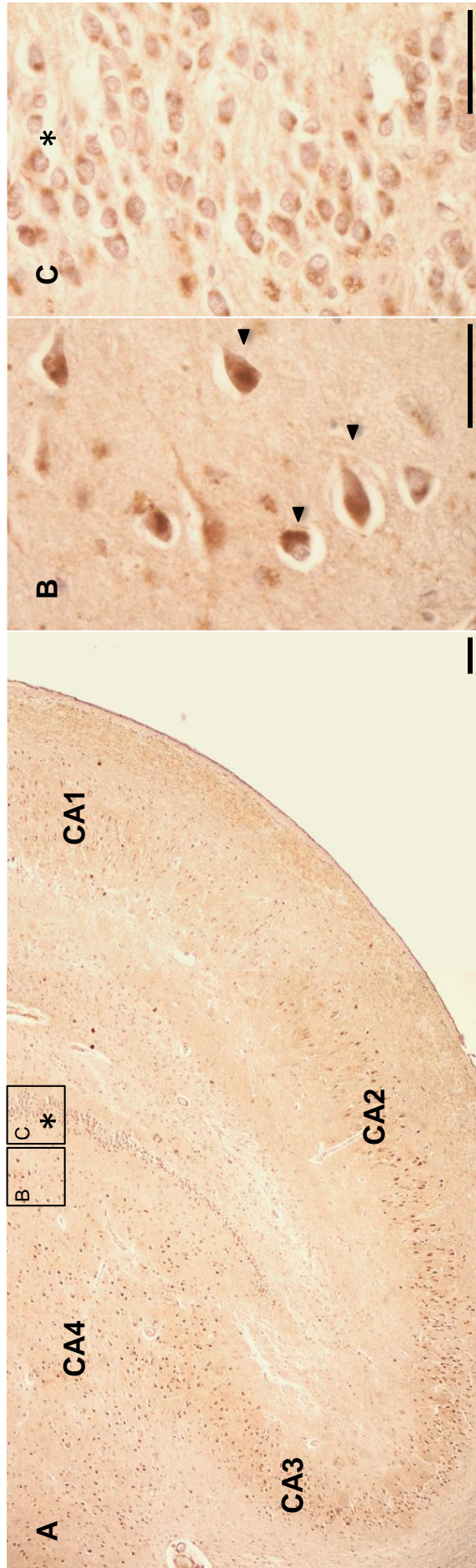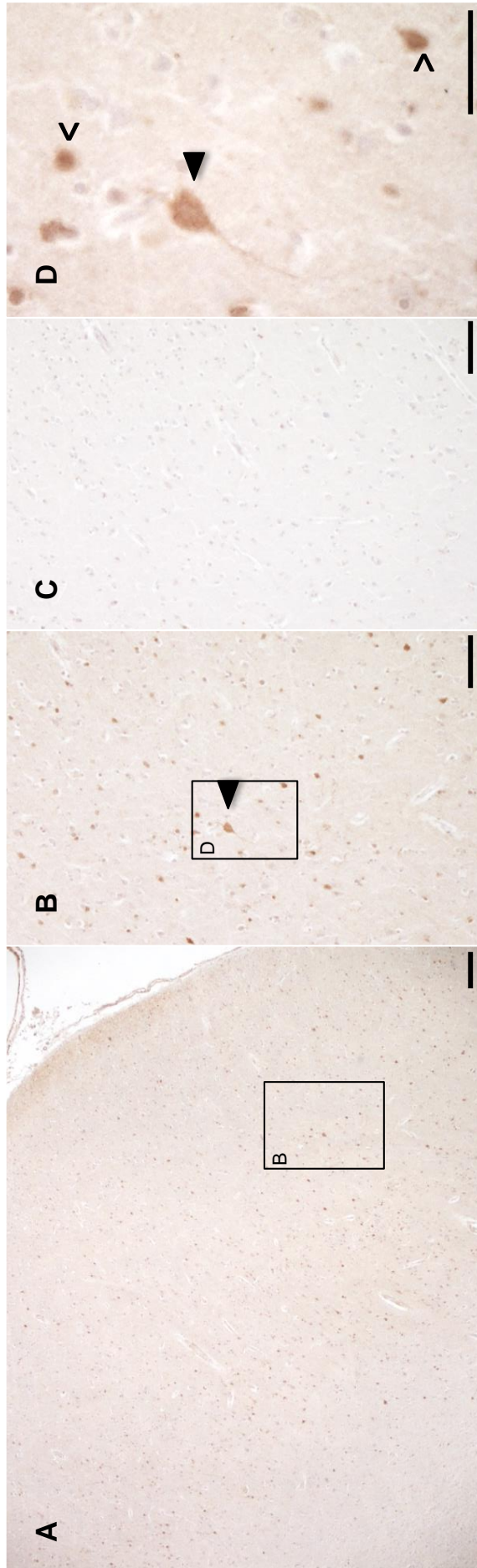
Figure 6. 4 Human cytosolic branched chain aminotransferase (hBCATc) staining in the hippocampus and temporal cortex ($n^i = 12$, $n^e = 6$). A: Overview of the hippocampus, staining for hBCATc was most intense in the CA4 region and decreased towards the CA1 region. B: Increased magnification of CA4 neurons (small arrows). C: Increased magnification of granule cells of the hippocampus (*), this staining was an infrequent occurrence. Magnifications: A, X4; B and C, X40. Scale bars: A, 200 µm; B and C, 50 µm.

Figure 6. 5 Human cytosolic branched chain aminotransferase (hBCATc) staining in the temporal cortex ($n^i = 12$, $n^e = 6$). A: Temporal cortex. B: Increased magnification of A showing large neuron (large arrow) and numerous small neurons. C: Antigen incubation of serial section of B, at 200X molar excess, immunoreactivity is completely removed by antigen incubation at 200X molar excess. D: Increased magnification of B showing large and small neuronal staining (<). Magnifications: A, X4; B and C, X10; D, X40. Scale bars: A, 200 µm; B and C, 100 µm; D, 50 µm.

Figure 6. 6 Human cytosolic branched chain aminotransferase (hBCATc) staining in the frontal cortex and white matter (n^i = 12, n^e = 6). A: Secondary antibody test of serial section of B and C. B: Antigen incubation of serial section of A and C, at 200X molar excess. C: Frontal cortex and white matter. D: Frontal cortex and white matter. E: Increased magnification of C. Staining of pyramidal neurons can be seen within the frontal cortex (Large arrows) as well as occasional staining of axons in the white matter (small arrow). Staining of the cortex appears to predominate in layers III-VI. Magnifications: A, B, and C, X4; D and E, X10. Scale bars: A, B and C, 200 µm. D and E, 100 µm.
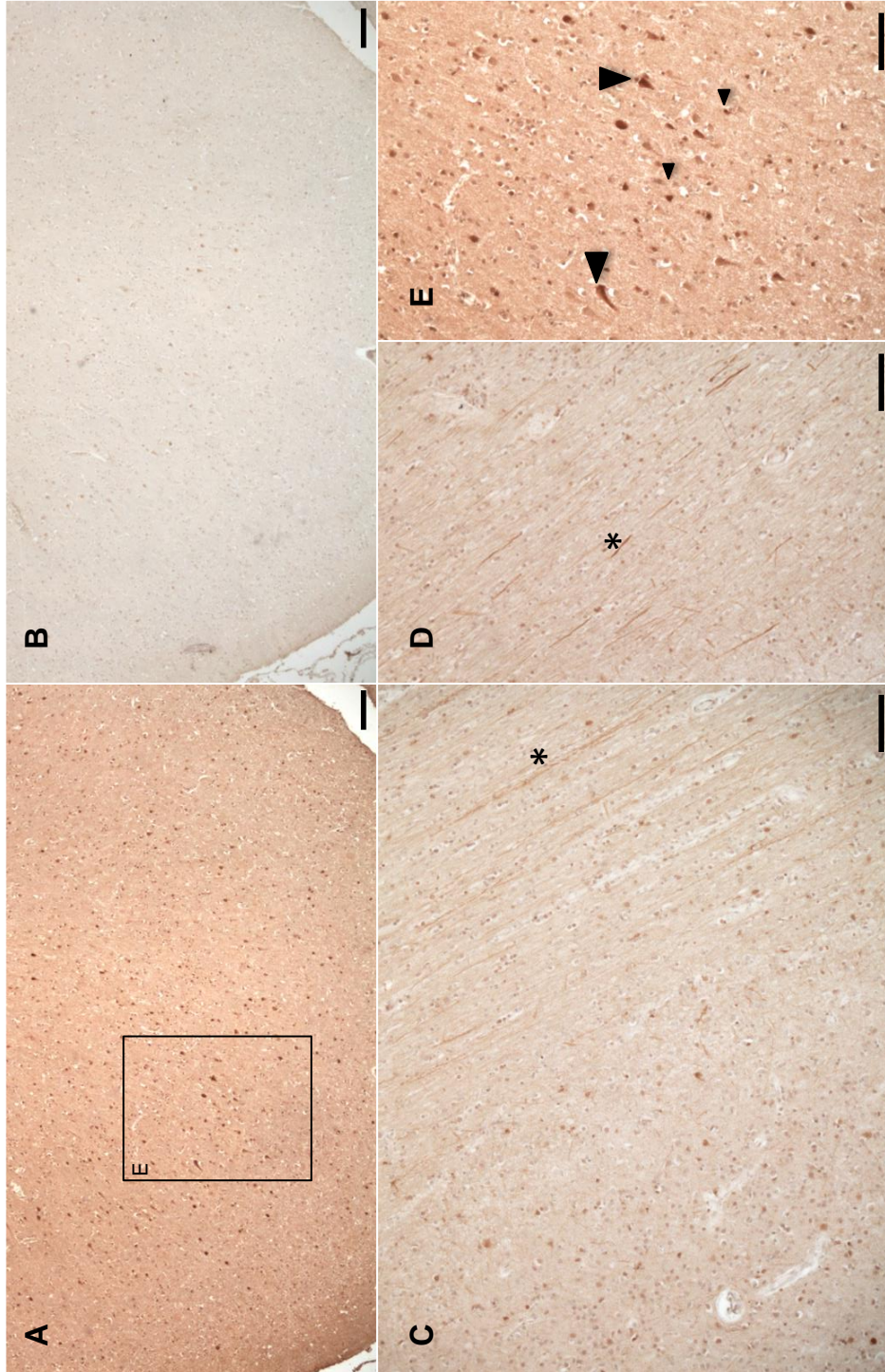
Figure 6. 7 Human cytosolic branched chain aminotransferase (hBCATc) staining in the occipital lobe ($n^i = 12$, $n^e = 6$). A: Occipital cortex. B: Antigen incubation of a serial section of A at 200X molar excess. C: Occipital white matter and cortex (*). D: Occipital white matter. E: Occipital cortex. Small neurons (small arrows) of the occipital cortex show hBCATc immunoreactivity, as well as pyramidal neurons (large arrows) of the occipital cortex and axons of the occipital white matter (*). Magnifications: A and B, 4X; C, D and E, 10X. Scale bars: A and B, 200 µm; C, D and E, 100 µm.

also weaker labelling of smaller neurons and numerous processes within the surrounding neuropil (Figure 6.8 A+C). The nucleus basalis of Meynert is part of the basal forebrain and is the predominant source of acetylcholine projections in the cortex; therefore neurons are cholinergic in nature. The nucleus basalis of Meynert also has a functional role in perception. The nucleus basalis of Meynert contained large hBCATc positive neurons supporting the role of the hBCATc protein in the production of intermediates for acetylcholine production.

Neurons in the globus pallidus were weakly labelled. The globus pallidus is part of the basal ganglia which regulates voluntary movement. Neurons of the thalamus were also weakly labelled however strong labelling of neuronal somata and processes were observed in the hypothalamus (Figure 6.9), particularly in the supraoptic and paraventricular nuclei. The thalamus processes sensory information, but the hypothalamus (localised just below the thalamus) creates a link between the nervous system and the endocrine system via the pituitary gland. The hypothalamus synthesises and secretes hormones (such as growth hormone releasing hormone) and these alter pituitary function. The specific function of the supraoptic and paraventricular nuclei is the production and release of oxytocin and vasopressin. The function of hBCATc in this instance is likely to be one of metabolite production for hormone manufacture, transamination for energy production from BCAAs, or as a protein that aids secretion. These functions are not mutually exclusive.
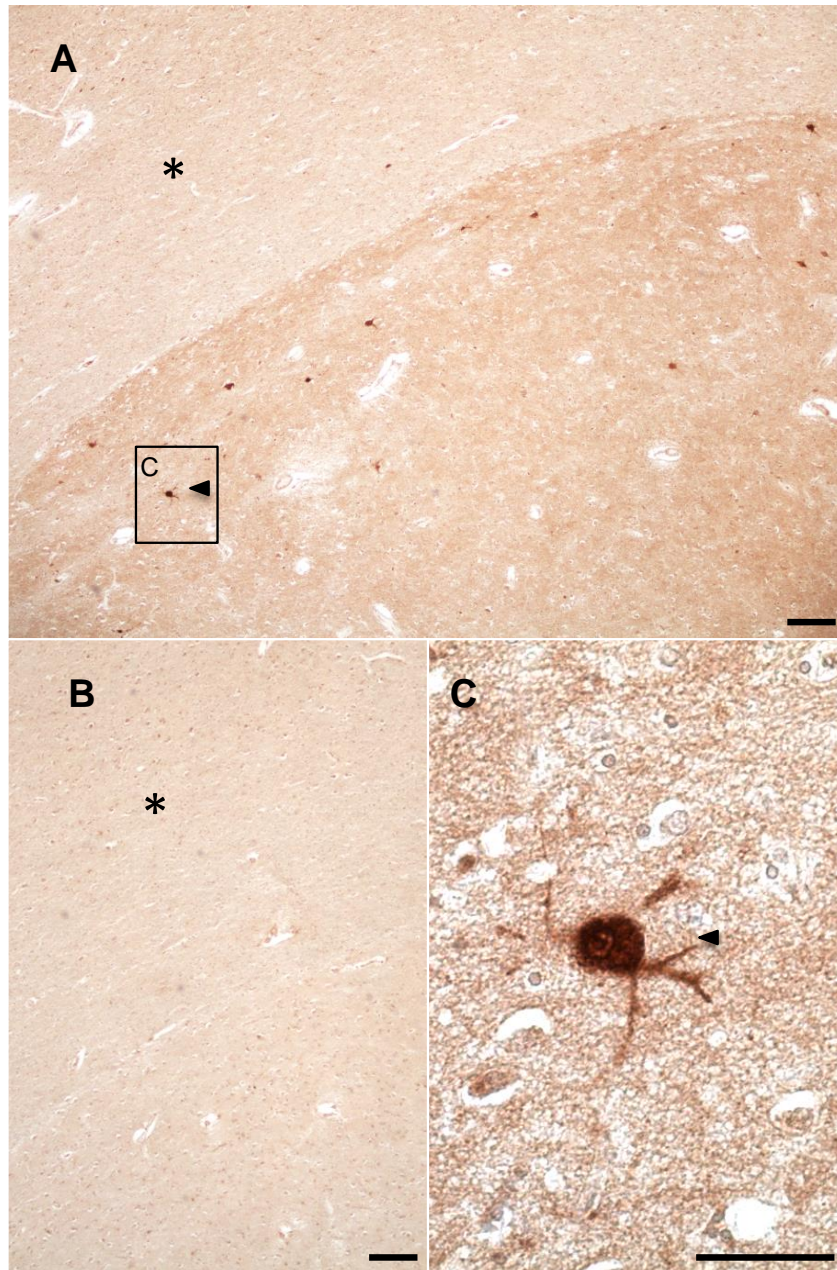
Figure 6. 8 Human cytosolic branched chain aminotransferase (hBCATc) staining in the Basal ganglia (putamen) (n^i = 12, n^e = 6). A: The capsula externa (*) of the basal ganglia showing staining of large neurons (small arrow) and surrounding processes. B: Antigen incubation of serial section of A, at 200X molar excess. C: Increased magnification of a single large neuron (small arrow). Magnifications: A and B, X4; C, X40. Scale bars: A and B, 200 µm; C, 50 µm.
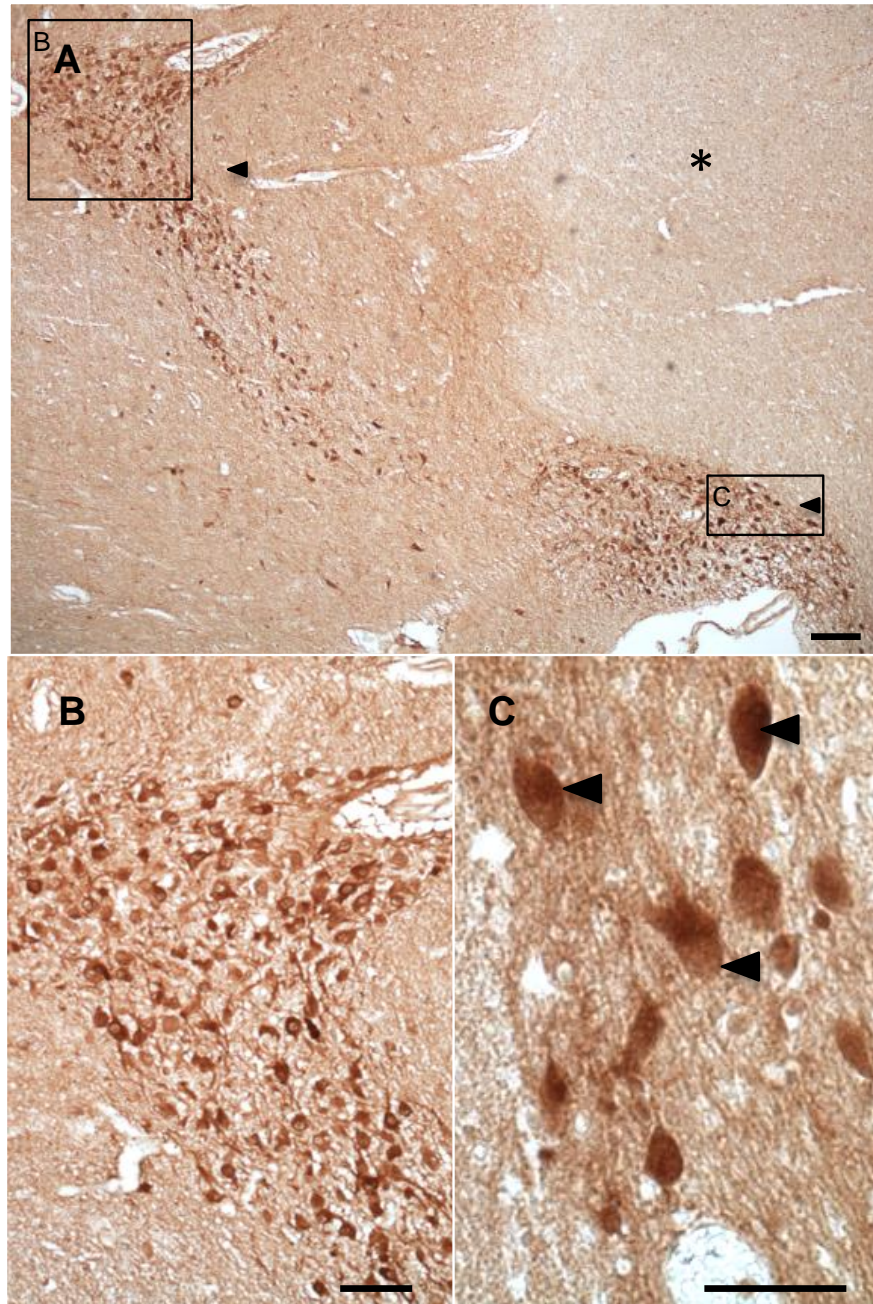
Figure 6. 9 Human cytosolic branched chain aminotransferase (hBCATc) staining in the hypothalamus (n^i = 4, n^e = 4). A: The optic tract (*) and the supraoptic nucleus (small arrows) of the hypothalamus. B: Increased magnification of the neurons of the supraoptic nucleus. C: Increased magnification of A to show clear neuronal cell body staining of neurons (large arrow) and process staining. Magnifications: A, X4; B, X10, C, X40; Scale bar: A, 200 µm; B, 100 µm; C, 50 µm.

Due to the brown pigment in neurons of the midbrain, substantia nigra and locus coeruleus, sections were stained with AEC (red) in place of DAB (brown). In the substantia nigra, hBCATc was detected in the nerve cell bodies and processes (Figure 6.10). The substantia nigra functions in eye movement and learning and serves as a source of GABAergic inhibition to other brain regions. It is therefore likely that hBCATc is producing intermediates for the production of GABA. Labelled neurons were observed throughout the midbrain with strongly labelled nerve cells in the inferior colliculus and relatively weakly labelled nerve cells in the periaqueductal grey matter. The inferior colliculus is part of the auditory pathway whereas the periaqueductal grey matter functions in the modulation of pain and defensive behaviour.

Within the granule cell layer of the cerebellar cortex the somata of basket, stellate and Golgi neurons were strongly immunopositive (Figure 6.2 E, 6.3 B). The cell bodies of the Purkinje cells were weakly immunopositive, as were the glomeruli (Figure 6.2 E+F, Figure 6.11). In some cases, there was distinct focal labelling of axons in the white matter, in a pattern suggesting nodal distribution (Figure 6.2 G), in addition to possible oligodendrocyte labelling. Basket cells, purkinje cells and golgi cells are all GABAergic inhibitory neurons. These cells make up the predominant neurons of the molecular and golgi cell layer and function in movement control. Purkinje atrophy occasionally occurs in domestic animals where it causes ataxia, tremors and an inability to determine space and distances (Sandy *et al*., 2002).
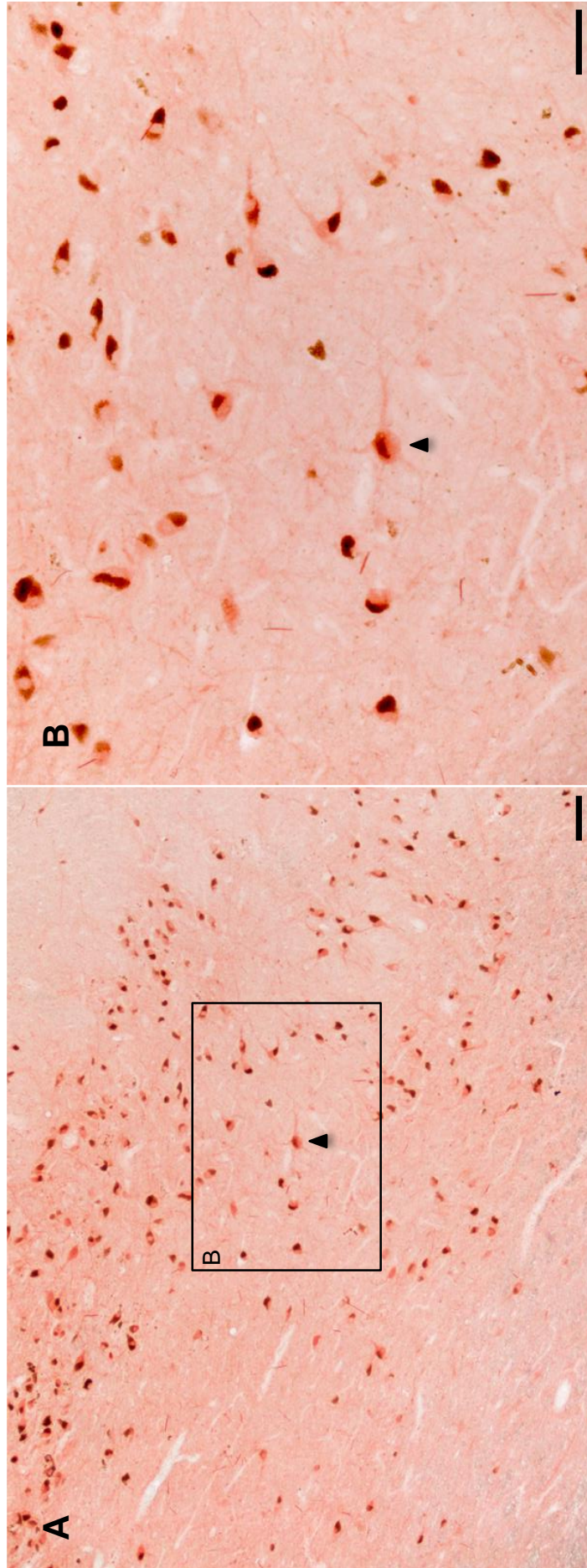
Figure 6. 10 Human cytosolic branched chain aminotransferase (hBCATc) staining in the mid brain ($n^i = 12$, $n^e = 6$). A: Pigment containing neurons of the substantia nigra. B: Increased magnification of A, staining of hBCATc localised to pigment containing neurons of the substantia nigra. Magnifications: A, X4; B, X10. Scale bars: A, 200 μm; B, 100 μm.
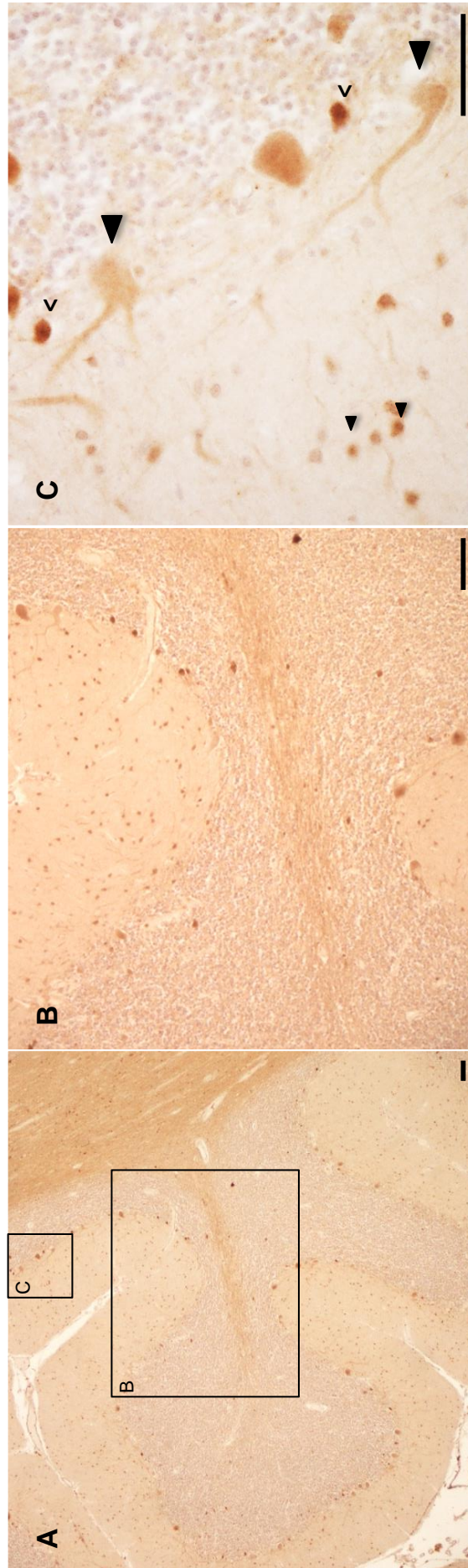
Figure 6. 11 Human cytosolic branched chain aminotransferase (hBCATc) staining in the cerebellum and white matter (n^i = 12, n^e = 6). A: Cerebellum showing molecular cell layer, nuclear layer and white matter. B: Magnification of A. C: Magnification of A. Cerebellum showing molecular cell layer, nuclear layer and white matter, shows staining of both the Golgi cell bodies (<), Purkinje cell bodies (large arrows), and stellate cells (small arrows). Magnifications: A, X4; B, X10; C, X40. Scale bars: A and B, 100 µm. C, 50 µm.

The pons functions as a connection between different brain regions, for example the cerebellar peduncles connect the cerebellum to the midbrain. Within the pons, hBCATc-positive neurons were present in the raphe nuclei and locus coeruleus both of which are hormone producing and secreting cells (Figure 6.12 B-D). The raphe nuclei function to produce and secrete serotonin so are serotonergic in nature. The locus coeruleus neurons are the primary site for the production and secretion of noradrenaline. There is up to 70% loss of these locus coeruleus neurons in AD (Bondareff *et al.*, 1982). Labelling also occurred in the basal pontine nuclei that contrasted to the lack of antigen in the corticospinal tract fibres (Figure 6.12 F). The pontine nuclei functions in motor activity and connect the primary motor cortex with the cerebellum whereas the corticospinal tract fibres connect the motor cortex to the spinal cord.

The medulla refers to the lower part of the brain stem and participates in autonomic, involuntary functions such as respiration, heart rate and reflexes. Additionally, the medulla connects the brain and spinal cord. In the medulla there was strong labelling of neurons in the gracile and cuneate nuclei, hypoglossal nucleus, the nucleus ambiguus and dorsal motor nucleus of the vagus nerve. The gracile and cuneate nuclei participate in fine touch and proprioception. The hypoglossal nucleus and the dorsal motor nucleus of the vagus are related to the cranial nerves the hypoglossal nerve (XII) and the vagus nerve. The hypoglossal nerve controls tongue movement, food manipulation and swallowing. The dorsal motor nucleus of the vagus nerve relays parasympathetic output of the brain to the viscera (particularly the
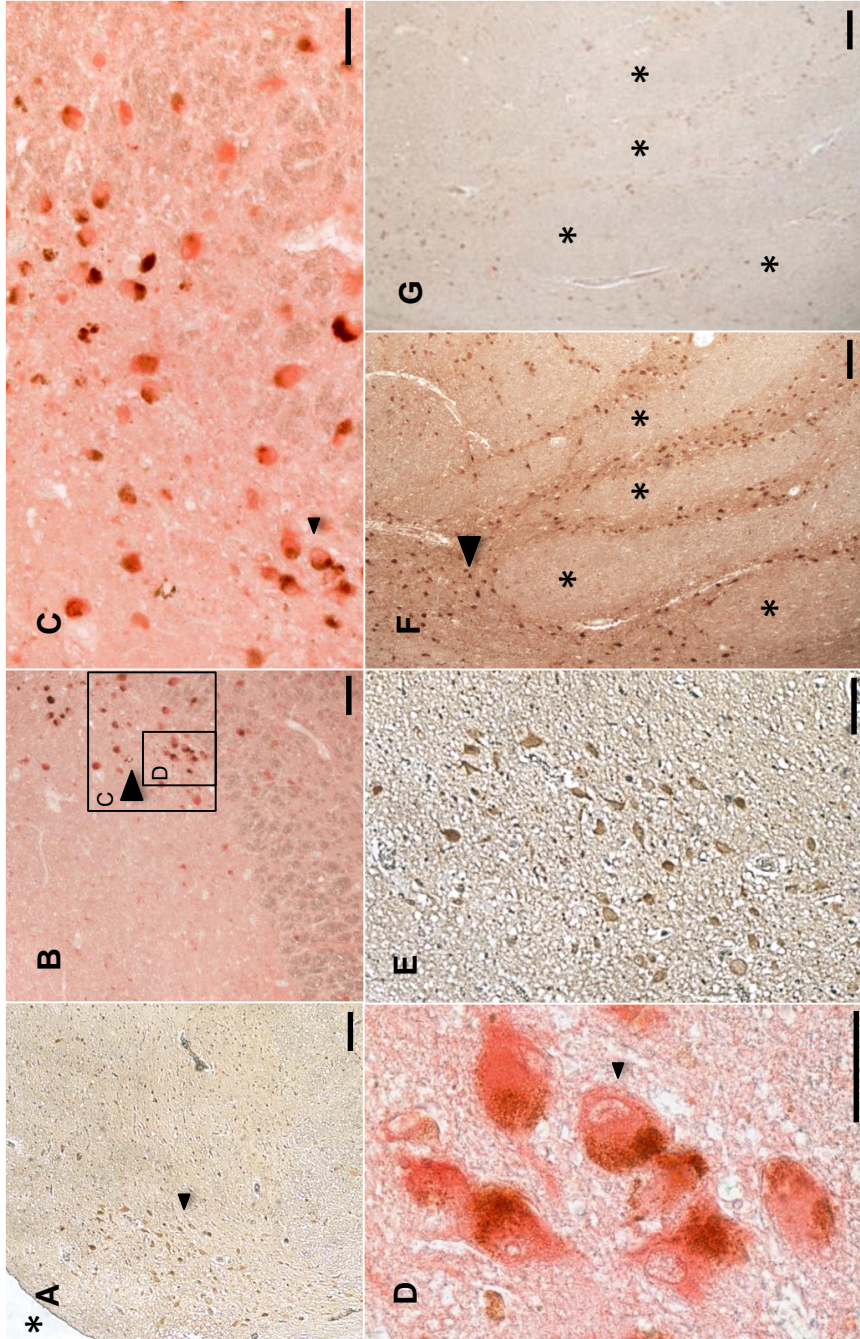
Figure 6. 12 Human cytosolic branched chain aminotransferase (hBCATc) staining in the Pons (n^i = 12, n^e = 6). A: The 4th ventricle of the Pons (*) with the Raphe nuclei (small arrow). B: Increased magnification of the locus coeruleus showing immunopositive neurons (large arrow). C: Increased magnification of immunopositive neuronal bodies of the locus coeruleus. D: Increased magnification of the raphe nuclei. E: Antigen incubation of serial section of D, at 200X molar excess. F: Immunopositive neurons and processes in the pontine nuclei (large arrow) and immunonegative corticospinal tract fibres (*). G: Antigen incubation of serial section of F, at 200X molar excess. Magnifications: A, B, F and G, X4; C and E, X10, D, X40. Scale bars: A, B, F and G, 200 μm; C and E, 100 μm; D, 50 μm.

intestines) whereas the nucleus ambiguus innervates the heart. Both resting heart rate and digestion are expected to be altered by hBCATc activity. The medulla also contained many hBCATc-positive neurons and nerve cell processes in the inferior olivary nucleus (discussed later) (Figure 6.15 A-C).

6.1.3 Distribution of hBCATm within the human brain

Immunoreactivity for hBCATm was present throughout the brain (Table 6.2) with consistent labelling of vascular endothelial cells in the grey and white matter (Figure 6.13 A-C E-G, Figure 6.14 A, B+D). A small population of glial cells in the subpial region in the inferomedial part of the temporal lobe showed coarse granular immunopositivity but this was not present in all brains. The endothelium of capillaries and larger blood vessels were immunopositive for hBCATm and showed punctate labelling in keeping with the mitochondrial location of this enzyme (Figure 6.14 A, B+D). The role of the vasculature in the human brain is as a separation device between the serum and the cells of the brain. The vasculature protects the brain from toxic substances within the blood and supplies the brain with nutrients and oxygen (Persidsky *et al.*, 2006). Transport across the vasculature is extremely limited and requires a great deal of energy, it is estimated that the cerebral vasculature has five times the mitochondria per cell than the vasculature of skeletal muscle (Oldendorf *et al.*, 1977).

Labelling of blood vessels was noted surrounding the hippocampus (Figure 6.13 A-C) and throughout the temporal cortex (Figure 13.E-G). There was also some labelling of the tunica media and occasional neuronal labelling

Table 6.2 An overview of hBCATm immunoreactivity throughout the human brain (n^i = 12, n^e = 35)

Area	¥Amount of staining in a cell population	§Intensity of stained cells
Temporal lobe		
-**Neuronal staining**	-/+	+
Cortex and white matter		
-**Capillaries/Endothelial cells (white matter and cortex)**	++	+++
Cerebellum		
-**Purkinje cells**	-/+	+
-**Capillaries/Endothelial cells.**	++	+++
-**Basket cells.**	-/+	+
-**Luminal staining**	-/+	+
-**Bergmann astrocytes (Purkinje cell layer)**	-/+	+
Putamen and Basal ganglia		
-**Tunica media**	+	++
-**Smooth muscle nuclei**	+	++
-**Pencillar fibres (white matter oligodendrocytes)**	++	++
-**Substantia innominata (hypothalamic neurons)**	++	++(+)
-**Mammillothalamic tract (hypothalamic neurons)**	++	++
Medulla		
-**Vessel/endothelial staining**	++	+++
Midbrain		
-**Supraoptic nucleus of the hypothalamic tract**	+	++
-**Periaqueductal grey matter (neurons)**	+	+
Pons		
-**Axons**	+(+)	+

¥Amount of staining: (-), no staining observed; (-/+), staining observed but not consistent and not in the majority of subjects; (+), minimal staining; (++), convincing amount of staining.
§Intensity of staining: (+), minimal staining; (++), low but convincing amount of staining; (+++), moderate staining.
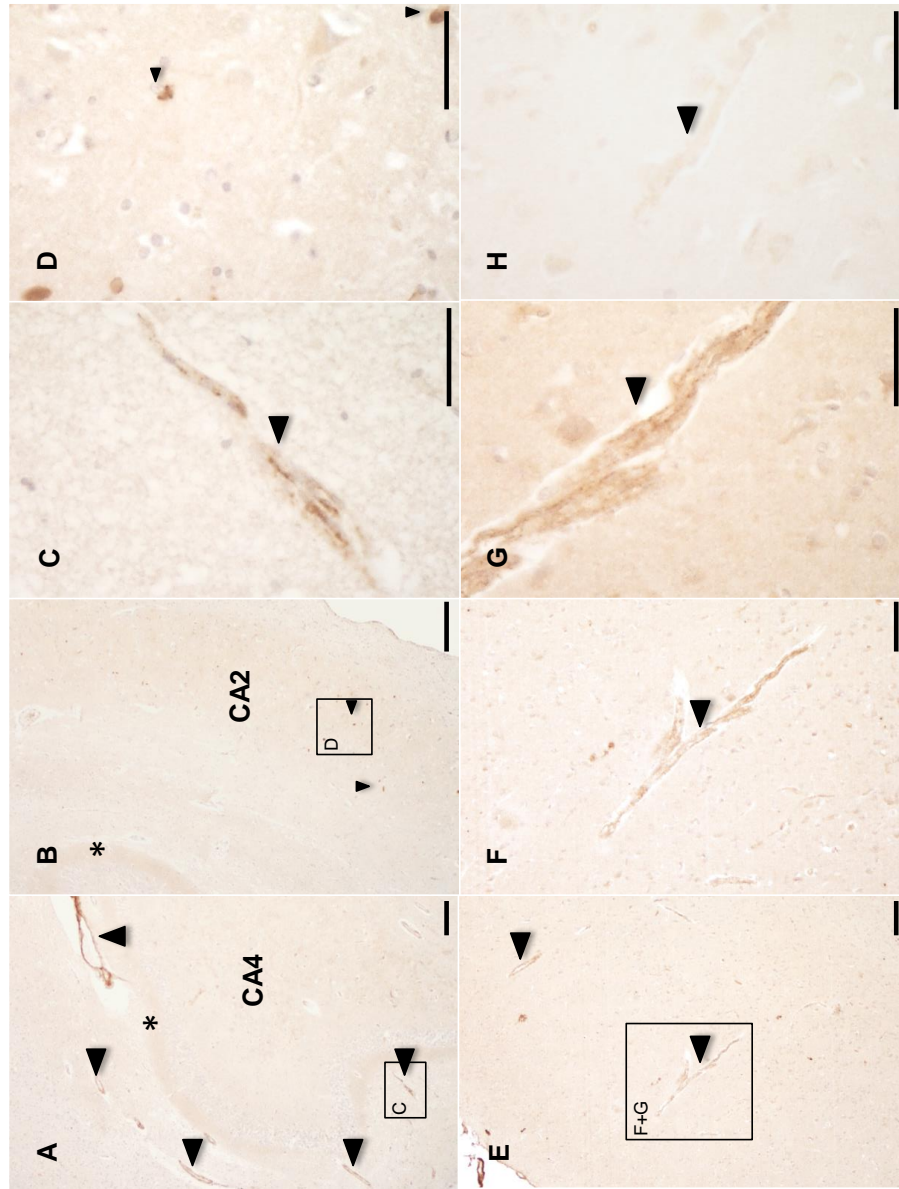
Figure 6. 13 Human mitochondrial branched chain aminotransferase (hBCATm) staining in the hippocampus and temporal cortex (n^i = 12, n^e = 6).
A: Overview of the CA4 region of the hippocampus. B: Overview of CA2 region of the hippocampus. C: Increased magnification of endothelial staining of vessels (large arrow) surrounding the hippocampus. D: Increased magnification of possible neuronal staining in B (small arrows). E: Temporal cortex showing endothelial staining (large arrows) without surrounding neuronal staining. F: Increased magnification of E. G: Increased magnification of F. H: Antigen incubation of serial section of E-G, at 200X molar excess. Magnifications: A, B and E, X4; F, X10; C, D, G and H, X40. Scale bars: A, B and E, 200 μm; F, 100 μm; C, D, G and H, 50 μm.
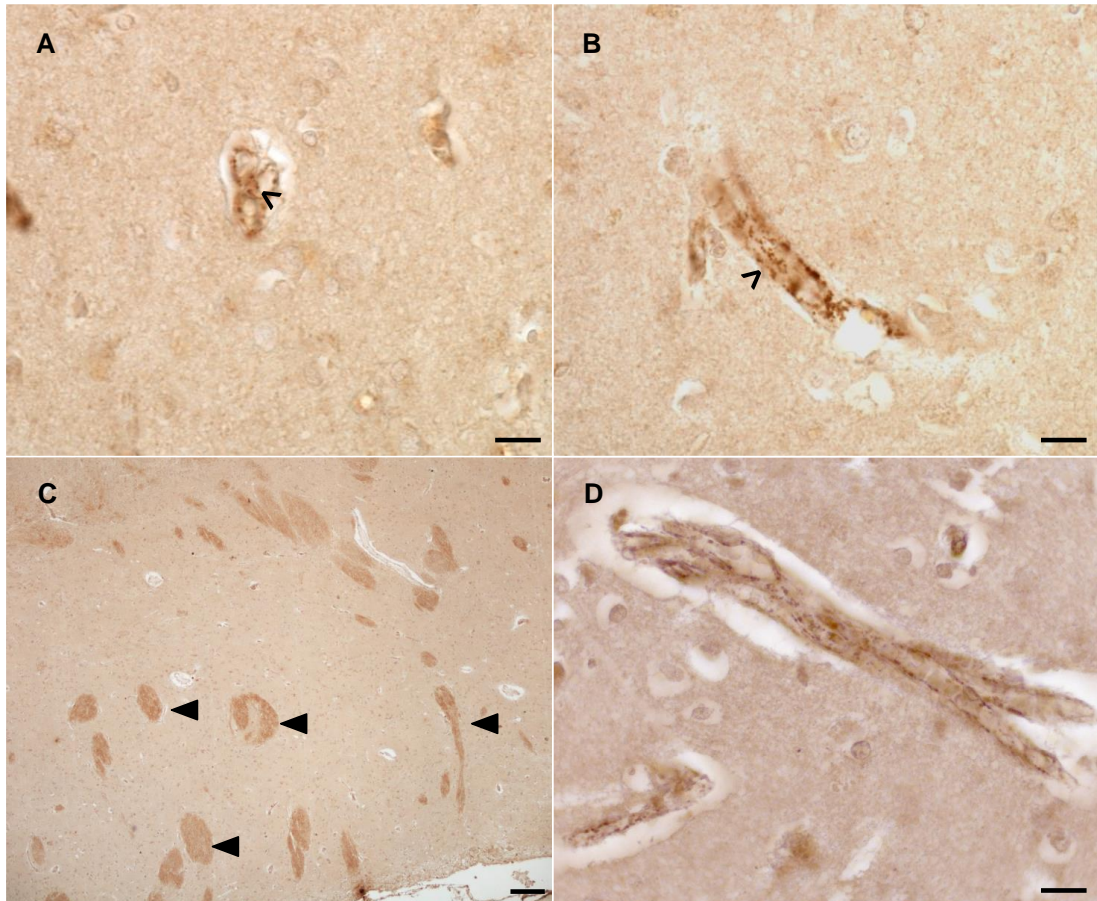
Figure 6. 14 Human mitochondrial branched chain aminotransferase (hBCATm) staining in the human brain (n^i = 12, n^e = 6). A: Punctate staining (arrowhead) appearing in small vessels in the Temporal lobe. B: Punctate staining (arrowhead) appearing in small vessels of the parietal lobe. C: Labelling of pencillar fibres (large arrowheads). D: Staining appearing in the vasculature of the parietal lobe. Magnifications: C, X4; A, B and D, X40. Scale bars: C, 200 μm; A, B and D, 50 μm.
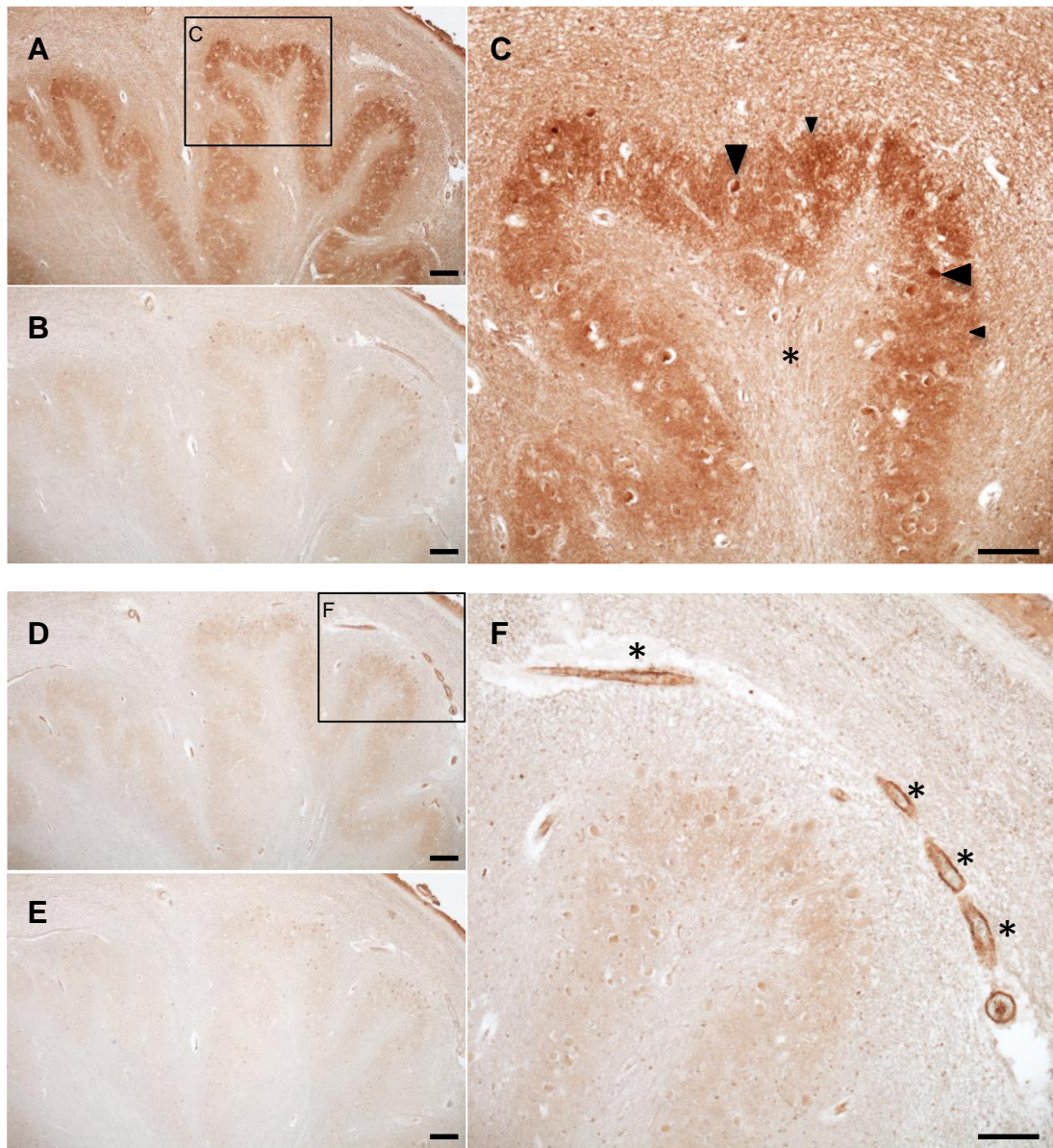
Figure 6. 15 Human cytosolic branched chain aminotransferase (hBCATc) and human mitochondrial branched chain aminotransferase (hBCATm) staining in the inferior olivary nucleus (n^i = 4, n^e = 4). A: Staining of hBCATc in the inferior olivary nucleus. B: Antigen incubation of serial section of A, at 200X molar excess. C: Increased magnification of the inferior olive showing staining of small neurons (large arrow) and neuropil staining (small arrow) along with immunonegative hylum (*). D: Staining of hBCATm in the inferior olive. E: Antigen incubation of serial section of D, at 200X molar excess. F: Vessel staining (*) within the amiculum of the inferior olivary nucleus. Magnifications: A, B, D and E, X4; C and F, X10. Scale bar: A, B, D and E, 200 µm; C and F, 100 µm.

(Figure 6.13 D).   The pencillar fibres in the basal ganglia were weakly positive in some brains (Figure 6.14 C) but elsewhere the white matter was unlabelled. These pencillar fibres (also referred to as pencil fibres of Wilson) are myelinated fibres that connect the striatum to the globus pallidus. This connection is important in learned movement (Kimura *et al.*, 1996).   The striatum showed weak hBCATm labelling of neuronal cell bodies and there was further weak labelling of neurons in the hypothalamus, periaqueductal grey matter and inferior olive that was reduced but not entirely removed by antigen incubation (Figure 6.15 D+E).

The distinct patterns of labelling for hBCATc and hBCATm are shown in Figure 6.15 and Figure 6.16. In Figure 6.15 hBCATm can be observed in the walls of blood vessels in amiculum of the inferior olivary nucleus (Figure 6.15 D-F) with hBCATc localised to the neurons and neuropil (Figure 6.15 A-C). The inferior olivary nucleus is closely associated with the cerebellum so functions as part of coordination of movements. Lesions to the inferior olivary nucleus have been associated with a decreased ability to perform specialised motor tasks (Martin *et al.*, 1996). In Figure 6.16 hBCATm is localised to the endothelial cells of the vasculature in the parietal cortex (Figure 6.16 D-F), with surrounding neurons labelled for hBCATc (Figure 6.16 A-C). The parietal lobe integrates sensory information and contains predominantly cholinergic neurons. The association of both hBCATc and hBCATm described here provides evidence of a BCAT shuttle between the two proteins and between the two cell types.
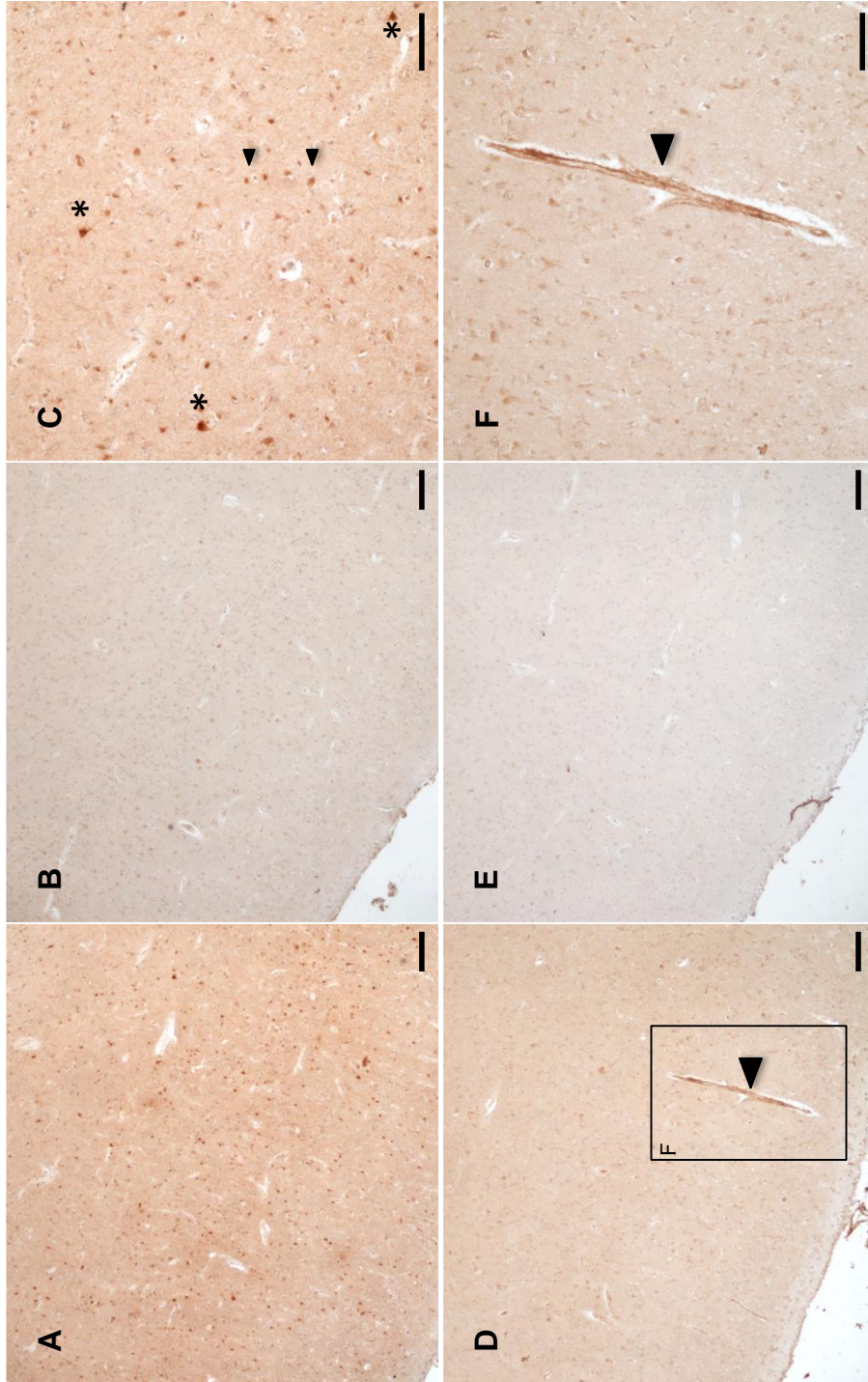
Figure 6. 16 Human cytosolic branched chain aminotransferase (hBCATc) and human mitochondrial branched chain aminotransferase (hBCATm) staining in the parietal cortex (n^i = 12, n^e = 6). A: Staining of hBCATc in the parietal cortex. B: Antigen incubation of serial section of A at 200X molar excess. C: Staining of hBCATc in small neurons (small arrows) and pyramidal neurons (*). D: Staining of hBCATm in the parietal cortex. E: Antigen incubation of serial section of D at 200X molar excess. F: Staining of hBCATm in vessel (large arrow). Magnifications: A, B, D and E, 4X; C and F, 10X. Scale bars: A, B, D and E, 200 μm; C and F, 100 μm.

In summary, hBCATc was observed in all brain regions and was largely neuron-specific throughout apart from occasional oligodendrocyte and axon labelling within the white matter. The intensity of hBCATc labelling varied between individuals; however, there was strongest labelling in putatively GABAergic neurons in the hippocampus, neocortex, putamen, hypothalamus, pons and medulla, with weaker labelling of putatively glutamatergic neurons. The hBCATm was predominantly vessel-associated, involving the endothelium and tunica media, with no labelling of astrocytes (with the exception of a small population of Bergman astrocytes observed in one individual). There was some labelling of neurons for hBCATm in the deep cerebral grey matter and brain stem but this was to a much lesser degree than that for hBCATc and was absent altogether from the majority of brains. Both hBCATc and hBCATm never co-localised within the same cell.

6.1.4 Distribution of hPDI within the human brain and co-localisation with hBCAT

A sub-aim of this work was to investigate the expression of hPDI within the human brain and to observe whether hPDI occurred in the same cell types as the hBCAT proteins. Further to this aim, electron microscopy was utilised to demonstrate co-localisation on the subcellular level. The human hPDI family contains over 20 proteins and has oxidoreductase, isomerase and chaperone function. In the human brain, hPDI and thiol proteins act as redox signalling buffers, which monitor changes in the redox environment, maintaining cell homeostasis (Laurindo *et al*., 2012). Although hPDI affects signalling

throughout the cell, it is predominantly expressed in the lumen of the endoplasmic reticulum (0.2-0.5 mM) (Lyles *et al.*, 1991; Zapun *et al.*, 1992).

The hippocampus showed hPDI labelling of all pyramidal cells and many interneurons, all large neurons were labelled (Figure 6.17 B+C). Granule cells of the dentate nucleus also showed positive labelling (Figure 6.17 A). The dentate nucleus is part of the hippocampal formation and functions in the formation of new memories. These granule cells are glutamatergic in nature. The temporal cortex showed almost all neurons labelled positive for hPDI (Figure 6.17 D-F) with some glial labelling in the white matter (mostly attributed to oligodendrocytes). However, it was noted that astrocyte labelling was absent.

In the cerebellum, blood vessels were labelled with vessels of the white matter also strongly labelled (Figure 6.18 B). Throughout the cerebellum purkinje cells were strongly labelled for hPDI, with labelling strongest in the cell body and weaker in the processes (Figure 6.18 A+B, D-F). Some labelling of hPDI was observed in the white matter (although axons were occasionally labelled); this was again attributed to oligodendrocytes and vessels (Figure 6.18 C). Blood vessels were also labelled, particularly in the white matter, with the labelling endothelial in nature. Labelling was complete compared to that observed for hBCATc and hBCATm, with the majority of vessels and neurons throughout the sections examined positive for hPDI. The hBCAT proteins were also localised in the same cells, as demonstrated by serial sectioning (Figure 6.19).
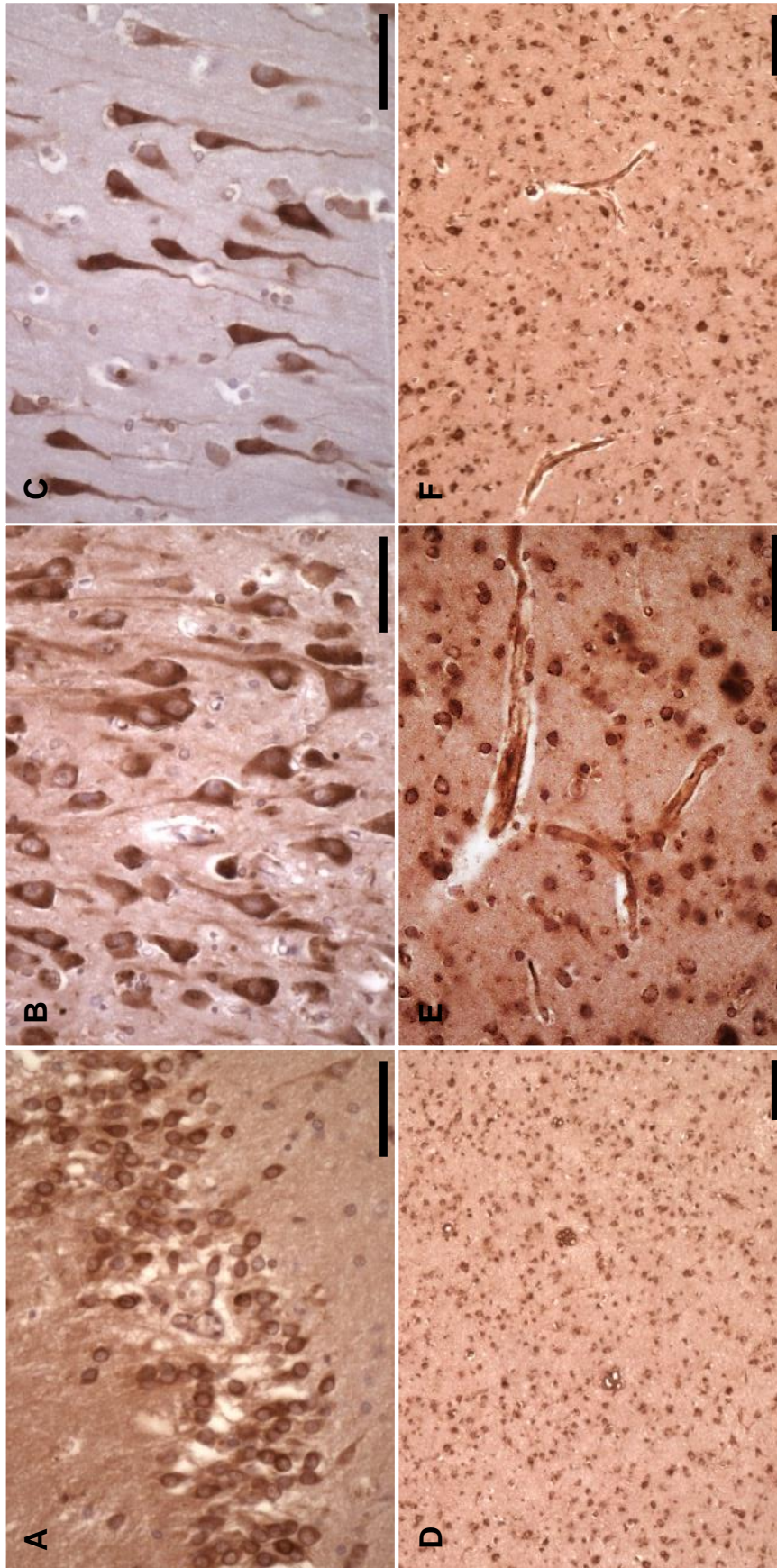
Figure 6. 17 Human protein disulphide isomerase (hPDI) staining in the hippocampus and temporal cortex ($n^i = 2$, $n^e = 2$). A: Dentate nucleus of the hippocampus, showing immunopositive cytoplasm of granule cells. B: CA4 region of the hippocampus, showing immunopositive neurons. C: CA3 region of the hippocampus, showing immunopositive pyramidal neurons. D: Temporal cortex, showing immunopositive labelling of both neuron cell bodies and endothelial cells of the vasculature. E: Increased magnification of the temporal cortex, showing immunopositive neuronal cell bodies and endothelial cells. F: Temporal cortex, showing immunopositive labelling of both neuron cell bodies and endothelial cells of the vasculature. Magnifications: A, B, C and E, X40; D and F, X10. Scale bars: A, B, C and E, 40 μm. D and F, 100 μm.
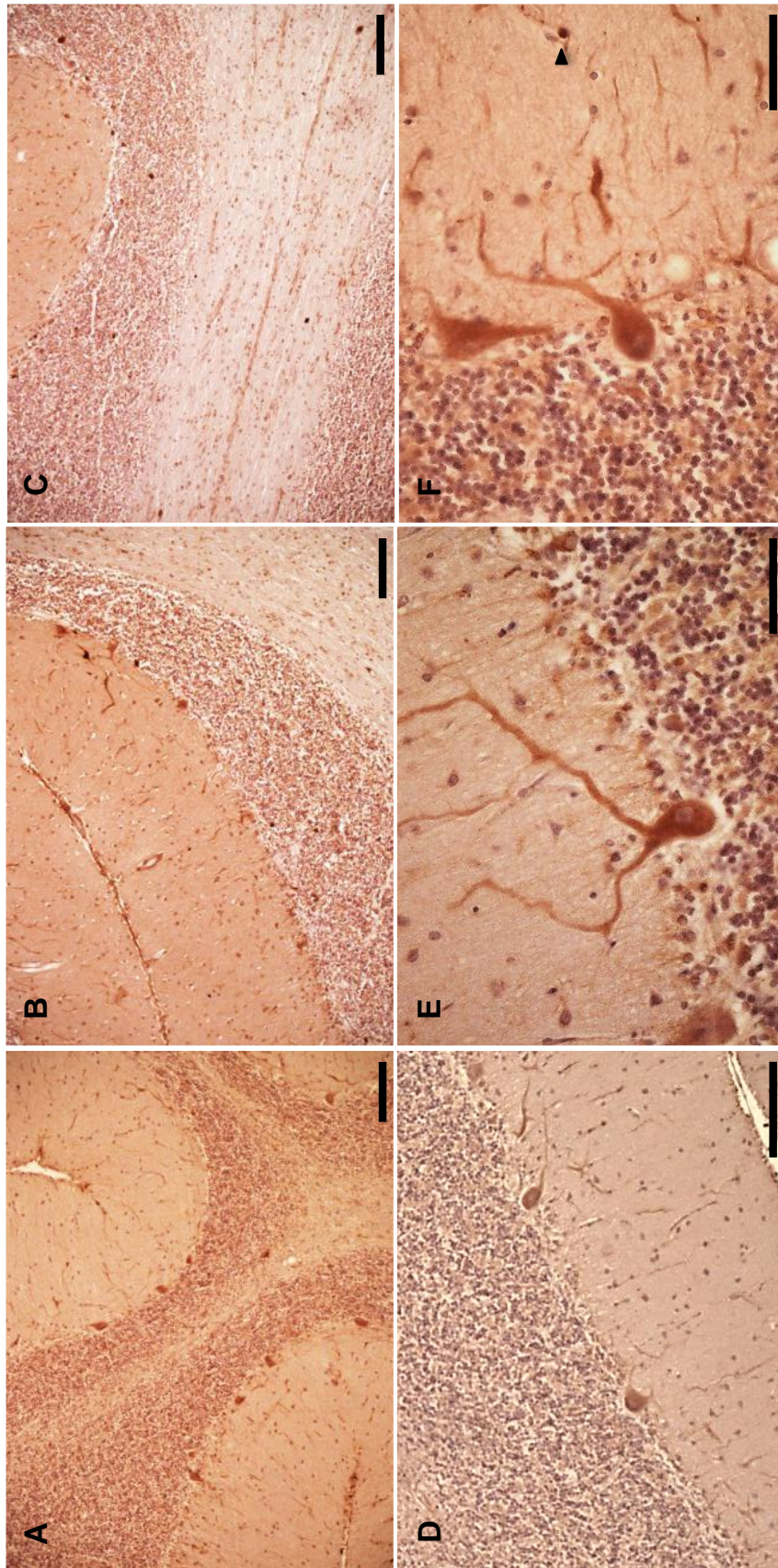
Figure 6. 18 Human protein disulphide isomerase (hPDI) staining in the cerebellum (n^i = 2, n^e = 2). A: Cerebellum, showing immunopositive cells within the molecular and nuclear cell layer. B: Cerebellum, showing immunopositive neurons and vasculature within the molecular and nuclear cell layer. C: White matter of cerebellum, showing immunopositive axons. D: Increased magnification of the boundary between the molecular and granule cell layer of the cerebellum, showing immunopositive purkinje cells. E: Increased magnification of the boundary between the molecular and granule cell layer of the cerebellum, showing a clearly immunopositive purkinje cell. F: Increased magnification of the boundary between the molecular and granule cell layer of the cerebellum, showing a immunopositive purkinje cell and stellate cell (small arrow). Magnifications: A, B, and C, X10; D, X20; E and F, X40. Scale bars: A, B, C and D, 100 µm. E and F, 40 µm.

hBCATc

PDI
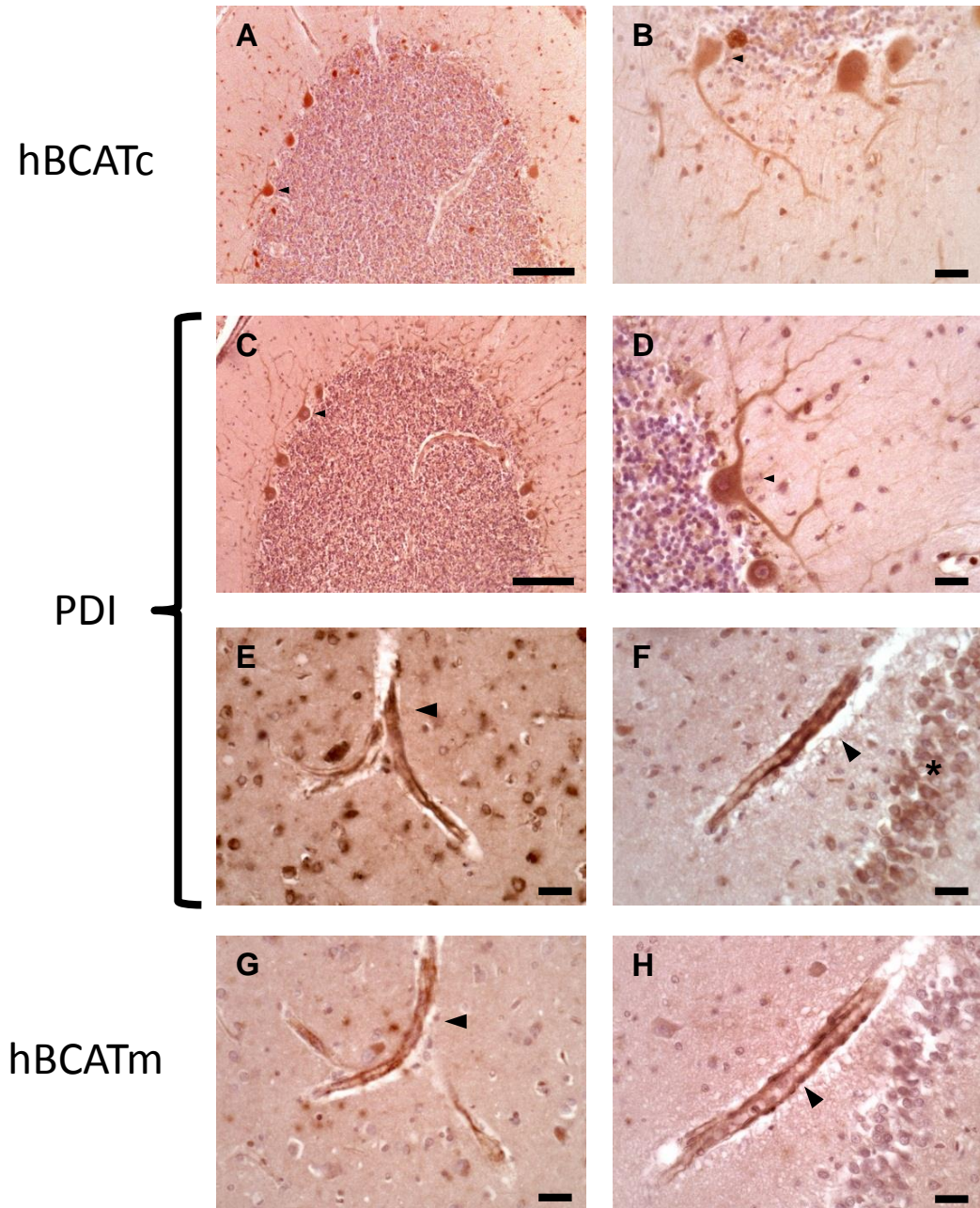
hBCATm

Figure 6. 19 Co-localisation of human cytosolic branched chain aminotransferase (hBCATc) and human mitochondrial branched chain aminotransferase (hBCATm) with human protein disulphide isomerase (hPDI) to the same cell types in the cerebellum, temporal lobe and hippocampus (n^i = 4, n^e = 4). Human brain sections were taken from 2 subjects (1 AD, 1 control). A-D show localisation of hPDI and hBCATc to the purkinje cells (small arrow) of the cerebellum. E-H shows the localisation of hPDI and hBCATm to the endothelial layer of vessels (large arrow) on serial sections of the temporal cortex (E+G) and the CA4 region of the hippocampus (F+H). Also shown in E+F is hPDI labelling of neurons of the temporal cortex (E) and granule cells (*) of the dentate nucleus (F). Magnifications: A and C, X10; B, D, E, F, G and H, X40. Scale bars: A and C, 100 μm; B, D, E, F, G and H 20 μm.

Electron microscopy observed hPDI localisation to the mitochondria (Figure 6.20) and co-localisation with the hBCATm protein. The ability of hPDI to localise to the mitochondria is likely related to mitochondrial associated membranes (MAMs). These MAMs serve as direct connections between the ER and the mitochondria, are increased under conditions of oxidative stress and facilitate the transfer of proteins from the ER to the mitochondria (Simmen *et al.*, 2010). It is also noted that hPDI has previously been reported in MAMs, and although it is predominantly an ER protein hPDI has previously been localised to the mitochondria, nucleus and cytosol (Hoffstrom *et al.*, 2010; Rigobello *et al.*, 2001; Turano *et al.*, 2002; Wilkinson *et al.*, 2004). Electron microscopy work also observed clustered formation of hPDI (Figure 6.20). The hPDI protein has the capacity to multimerise to >600 kDa multimers (Solovyov & Gilbert, 2004) and the role of hPDI in chaperone mediated autophagy is already well established (Bejarano & Cuervo, 2010; Rich *et al.*, 2003). These clusters may represent the initial multimerisation of the protein for chaperone mediated autophagy, or a response to an oxidative environment.

In summary, the labelling for hPDI was extensive, particularly when compared to that of either hBCATc or hBCATm. Labelling for hPDI was in every section of the slide but was largely absent from white matter except for occasional axonal labelling. Localisation of hPDI to mitochondria, in close proximity to hBCATm suggests that the two proteins may interact *in vivo*. As hBCAT have thiol isomerase activity and are expressed in the same brain

cells as hPDI, these studies suggest that their redox role in cells may be physiologically relevant.
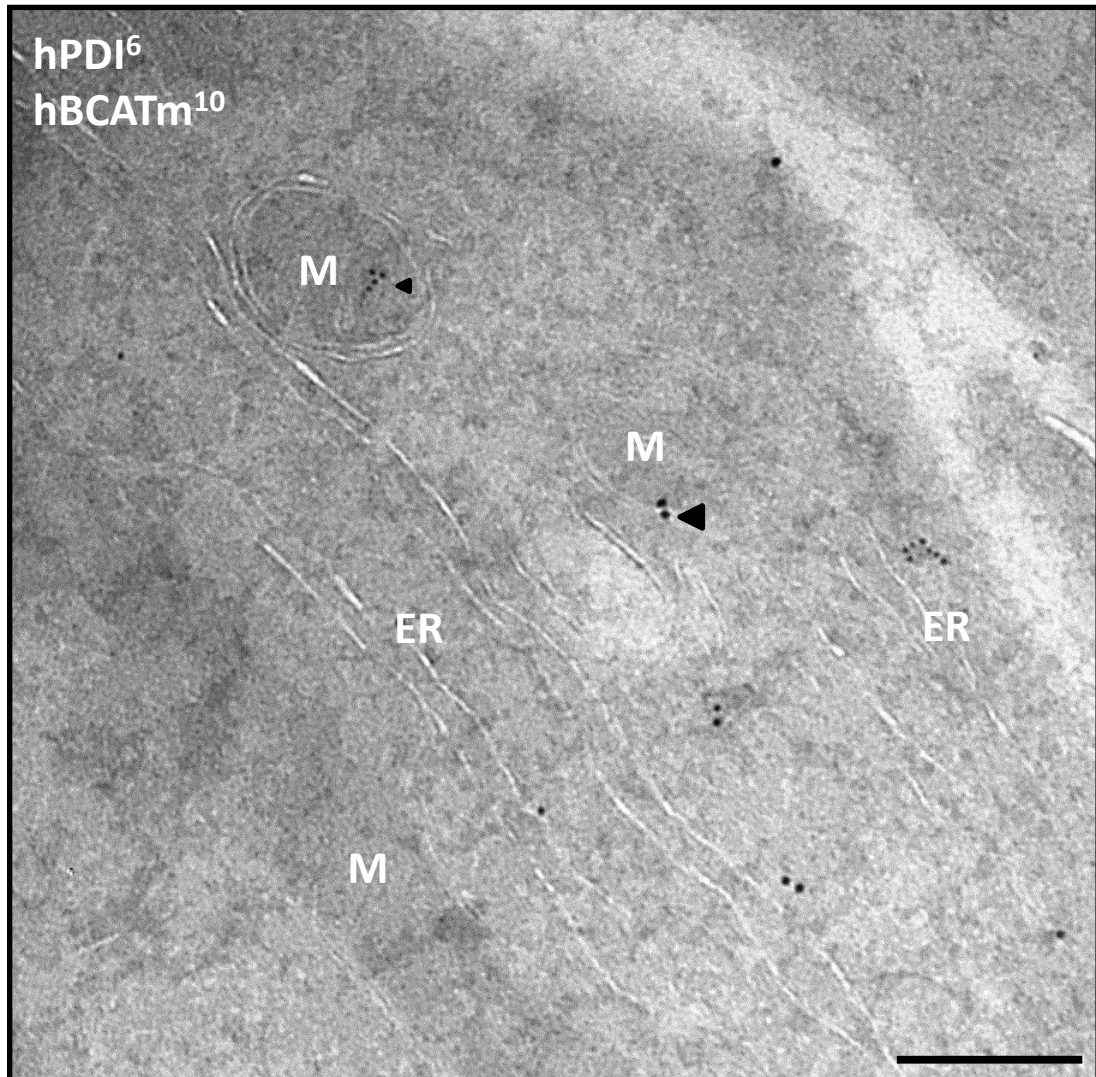
Figure 6. 20 Transmission electron microscopy showing PDI localisation to the mitochondria of IMR-32 neuronal cells. IMR32 cells were fixed using 2% formaldehyde and 0.2% paraformaldehyde, cells were then processed for sectioning at the Wolfson bioimaging institute (University of Bristol). Sections were then treated with a rabbit polyclonal antibody specific to hBCATm (PA1/10) (Insight biotechnologies, Wembley, UK) and a mouse polyclonal antibody to PDI (1/10) (Abcam, Cambridge, UK) as described in Method 3.6. Images were acquired using a Technai 12 (FEI) transmission electron microscope at University of Bristol. Abbreviations: hBCATm – mitochondrial branched chain aminotransferase, M – mitochondria, PDI – protein disulphide isomerase. Scale bars: A, 200 nm.

6.2 Investigation of protein alteration in Alzheimer's disease

With the proposed role of the hBCAT proteins in glutamate signalling it was hypothesized that their expression in diseases where glutamate toxicity features, such as AD and MND, would be altered. As changes in the redox environment is another key pathological mechanism of AD, the presence of S-glutathionylated protein was also investigated. This was further correlated with other variables such as tissue integrity (i.e. tissue pH, PM delay), physiological factors (i.e. age, brain weight, sex), genetic factors (i.e. ACE genotype, IRAP genotype, APOE genotype) and pathological features (i.e. Braak stage, Tau %, Aβ %) to investigate what factors were associated with hBCAT or S-glutathionylated protein expression.

The key features of AD pathology are amyloid deposition and hyper-phosphorylated tau. The Braak staging system is a post-mortem differentiation of AD pathology into seven stages of increasing severity of neurofibrillary changes (0-VI) (Braak & Braak, 1991). The cohort database was characterised by correlating Braak stage of the complete database cohort with both Aβ average (%) and Tau average (%) of the temporal cortex. Sections were labelled with antibodies raised to the Aβ peptide (or hyper phosphorylated tau) and used for analysis of parenchymal Aβ load. Parenchymal Aβ plaque load was calculated utilising Histometrix software, driving a Leica microscope with a motorized stage, as percentage area of cerebral cortex (measured in the temporal lobe) immunopositive for Aβ (or tau) after manual editing for exclusion of Aβ-laden vessels. It was demonstrated that both Aβ (Figure 6.21 A, $p = 3.19 \times 10^{-7}$, ρ +0.358) and
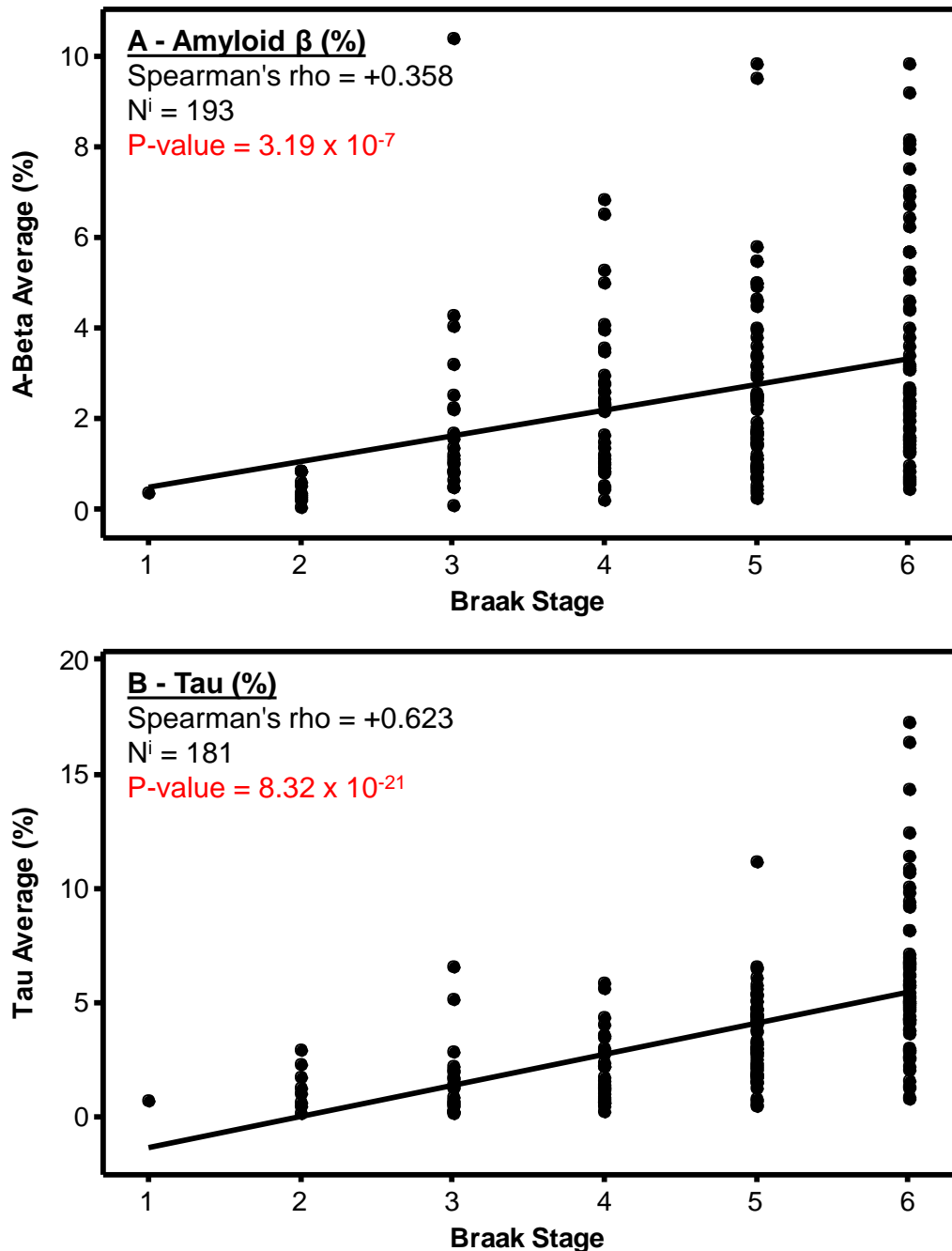
Figure 6. 21 Scatterplots of Braak staging correlated with Amyloid β average (%) and Tau average (%) of the temporal cortex. Sections were stained with the anti-Aβ or anti-hyper phosphorylated tau antibody. Amyloid β and hyper phosphorylated tau average (%) was calculated using Histometrix software, driving a Leica microscope with a motorized stage, as the percentage area of cerebral cortex (measured in the temporal lobe) immunopositive for Aβ senile plaques (M0872, Dako) or hyper phosphorylated tau (BR03, Autogen Bioclear). This work was carried out by the SWDBB. Data was then analysed for significance using Spearman's rho test in Minitab™.

hyper phosphorylated tau (Figure 6.21 B, p = 8.32 x10^{-21}, ρ +0.623) positively correlated with Braak stage, with hyper phosphorylated tau demonstrating stronger correlation.

6.2.1 The effect of post-mortem delay and pH on hBCAT expression

Subject post-mortem delay is the length of time it takes from death to storage of the tissue at -80°C. As post-mortem delay increases the proteins in the sample degrade, however the speed of this degradation can vary wildly and is likely to be specific to the protein (Siew *et al.*, 2004). Subject post-mortem delay has no correlation with either frontal expression of hBCATc (Figure 11.1 A, p = 0.632, ρ -0.055), frontal and temporal expression of hBCATm (Figure 11.2 A, p = 0.620, ρ -0.056 and Figure 11.2 B, p = 0.419, ρ -0.092 respectively) or temporal expression of S-glutathionylated proteins (Figure 11.3 B, p = 0.937, ρ -0.014).

The post mortem delay was mimicked in individual subjects by extracting tissue from the frontal cortex of frozen brain sections and storing them at 4°C for increasing time points (representing post-mortem delay). Western blot analysis demonstrated a 10% decline in hBCATc expression with 72 hour post-mortem delay (Figure 6.22 A, Figure 6.23 A). Expression of hBCATm also demonstrated a larger effect of 15% decrease in expression (Figure 6.22 B, Figure 6.23 B). However, it should be noted that the post-mortem delay was on average 4.5 hours longer in the AD cohort compared to the control cohort. This implies that a supposed detrimental effect on expression caused

Results

Figure 6. 22 Frontal cortex expression of the hBCAT protein in PM delay samples ($n^i = 2$, $n^e = 2$). Control frontal cortex tissue was acquired from South West Dementia Brain Bank. Western blot analysis was carried out using rabbit polyclonal antibodies specific to hBCATc or hBCATm (PA 1/10,000, SA 1/5000) (Insight Biotechnologies, Wembley, UK) in 5% Marvel as described in Method 4.3. Equal amounts of protein was loaded into each lane (10 μg/well) with a 15 ng pure protein (hBCATc or hBCATm) control included on each gel. The same membrane was stripped in 0.5 M sodium hydroxide and re-probed with mouse monoclonal anti-GAPDH antibody (PA 1/10,000, SA 1/5000) (Santa Cruz, California, USA) as an internal control. Panel A: Western blot of hBCATc in the frontal cortex region. Panel B: Western blot of hBCATm in the frontal cortex region. Gel map: hBCATc (C), hBCATm (M), 1 – 0 hrs PM delay, 2 – 6 hrs PM delay, 3 – 12 hrs PM delay, 4 – 24 hrs PM delay, 5 – 48 hrs PM delay, 6 – 72 hrs PM delay. The density of each band was measured using ImageJ™ software (Wayne Rasband, National Institute of Health, USA).
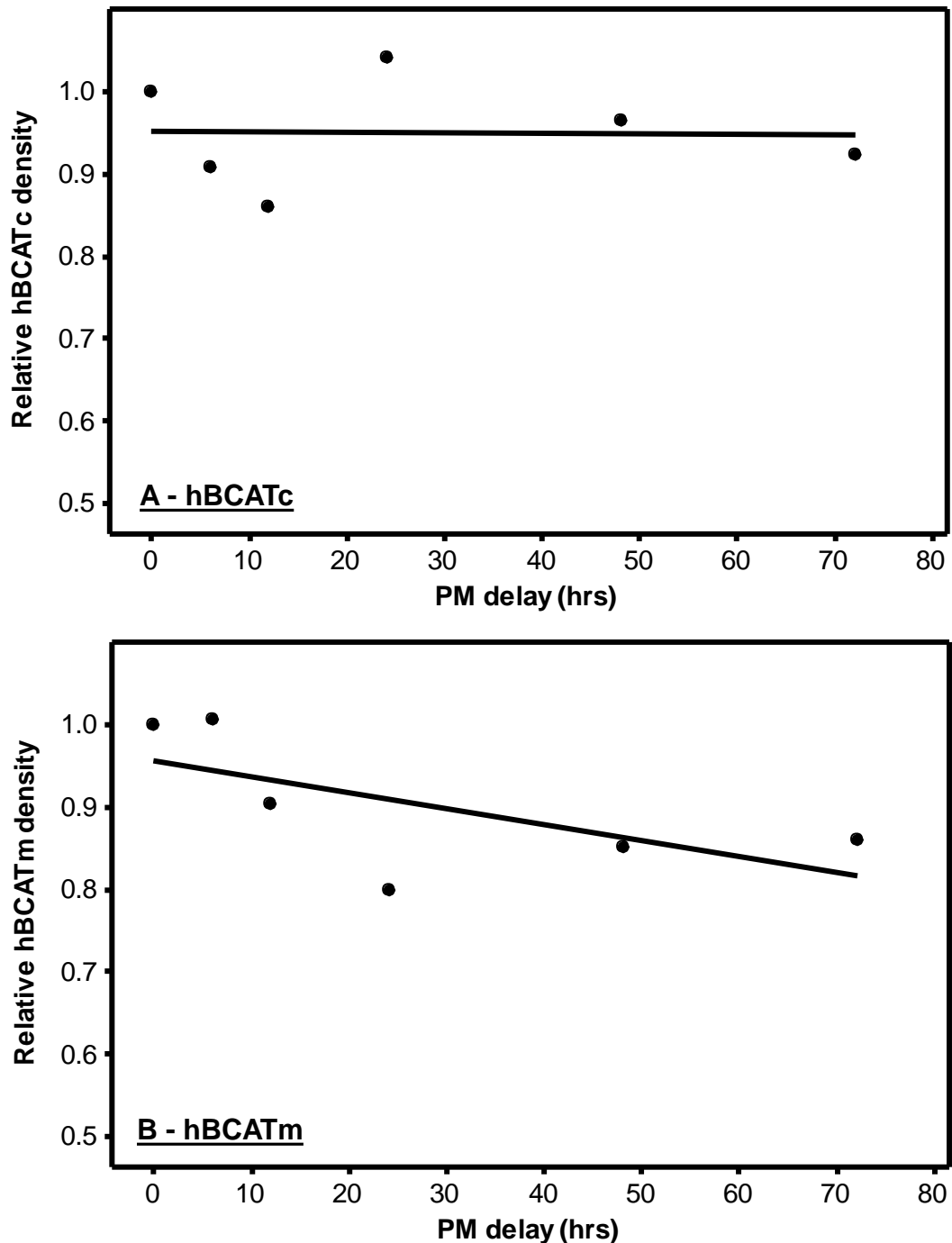
Figure 6. 23 Scatterplots of frontal hBCATc and hBCATm protein levels with increasing PM delay (n^i = 2, n^e = 2). Frontal cortex tissue was acquired from South West Dementia Brain Bank. PM delay was mimicked by the cutting of frozen tissue and then leaving the tissue at 4 ^{o}C (to mirror morgue conditions). The density of bands were measured using ImageJ^{TM} software (Wayne Rasband, National Institute of Health, USA) and expressed relative to the density for GAPDH. The results from two PM delay experiments were then averaged. Abbreviations: PM – post mortem.

by post-mortem delay could potentially lower the AD cohort levels and mask slight increases in expression.

To further investigate tissue quality, tissue pH was investigated, with decreased pH associated with poorer quality tissue (Stan *et al.*, 2006). However this decrease in tissue quality is not associated with a decrease in protein degradation but mRNA degradation. Frontal cortex tissue was homogenised in a neutral buffer and the pH was measured. However in this study, none of the variables investigated correlated with tissue pH (Figure 11.4, Figure 11.5, Figure 11.6). This is likely due to the more stable nature of proteins when compared to mRNA.

6.2.2 Effect of AD on hBCAT protein expression

Alzheimer's disease is an age related neurodegenerative disorder. This pathology follows a characteristic pathway, starting in the hippocampus and progressing to the temporal and frontal cortex. Protein density of hBCATc, hBCATm and S-glutathionylated proteins was calculated utilising ImageJ^{TM} software (Wayne Rasband, National Institute of Health, USA) and these protein levels were normalised relative to GAPDH. This was used as an internal control as GAPDH levels have been used previously as a loading control in this disease and appears to have unaltered expression in AD (Grathwohl *et al.*, 2009; Hebert *et al.*, 2008; Smith *et al.*, 2006). Frontal protein expression of hBCATc was increased in AD subjects by 32%, when compared to matched controls but was not mirrored in the temporal cortex and also did not reach significance (Figure 6.24 A, Figure 6.25 A, $p = 0.079$
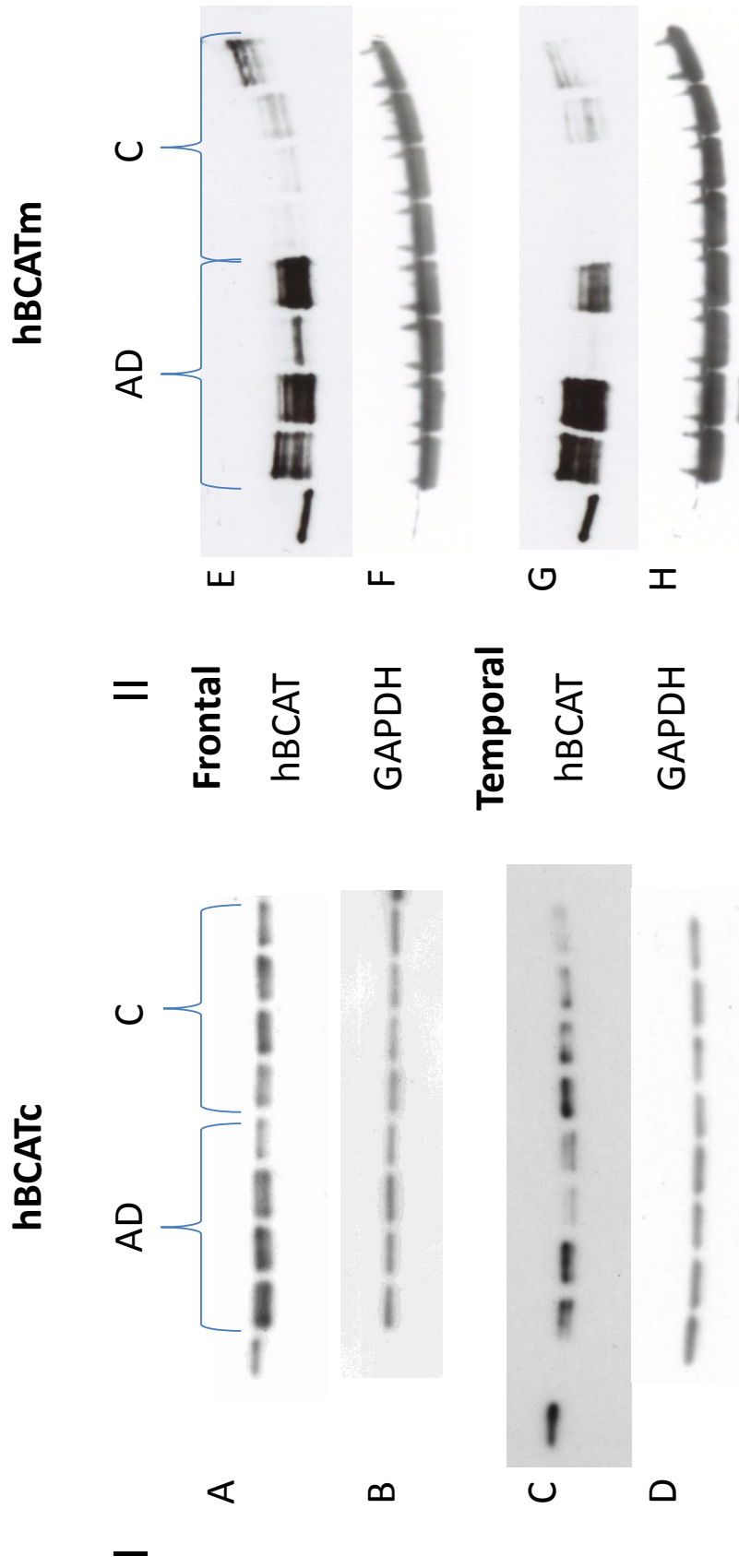
Figure 6. 24 Frontal and temporal cortex expression of the hBCAT protein in AD subjects compared to age and gender matched controls (n[i] = 80, n[e] = 30 for each protein). AD and control frontal and temporal cortex tissue was acquired from South West Dementia Brain Bank. Western blot analysis was carried out using rabbit polyclonal antibodies specific to hBCATc or hBCATm (PA 1/10,000, SA 1/5000) (Insight Biotechnologies, Wembley, UK) in 5% Marvel as described in Method 4.3. Equal amounts of protein was loaded into each lane (10 µg/well) with a 15 ng pure protein (hBCATc or hBCATm) control included on each gel. The same membrane was stripped in 0.5 M sodium hydroxide and re-probed with mouse monoclonal anti-GAPDH antibody (PA 1/1,000, SA 1/5000) (Santa Cruz, California, USA) as an internal control. Panel I: Western blot of hBCATc in the frontal (A) and temporal (C) cortex regions, with GAPDH loading controls (B+D). Panel II: Western blot of hBCATm in the frontal (E) and temporal (G) cortex regions, with GAPDH loading controls (F+H). The density of each band was measured using ImageJ[TM] software (Wayne Rasband, National Institute of Health, USA).

A - Frontal
Mean = 0.946 ● 0.716
N^i = 36 ● 35
N^e = 15
P-values
Sex = 0.192
Diagnosis = 0.079

B - Temporal
Mean = 0.685 ● 0.745
N^i = 38 ● 37
N^e = 15
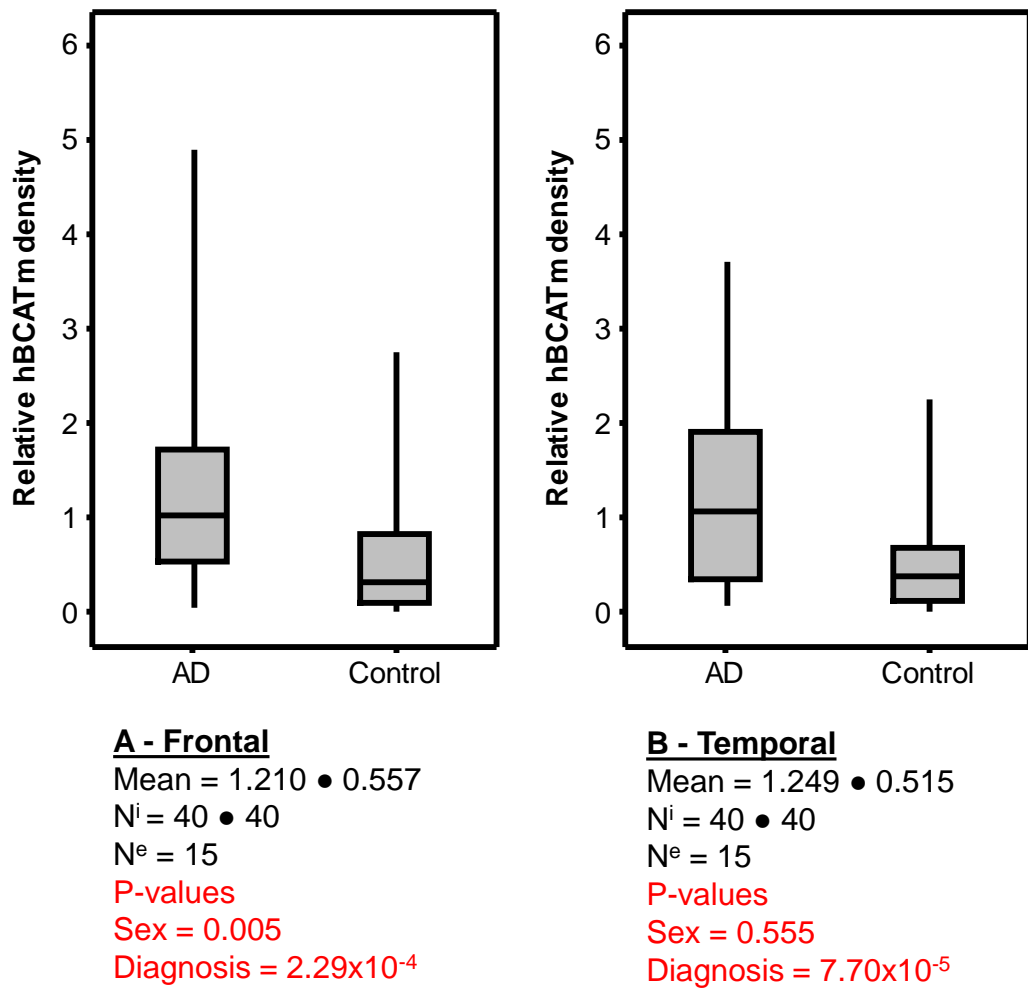P-values
Sex = 0.514
Diagnosis = 0.357
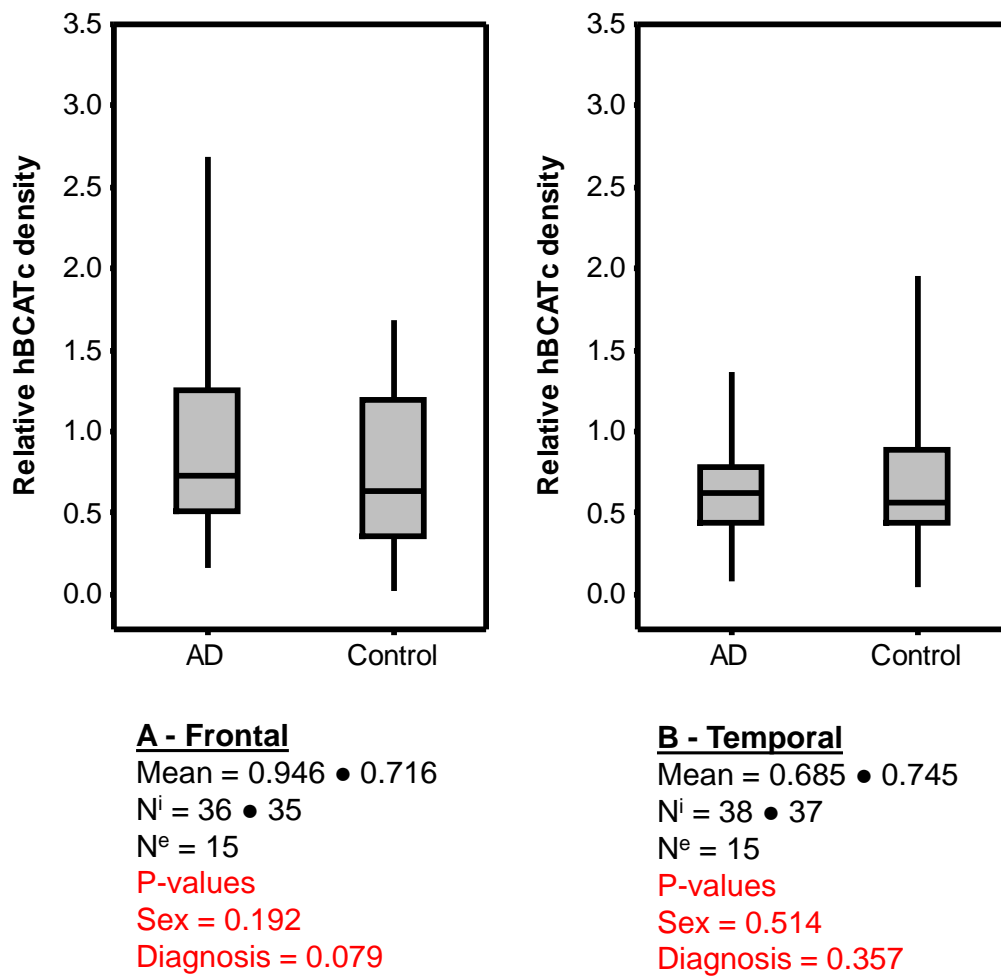
Figure 6. 25 Boxplots of frontal and temporal hBCATc protein levels in AD subjects compared to matched controls. The density of bands were measured using ImageJ™ software (Wayne Rasband, National Institute of Health, USA) and expressed relative to the density of GAPDH. Data was then analysed for significance using a two way anova test in Minitab™. Panels show interquartile range (box) sample range (whiskers) and the median (horizontal line within the interquartile range).

and Figure 6.24 A, Figure 6.25 B, p = 0.357 respectively). However, protein expression of hBCATm was significantly increased in the frontal and temporal cortex by 117% and 143%, respectively relative to age and gender matched control subjects (Figure 6.24 B, Figure 6.26 A, p = 2.29 x 10^{-4} and Figure 6.24 B, Figure 26 B, p = 7.70 x 10^{-5}). Furthermore, levels of S-glutathionylated protein were observed to be significantly decreased by 36% in AD compared to controls in the frontal cortex (Figure 6.27 A, Figure 6.28 A, p = 0.023). However, the decrease of 10% observed in the temporal cortex did not reach significance (Figure 6.27 B, Figure 6.28 B, p = 0.580).

In summary, increased levels of hBCATm by over 140% indicates that this protein may have a role in the regulation of brain glutamate through metabolism in the endothelial cells in AD. An increase of hBCATc was also observed within the frontal cortex, although this did not reach statistical significance. It is probable that this would impact neuronal glutamate pool within neuronal cells. Furthermore, the decreased level of S-glutathionylated proteins potentially relates to a decrease in free GSH occurring in AD, rather than a decreased rate of S-glutathionylation (Bermejo *et al*., 2008).

6.2.3 Effect of MND on hBCAT protein expression

The disease MND is a rapidly progressive neurodegenerative disease characterised by progressive muscle weakness, muscle atrophy and difficulty breathing. The defining pathology of MND is a loss of upper and lower motor neurons of the motor cortex (Deng *et al*., 2011). Individuals with MND have

A - Frontal
Mean = 1.210 ● 0.557
N^i = 40 ● 40
N^e = 15
P-values
Sex = 0.005
Diagnosis = 2.29×10^{-4}

B - Temporal
Mean = 1.249 ● 0.515
N^i = 40 ● 40
N^e = 15
P-values
Sex = 0.555
Diagnosis = 7.70×10^{-5}

Figure 6. 26 Boxplots of frontal and temporal hBCATm protein levels in AD subjects compared to matched controls. The density of bands were measured using ImageJ[TM] software (Wayne Rasband, National Institute of Health, USA) and expressed relative to the density for GAPDH. Data was then analysed for significance using a two way anova test in Minitab™. Panels show interquartile range (box) sample range (whiskers) and the median (horizontal line within the interquartile range).
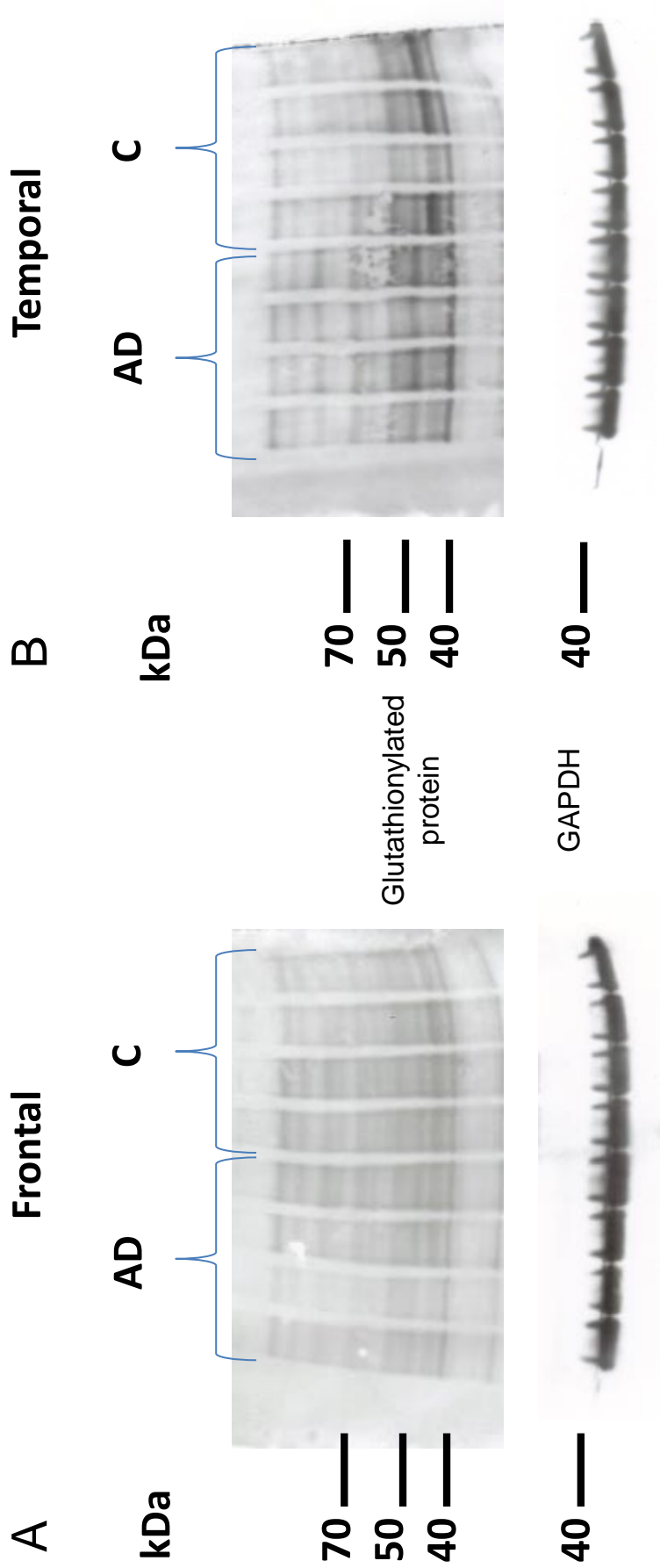
Figure 6. 27 Frontal and temporal cortex levels of glutathionylated protein in AD subjects compared to matched controls (n^i = 50 and 36, n^e = 10 and 10). AD and control frontal and temporal cortex tissue was acquired from the South West Dementia Brain Bank. Western blot analysis was carried out using a mouse monoclonal antibody specific to glutathione (PA 1/300, SA 1/5000) (Source Bioscience, Nottingham, UK) in 0.5% Marvel as described in Method 4.3. Equal amounts of protein was loaded into each lane (20 μg/well). The same membrane was stripped in 0.5 M sodium hydroxide and re-probed with mouse monoclonal anti-GAPDH antibody (PA 1/1,000, SA 1/5000) (Santa Cruz, California, USA) as an internal control. Panel A: Western blot of glutathionylated protein in frontal cortex region. Panel B: Western blot of glutathionylated protein in the temporal cortex region. The density of each band was measured using ImageJ™ software (Wayne Rasband, National Institute of Health, USA).
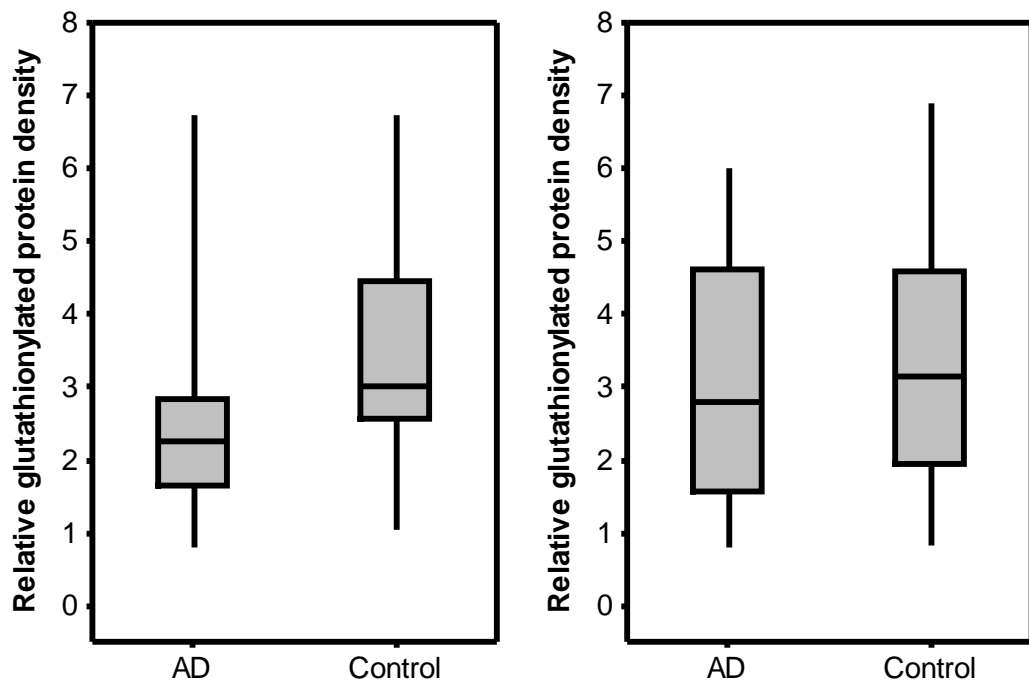
A - Frontal
Mean = 2.53 ● 3.43
N^i = 25 ● 25
N^e = 10
P-values
Sex = 0.086
Diagnosis = 0.023

B - Temporal
Mean = 3.11 ● 3.42
N^i = 18 ● 18
N^e = 10
P-values
Sex = 0.711
Diagnosis = 0.580

Figure 6. 28 Box plots of frontal and temporal glutathionylated protein levels in AD subjects compared to matched controls. The density of bands were measured using ImageJ[TM] software (Wayne Rasband, National Institute of Health, USA) and expressed relative to the density for GAPDH. Data was then analysed for significance using a two way anova test in Minitab™. Panels show interquartile range (box) sample range (whiskers) and the median (horizontal line within the interquartile range).

higher levels of glutamate in their serum and spinal fluid (Al-Chalabi *et al.*, 2000). This led to the hypothesis that hBCAT is altered in this disease and a pilot study investigated if the effect on hBCAT expression was mirrored in other diseases where glutamate was a pathological mechanism or whether the effect was specific to AD. It was demonstrated that overall levels of hBCATc were non-significantly increased by 18% (Figure 6.29 A, Figure 6.30 A, $p = 0.529$) and levels of hBCATm were non-significantly increased by 38% (Figure 6.29 B, Figure 6.30 B, $p = 0.548$) in MND motor cortex samples compared to controls. This indicates that either the sample set is too small to detect the difference (significantly) between MND and controls, or that expressional alteration to the hBCAT protein is unique to AD. It should be noted that the samples were gender matched, however the control cohort was on average 4.4 years older and the post-mortem delay 4 hours shorter. It should also be noted that one of the MND control cases also had mild Braak pathology. When this study is expanded upon in the future it is necessary that all controls are absent of Braak pathology and appropriately age, gender and PM delay matched (at least in terms of the complete cohort) – in part due to what has been demonstrated in this work.

6.2.4 Distribution of the hBCAT proteins in AD compared to controls

To evaluate the increased expression of hBCAT demonstrated utilising Western blot analysis, immunohistochemistry was used. The aims of immunohistochemistry analysis were (i) to evaluate the cellular distribution of the increased expression observed using Western blot analysis and (ii) to evaluate expression in the hippocampus. It is known that neuronal, glial and

Results
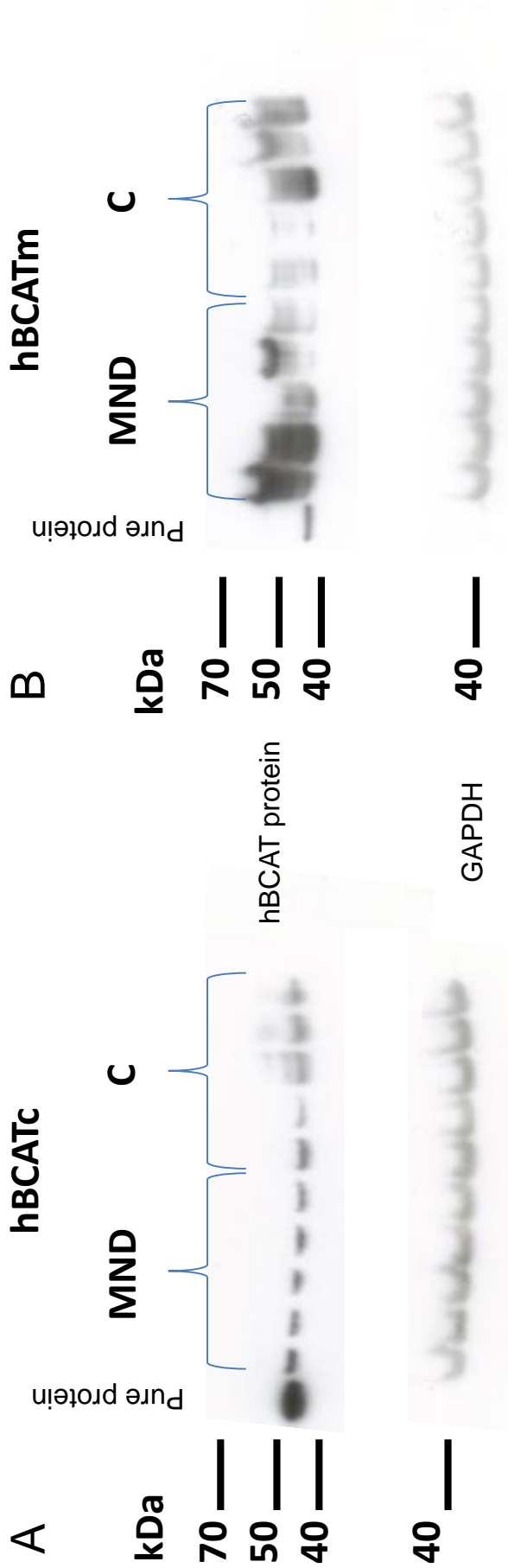
Figure 6. 29 Motor cortex expression of the hBCAT protein in MND subjects compared to matched controls (n^i = 10, n^e = 2). MND and control motor cortex tissue was acquired from the London Neurodegenerative Disease Brain Bank. Western blot analysis was carried out using rabbit polyclonal antibodies specific to hBCATc or hBCATm (PA 1/1000 and 1/1500 respectively, SA 1/5000) (Insight Biotechnologies, Wembley, UK) in 0.5 % Marvel as described in Method 4.3. Equal amounts of protein was loaded into each lane (20 µg/well) with a 20 ng pure protein (hBCATc or hBCATm) control included on each gel. The same membrane was stripped in 0.5 M sodium hydroxide and re-probed with mouse monoclonal anti-GAPDH antibody (PA 1/1,000, SA 1/5000) (Santa Cruz, California, USA) as an internal control. Panel A: Western blot of hBCATc in the motor cortex region. Panel B: Western blot of hBCATm in the motor cortex region. The density of each band was measured using ImageJ™ software (Wayne Rasband, National Institute of Health, USA).

Jonathon Hull (2014)   Page 125

A - hBCATc
Mean = 0.502 ● 0.593
N^i = 5 ● 5
N^e = 2
P-value = 0.529

B - hBCATm
Mean = 1.749 ● 2.413
N^i = 5 ● 5
N^e = 2
P-value = 0.548
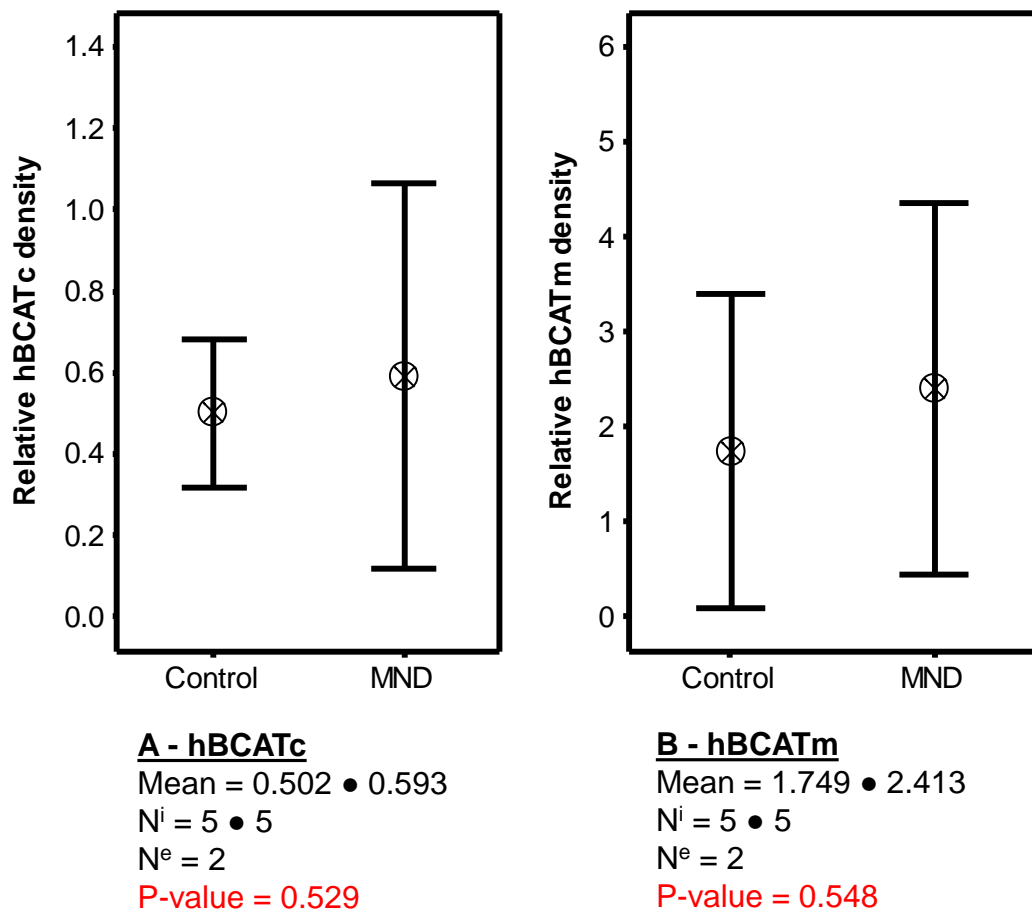
Figure 6. 30 Interval plots of motor cortex hBCATm and hBCATc protein expression in MND subjects compared to matched controls. The density of bands was measured using ImageJ^{TM} software (Wayne Rasband, National Institute of Health, USA) and expressed relative to the density for GAPDH. Data was then analysed for significance using an unpaired t-test in Minitab™. Interval plots show 95% confidence interval and the mean.

vascular cells all have different roles in AD pathology with neuronal pathology initiating in the hippocampus in a well-defined manner but both vascular and glial abnormalities considered prior events. Therefor it is appropriate to observe which cell type contain hBCATm and whether a new cell type is observed in AD pathology.

In the hippocampal region, labelling for hBCATc in AD sections was pronounced relative to the equivalent section from control subjects in both the CA4 (Figure 6.31 A, Figure 6.31 F, Figure 6.35, p = 0.026) and the CA1 region (Figure 6.31 B, Figure 6.31 G, Figure 6.35, p = 0.011); with no observable increase in labelling within the temporal cortex (Figure 6.31 C-E+H-J, Figure 6.32, Figure 6.35, p = 0.496). Increased presence of hBCATm labelling in the vasculature relative to matched controls was also noted within the CA4 region of the hippocampus (Figure 6.33 A+E). For hBCATm the increase in expression was observed in the vasculature of AD subjects in the temporal cortex (but also throughout the brain), where the expression of hBCATm was pronounced in AD subjects relative to control subjects (Figure 6.33, Figure 6.34, Figure 6.35, p= 0.025). These results demonstrate that the increased expression of hBCATm is not occurring in a new cell type but remains restricted to the vasculature. It is also proposed that hBCATc expression in the hippocampus is increased in AD subjects relative to controls.
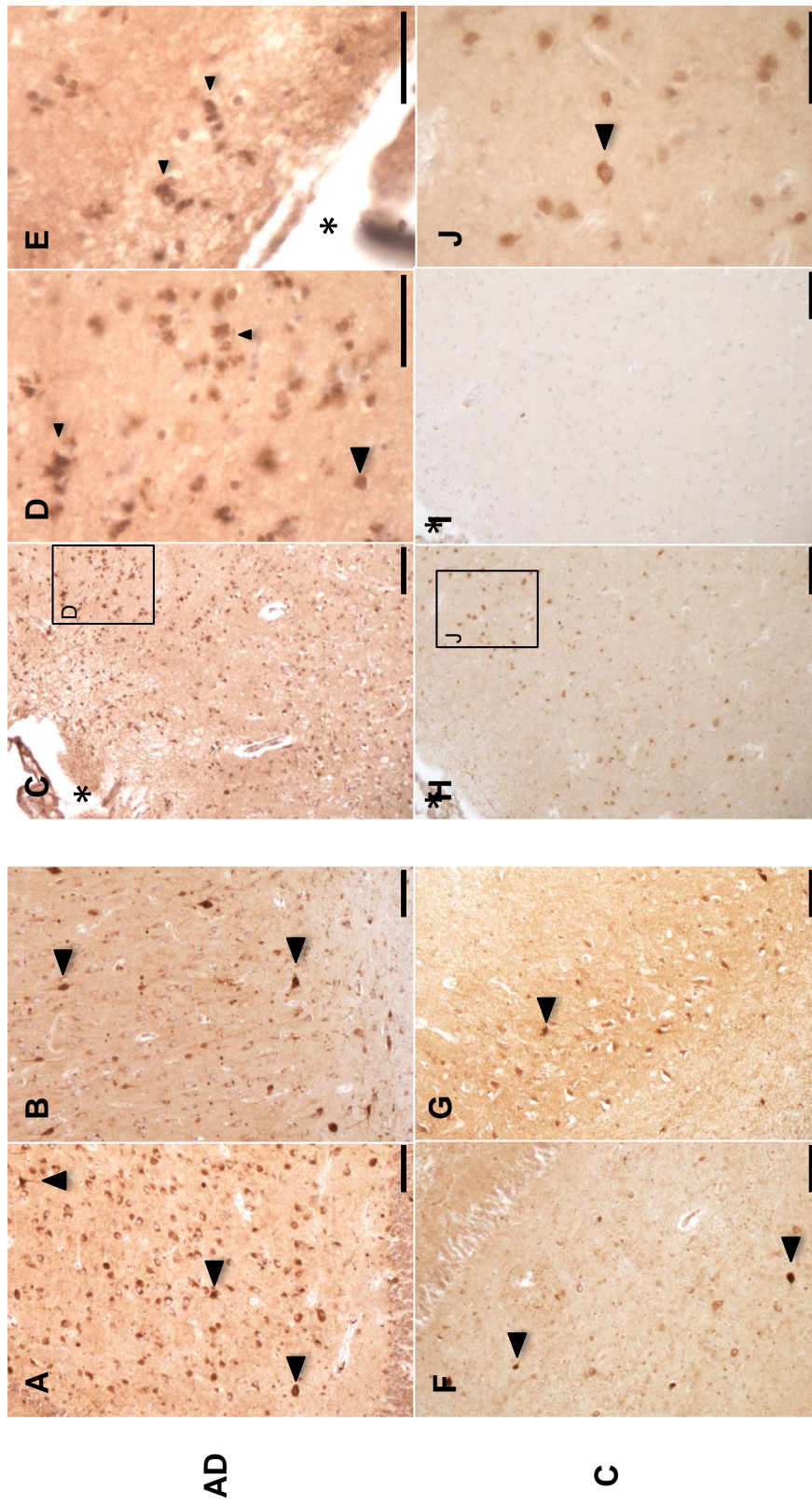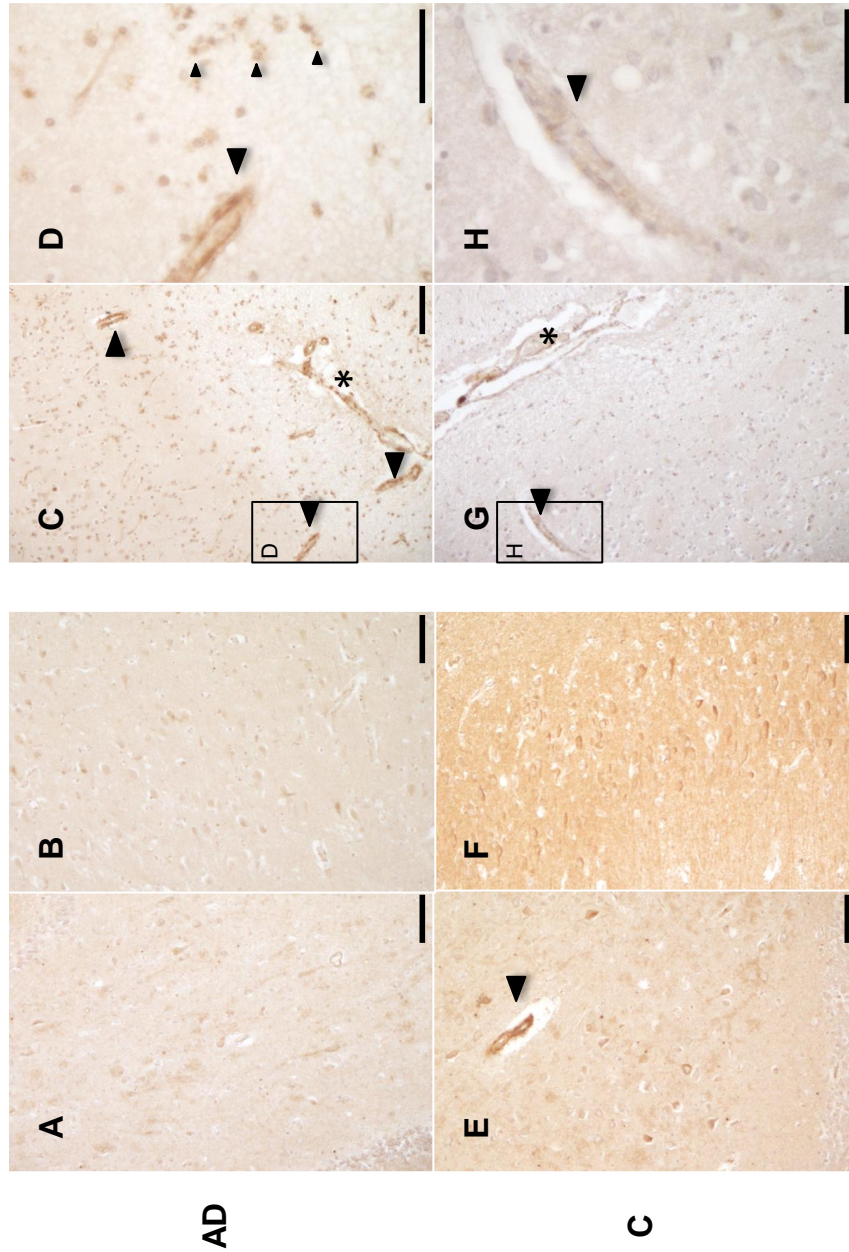
Figure 6. 31 Staining of hBCATc in the hippocampus and temporal of AD and control subject (n^i = 60, n^e = 30). Panel A: CA4 region of the hippocampus in an AD subject showing intensely stained neurons (large arrows). Panel B: CA1 of the hippocampus in an AD subject. Panel C: Temporal cortex of an AD subject showing the collateral sulci (*). Panel D & E: Increased magnification of the collateral sulci showing 'non-neuronal' staining. Panel F: CA4 region of the hippocampus in a control subject. Panel G: CA1 region of the hippocampus in a control subject. Panel H: Temporal cortex of control subject. Panel I: Antigen incubation of serial section of H, at 200X molar excess. Panel J: Increased magnification of H. It can be seen that immunoreactivity is completely removed by antigen incubation at 200X molar excess. Magnification for A, B, C, F, G, H and I, X10. Magnification for D, E and J, X40. Scale bar: A, B, C, F, G, H and I, 200 μm; D, E and J, 50 μm.
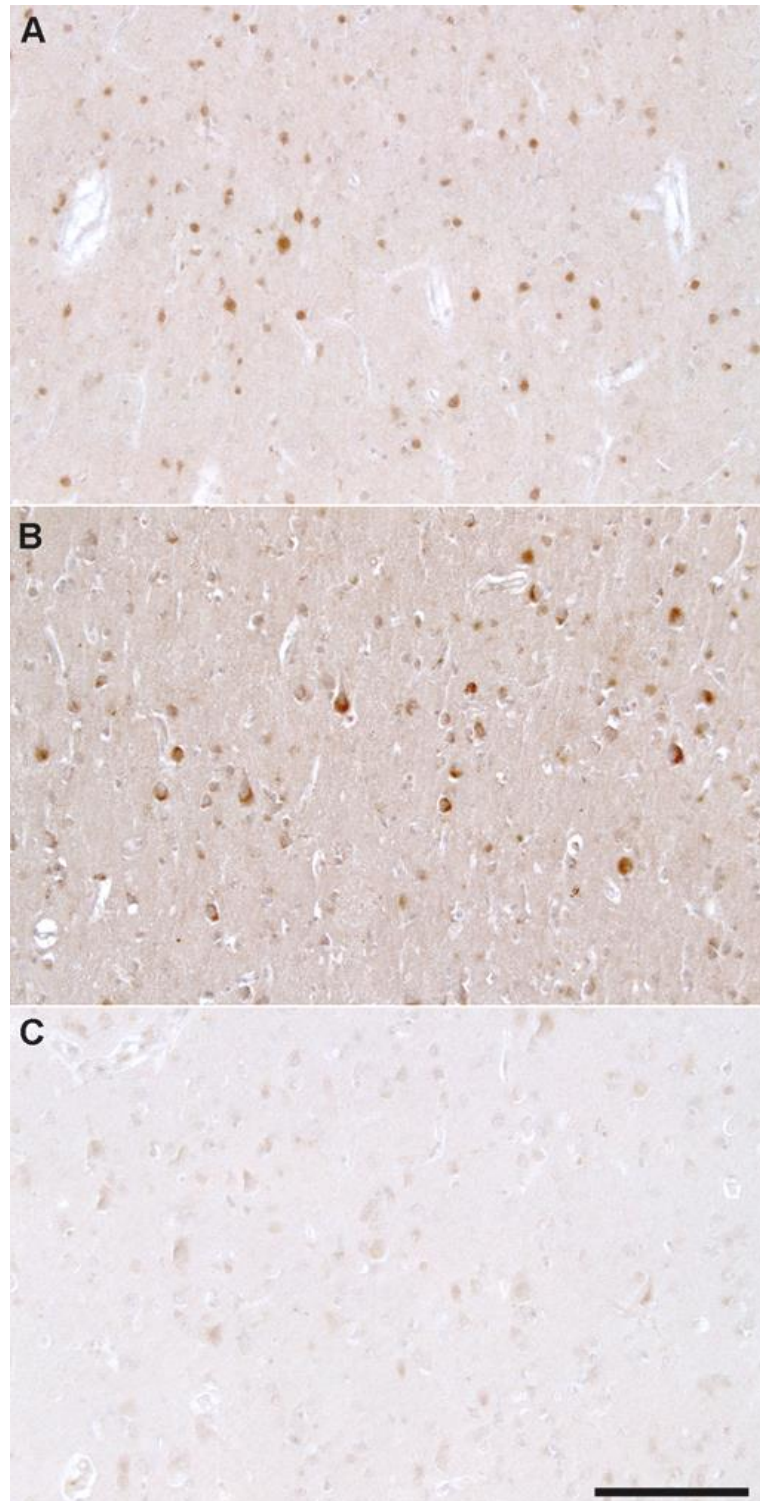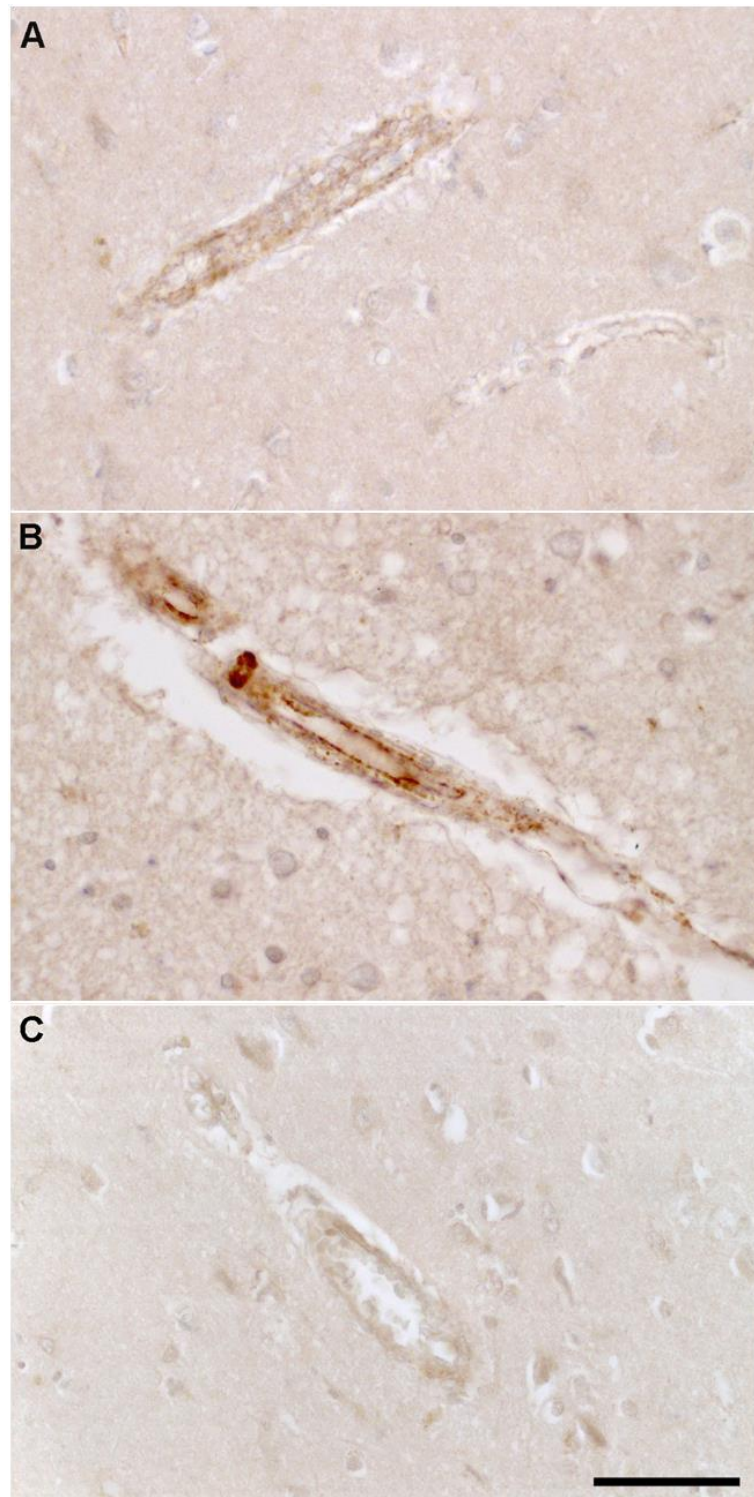
Figure 6. 32 Neuronal staining of hBCATc in the temporal cortex of AD and control individuals (n^i = 60, n^e = 30). Panel A: hBCATc staining in a control subject. Panel B: hBCATc staining in an AD subject. Panel C: Antigen incubation of serial section of B, at 200X molar excess. Scale bar: A, B and C, 50 μM.

Figure 6. 33 Staining of hBCATm in the hippocampus and temporal of AD and control individuals (n^i = 60, n^e = 30) Panel A: CA4 region of the hippocampus in an AD subject. Panel B: CA1 of the hippocampus in an AD subject. Panel C: Temporal cortex of an AD subject showing the collateral sulci (*). Panel D: Increased magnification of C showing 'non-neuronal' staining (small arrows) and vessel staining (large arrow). Panel E: CA4 region of the hippocampus in a control subject. Panel F: CA1 region of the hippocampus in a control subject. Panel G: Temporal cortex of control subject. Panel H: Increased magnification of G. Neuronal staining of the hippocampus was largely non-existent in AD and control individuals, however an increase in vessel and 'non-neuronal' staining was noted in the temporal cortex. Magnification for A, B, C, E, F, and G, X10. Magnification for D, and H, X40. Scale bar: A, B, C, E, F and G, 100 μm; D and H, 50 μm.

Figure 6. 34 Vessel staining of hBCATm in temporal cortex of AD and control individuals (n^i = 60, n^e = 30). Panel A: hBCATm staining in a control subject. Panel B: hBCATm staining in an AD subject. Panel C: Antigen incubation of serial section of B, at 200X molar excess. Scale bar: A, B and C, 50 µM.
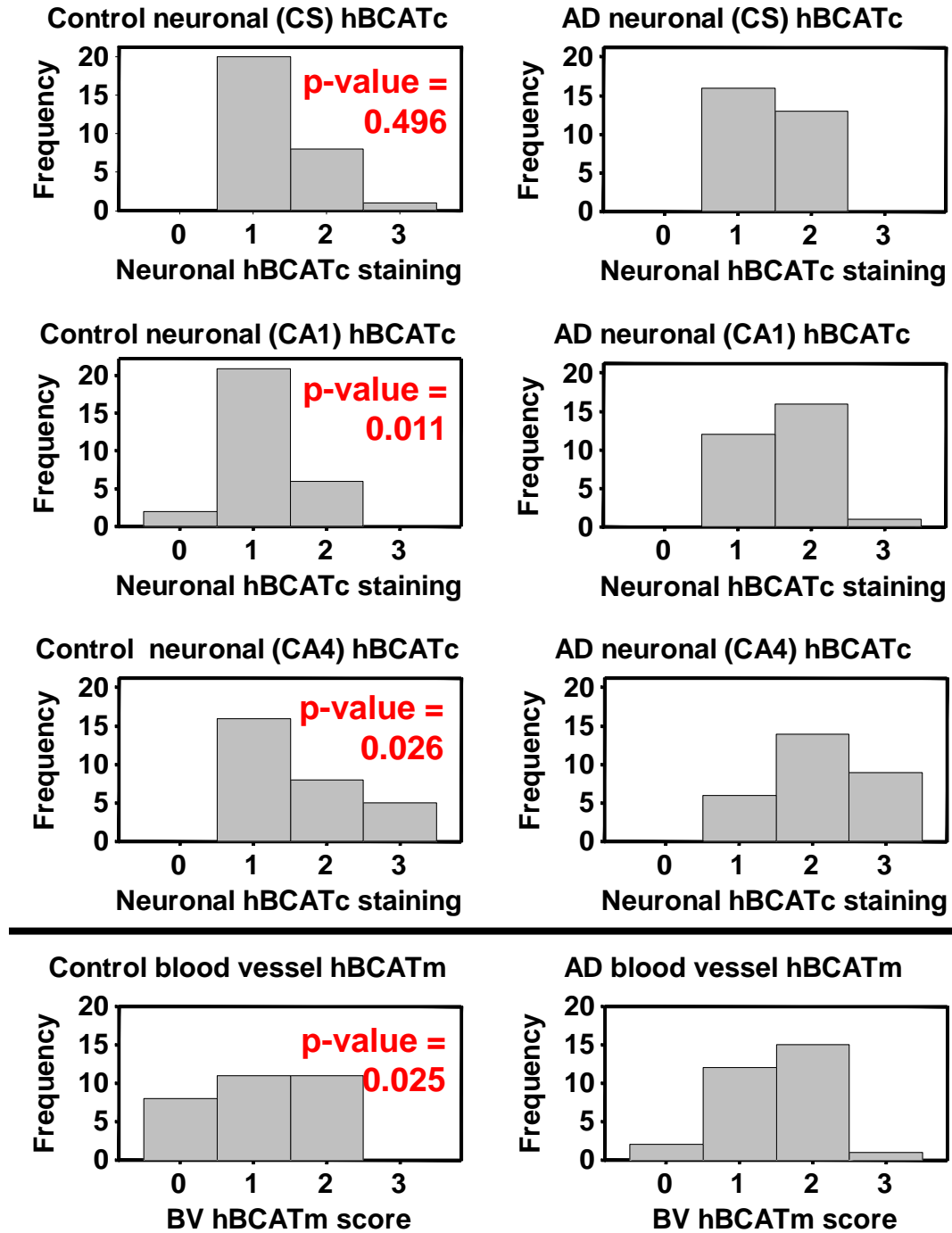
Figure 6. 35 Histograms of temporal and hippocampal hBCATc and hBCATm protein level scores in AD subjects compared to matched controls (n^i = 60, n^e = 30). The staining score of cell types were repeated by another individual for consistency and analysed for significance using Wilcoxon-Mann-Whitney test in Minitab™.

In conclusion, this work demonstrates that increased expression observed using Western blot analysis was not occurring in a new cell type – hBCATm expression remained vascular in nature and the increased expression was replicated in this work. It is further observed that hBCATc expression was significantly up-regulated in the hippocampus of AD subjects relative to controls and this may have pathological implications for BCAA metabolism and glutamate production in AD.

6.2.5 Correlation of hBCATc, hBCATm and S-glutathionylated protein to key physiological and genetic factors

Relative densitometry was comparable across Western blots, therefore expression of hBCATc, hBCATm and S-glutathionylated protein were compared to data stored at the SWDBB. For AD it is already known that the greatest risk factor is age, with increasing age increasing the risk of AD (Lindsay *et al.*, 2002). Further to age, the most common risk factors include gender, levels of education and APOE genotype (Launer *et al.*, 1999; Lindsay *et al.*, 2002). For gender it appears that females are at greatest risk of AD pathology although it is suspected that this increase in incidence of AD was due to the increased life expectancy associated with females (Hebert *et al.*, 2000). Molecular genetics has revealed risk factors for sporadic AD in the form of alipoprotein E (APOE), BIN1, CLU, CR1 and PICALM genotype in addition to positive family history (Bertram *et al.*, 2010)*.* The strongest association is with the APOE genotype, the ε4 genotype associated with an increased risk of AD by approximately 4-fold (reviewed by Brouwers *et al.*, 2008)*.* Finally, increasing age is associated with a decrease in brain weight.

This decrease is exacerbated in AD and is thought to relate to a functional loss of brain mass (Fox & Schott, 2004).

Age is the largest risk factor for AD (Lindsay *et al.*, 2002). Increasing age increases the risk of AD due to an increased oxidative stress associated with aging and the key role oxidative stress is thought to play in disease manifestation. Although a negative correlation between hBCATc expression in the frontal cortex and age was observed (Figure 6.36 A, $p = 0.004$, ρ -0.342) there was no significant correlation between hBCATc or hBCATm expression in the temporal region or the frontal region for hBCATm (Figure 6.36, $p = 0.305$, ρ -0.120 B; Figure 6.37 A, $p = 0.137$, ρ +0.168 and Figure 6.37 B, $p = 0.142$, ρ +0.166 respectively). However, levels of S-glutathionylated protein significantly increased with age in both the frontal and temporal region (Figure 6.38 A, $p = 0.012$, ρ +0.354 and Figure 6.38 B, $p = 0.042$, ρ +0.340 respectively). It is probable that this correlation is related to the oxidative stress associated with ageing. It follows that this increased S-glutathionylated protein levels would correlate with a decrease in free S-glutathione levels observed in the aged brain.

Brain weight showed no correlation with frontal and temporal hBCATc (Figure 6.39 A, $p = 0.658$, ρ -0.055 and Figure 6.39 B, $p = 0.777$, ρ -0.034) or S-glutathionylated (Figure 11.7 A, $p = 0.350$, ρ -0.141 and Figure 11.7 B, $p = 0.997$, ρ -0.00073) protein levels but negatively correlated with hBCATm expression (Figure 6.40 A, $p = 9.3 \times 10^{-5}$, ρ-0.438 and Figure 6.40 B, $p = 2.3 \times 10^{-3}$, ρ-0.349). This implies a physiological relationship between hBCATm
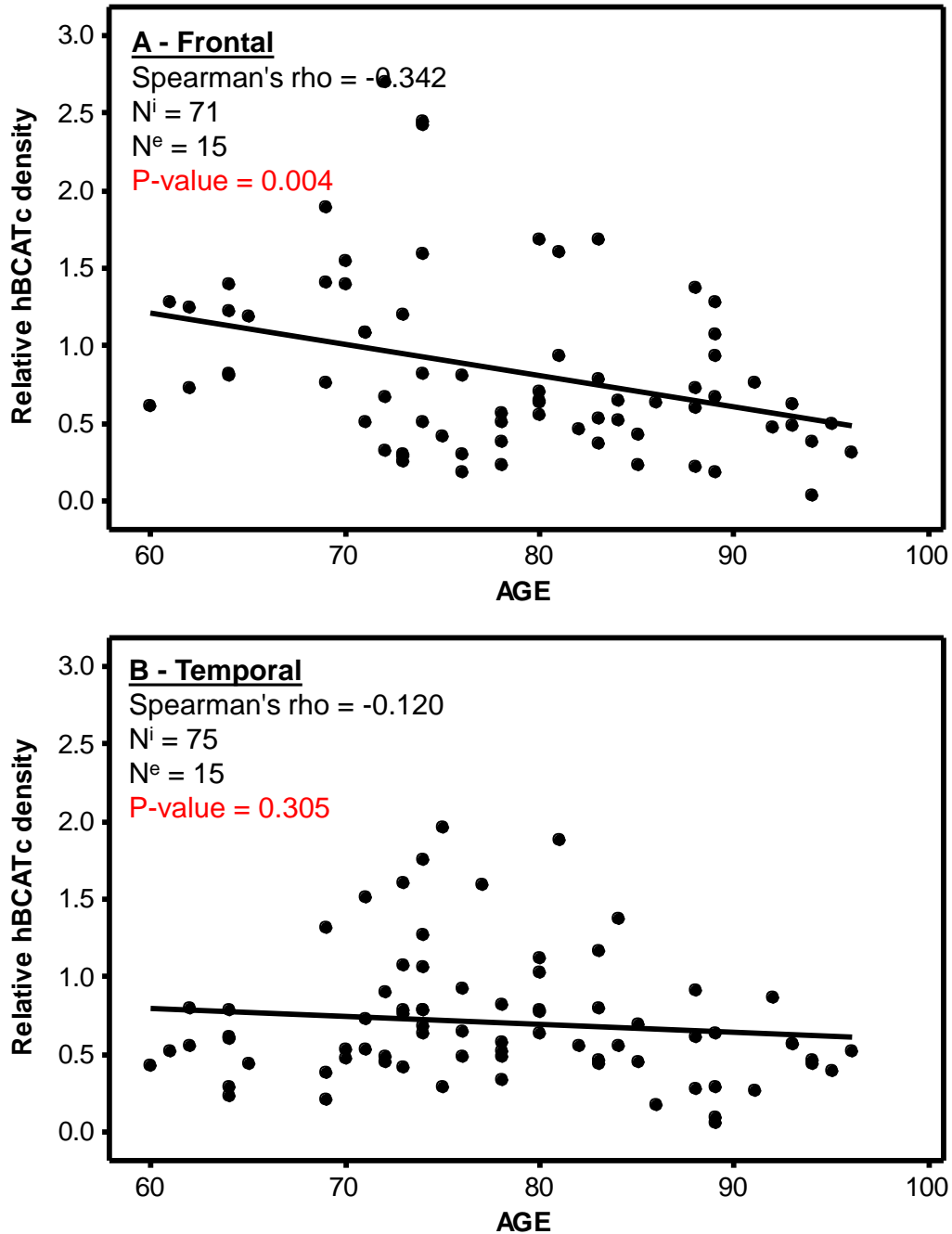
Figure 6. 36 Scatterplots of frontal and temporal hBCATc protein levels correlated with age. The density of bands were measured using ImageJ™ software (Wayne Rasband, National Institute of Health, USA) and expressed relative to the density for GAPDH. Data was then analysed for significance using Spearman's rho test in Minitab™.
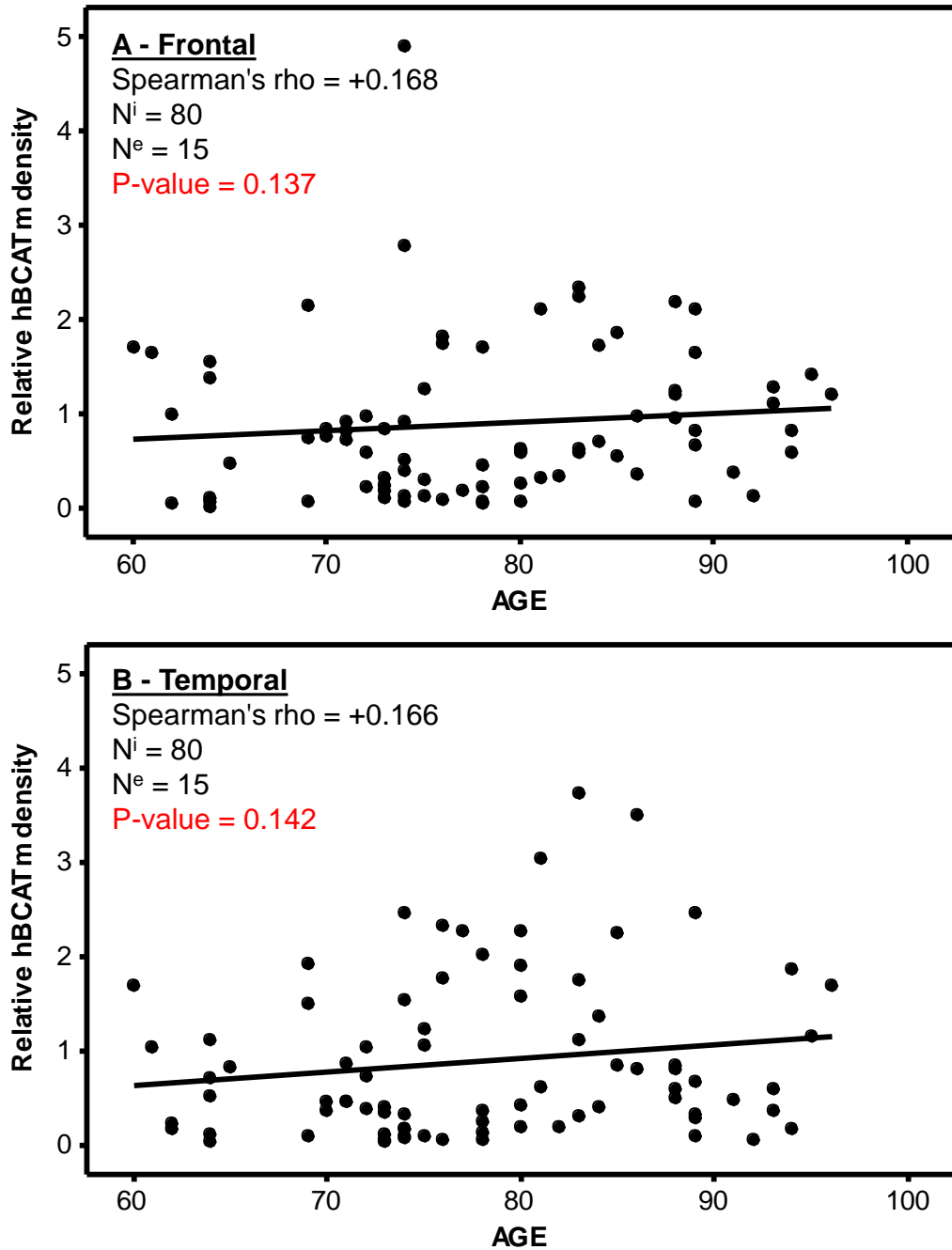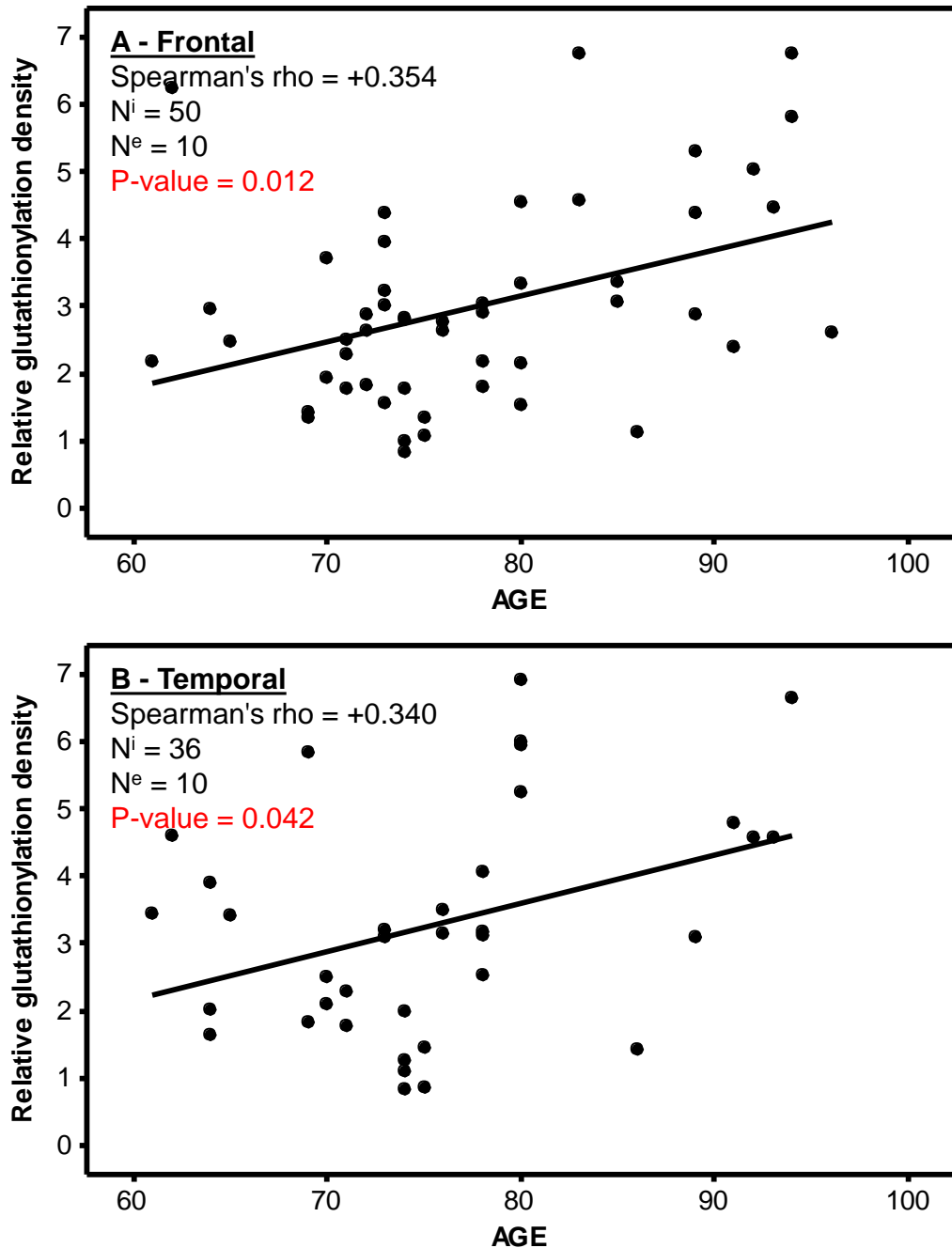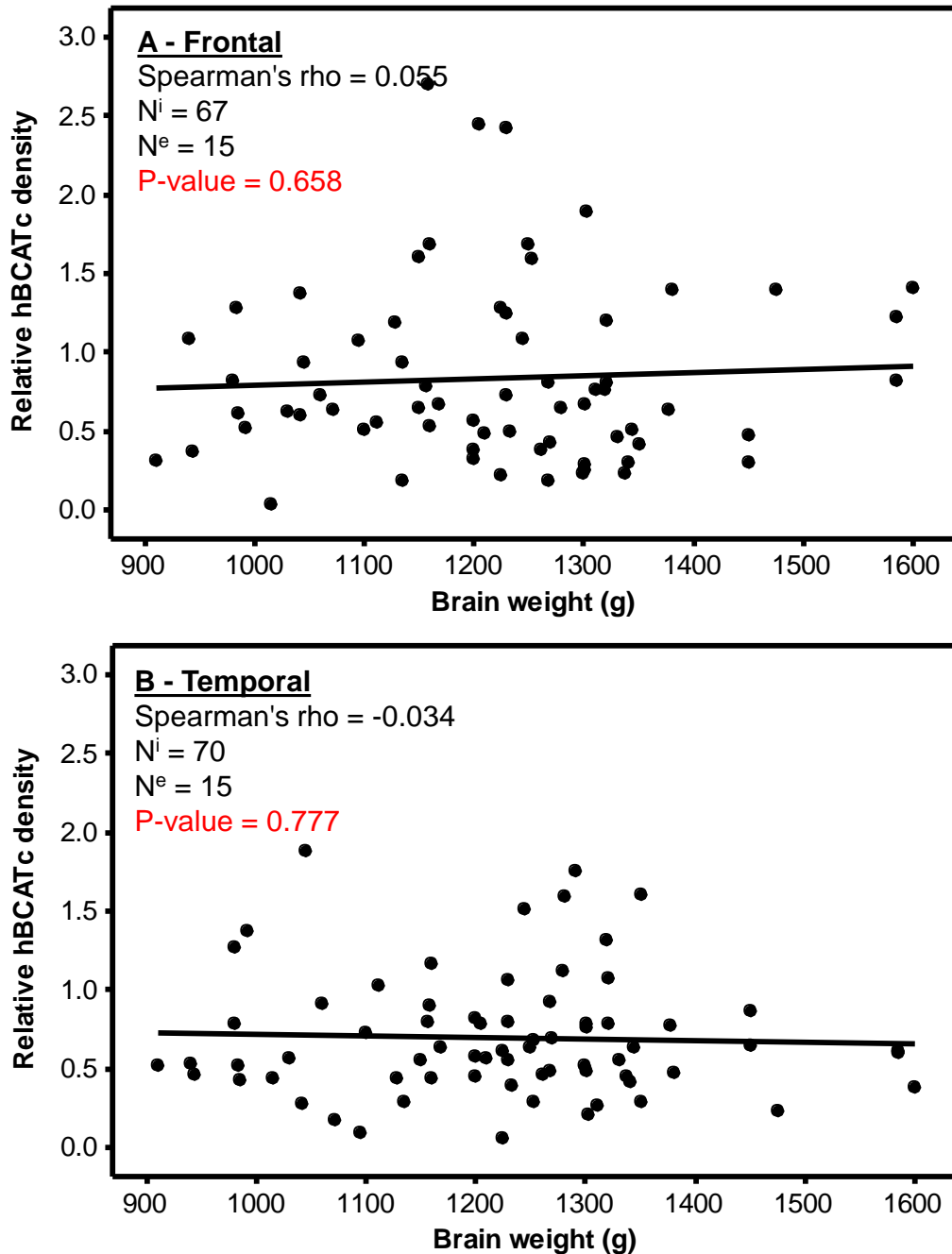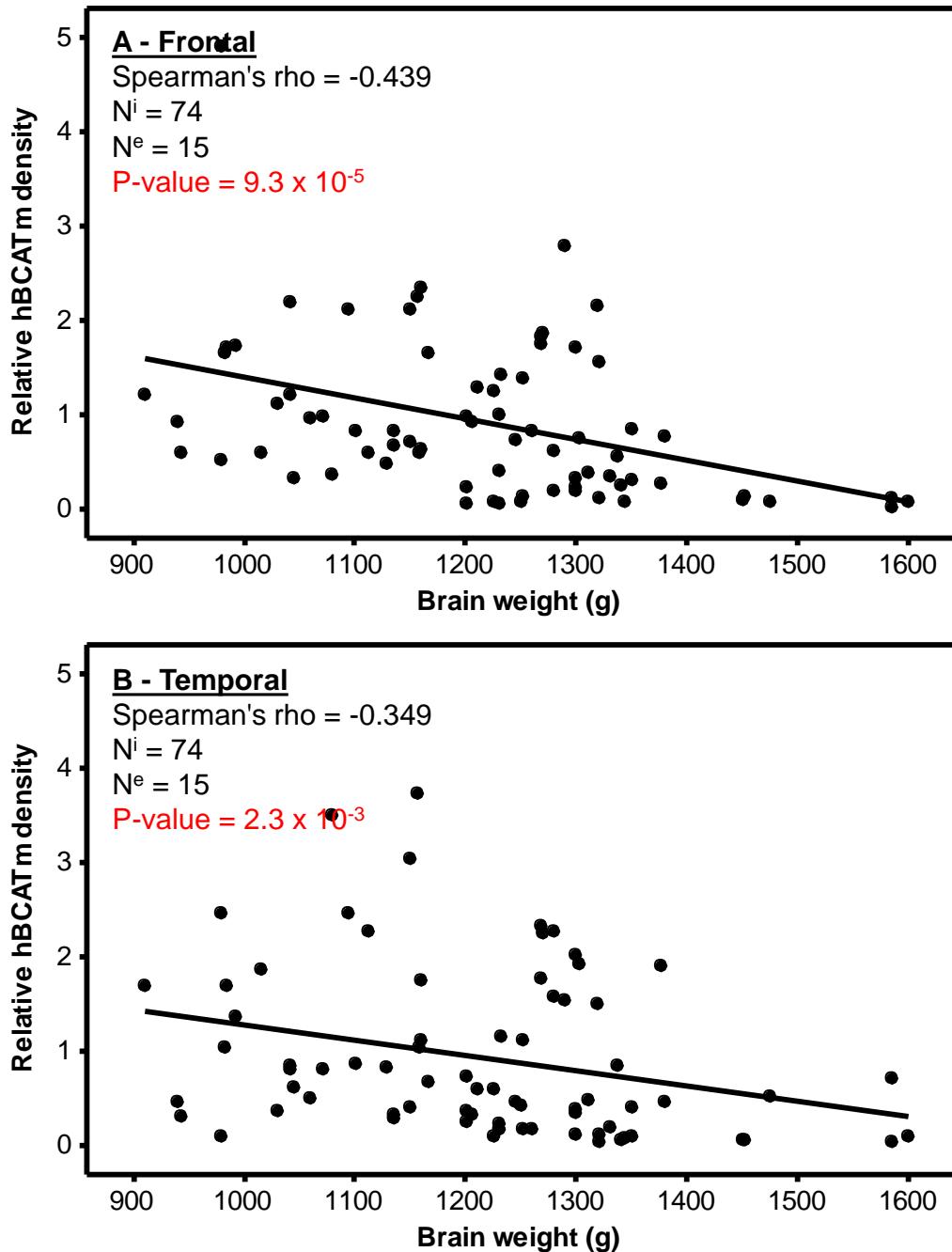
Figure 6. 37 Scatterplots of frontal and temporal hBCATm protein levels correlated with age. The density of bands were measured using ImageJ™ software (Wayne Rasband, National Institute of Health, USA) and expressed relative to the density for GAPDH. Data was then analysed for significance using Spearman's rho test in Minitab™.

Figure 6. 38 Scatterplots of frontal and temporal glutathionylated protein levels correlated with age. The density of lanes were measured using ImageJ™ software (Wayne Rasband, National Institute of Health, USA) and expressed relative to the density for GAPDH. Data was then analysed for significance using Spearman's rho test in Minitab™.

Figure 6. 39 Scatterplots of frontal and temporal hBCATc protein levels correlated with brain weight. The density of bands were measured using ImageJ™ software (Wayne Rasband, National Institute of Health, USA) and expressed relative to the density for GAPDH. Data was then analysed for significance using Spearman's rho test in Minitab™.

Figure 6. 40 Scatterplots of frontal and temporal hBCATm protein levels correlated with brain weight. The density of bands were measured using ImageJ™ software (Wayne Rasband, National Institute of Health, USA) and expressed relative to the density for GAPDH. Data was then analysed for significance using Spearman's rho test in Minitab™.

and brain weight; however it may also be related to the progression of AD or the aging process itself (i.e. increased AD or age progression, decreased brain mass due to atrophy, increased hBCATm expression).

Females are at additional risk of AD than males, although this is not the largest of predisposing factors (Launer *et al.*, 1999). Differences in female/male expression of hBCATc, hBCATm or S-glutathionylated protein reached significance in one instance –frontal expression of hBCATm was increased by 71% in females (Figure 6.42 A, p = 0.010). It was further noted that frontal and temporal hBCATc was non-significantly 25% and 11% higher in males respectively (Figure 6.41 A, p = 0.179 and Figure 6.41 B, p = 0.471 respectively) with S-glutathionylated protein consistently higher in females by 26% and 8% respectively (Figure 6.43 A, p = 0.122 and Figure 6.44 B, p = 0.905).

Genetic factors currently linked with AD pathology or possible treatment include Angiotensin converting enzyme (ACE), insulin regulated amino-peptidase (IRAP) and Alipoprotein E (APOE) genotypes and were correlated with hBCAT expression. In addition to this, family history of AD was also correlated with hBCAT expression as a positive family history is a predisposing factor to the disease (Lindsay *et al.*, 2002). The ACE protein converts angiotensin I to angiotensin II which constricts vessels but there is also evidence that the protein can cleave Aβ. The ACE genotype is separated into D (deletion) allele and I (insertion) allele, with I associated with a lower activity of the ACE protein and a higher risk of AD (Zhang *et al.*,
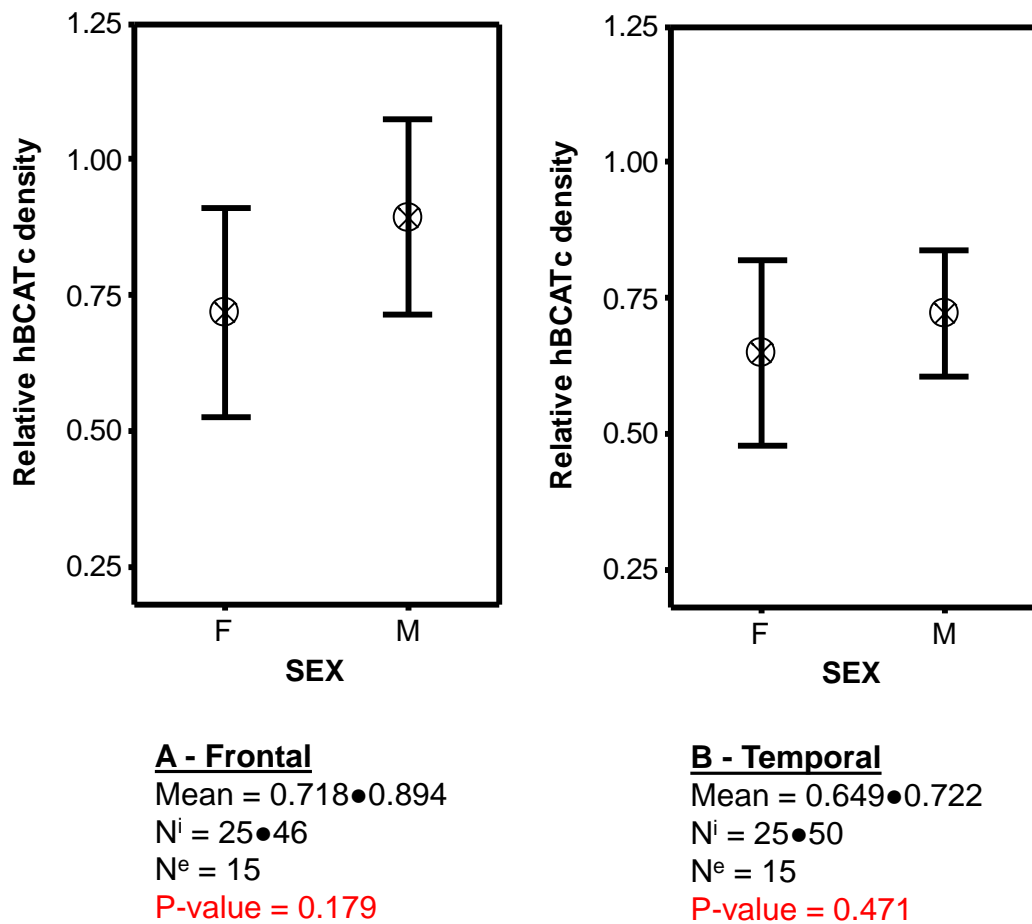
A - Frontal
Mean = 0.718●0.894
N^i = 25●46
N^e = 15
P-value = 0.179

B - Temporal
Mean = 0.649●0.722
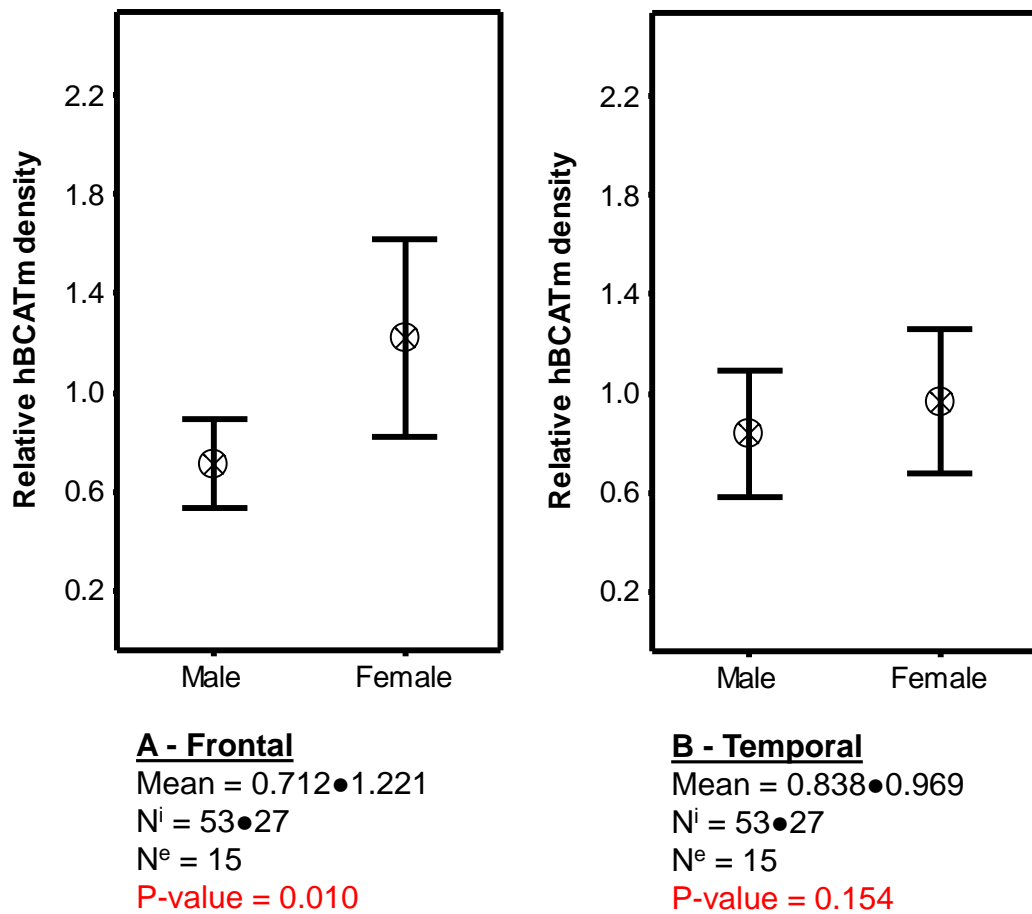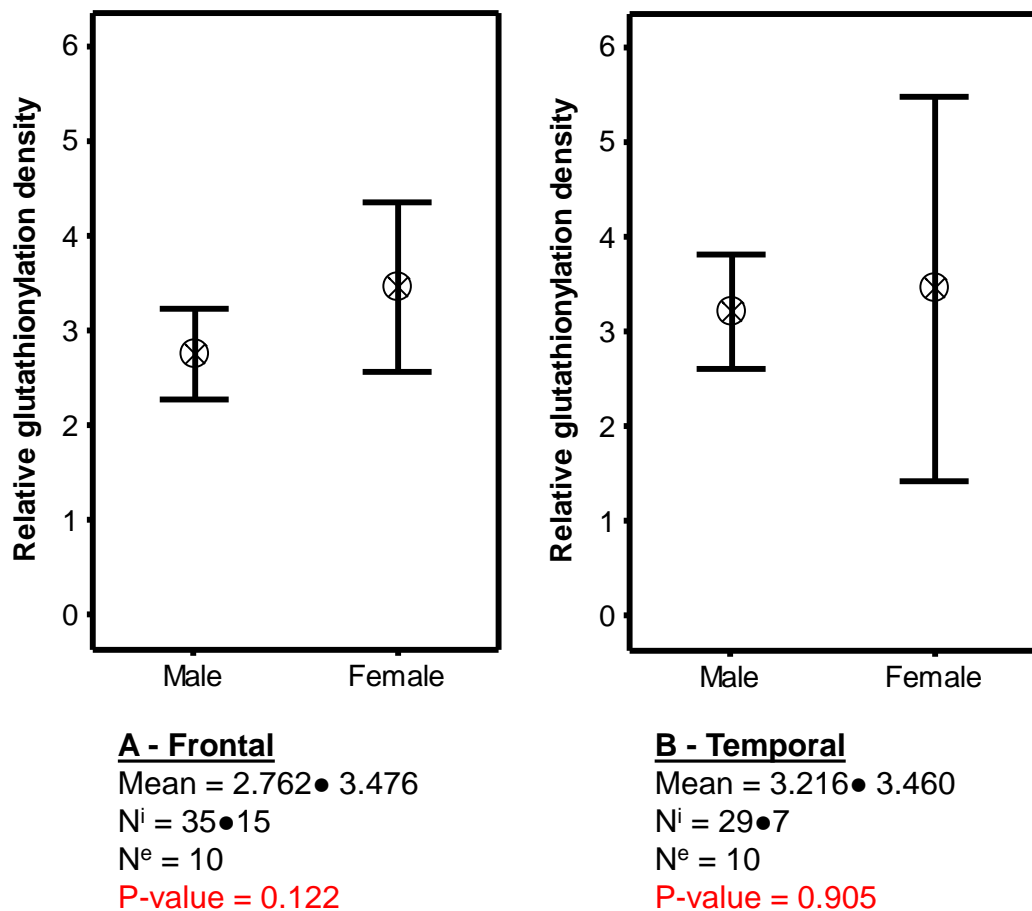N^i = 25●50
N^e = 15
P-value = 0.471

Figure 6. 41 Interval plot of frontal and temporal hBCATc protein levels in females compared to males. The density of bands were measured using ImageJ™ software (Wayne Rasband, National Institute of Health, USA) and expressed relative to the density for GAPDH. Data was then analysed for significance using an unpaired t-test in Minitab™.
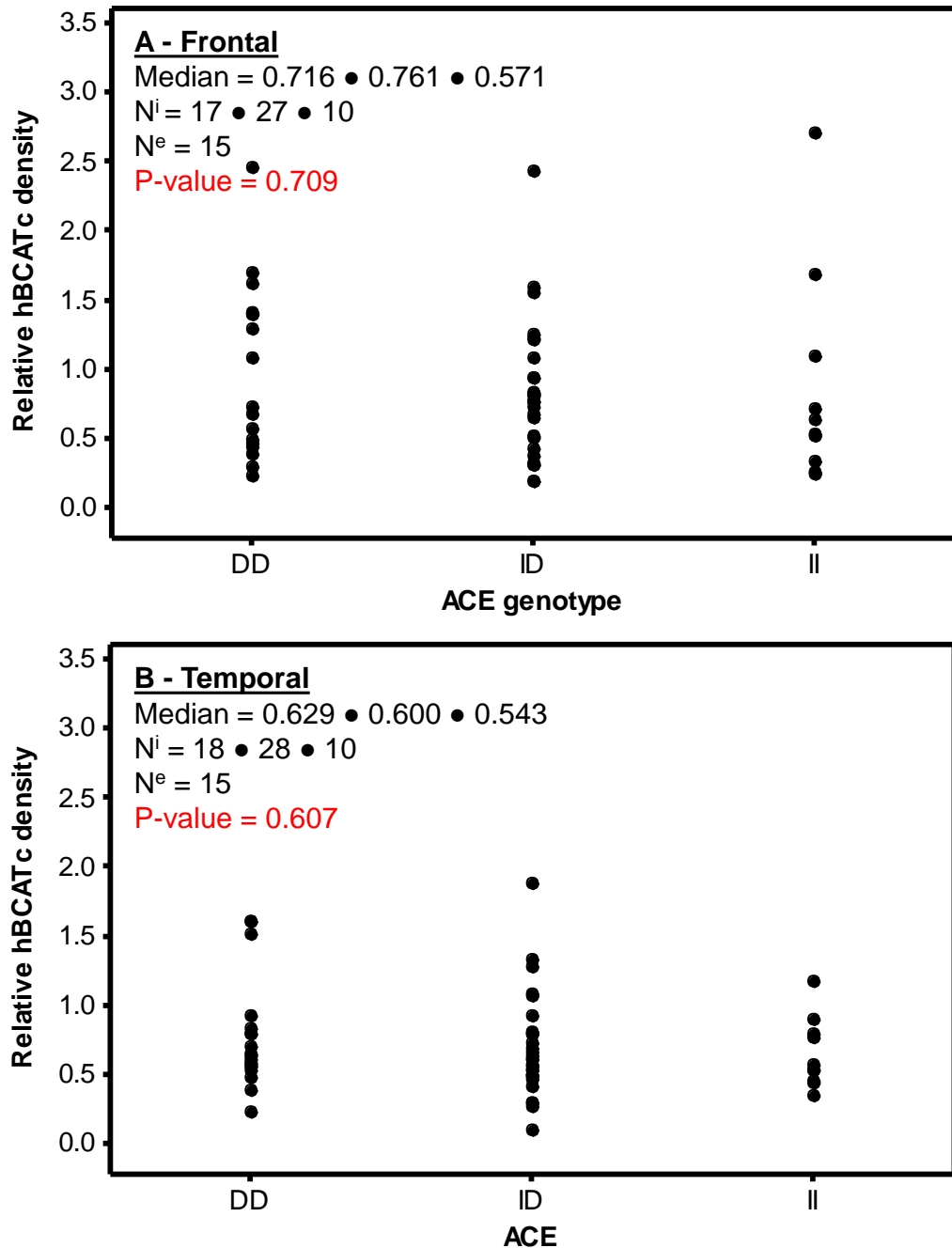
A - Frontal
Mean = 0.712●1.221
N^i = 53●27
N^e = 15
P-value = 0.010

B - Temporal
Mean = 0.838●0.969
N^i = 53●27
N^e = 15
P-value = 0.154

Figure 6. 42 Interval plot of frontal and temporal hBCATm protein levels in females compared to males. The density of bands were measured using ImageJ™ software (Wayne Rasband, National Institute of Health, USA) and expressed relative to the density for GAPDH. Data was then analysed for significance using an unpaired t-test in Minitab™.

A - Frontal
Mean = 2.762● 3.476
N^i = 35●15
N^e = 10
P-value = 0.122

B - Temporal
Mean = 3.216● 3.460
N^i = 29●7
N^e = 10
P-value = 0.905

Figure 6. 43 Interval plot of frontal and temporal glutathionylated protein levels in females compared to males. The density of lanes were measured using ImageJ™ software (Wayne Rasband, National Institute of Health, USA) and expressed relative to the density for GAPDH. Data was then analysed for significance using an unpaired t-test in Minitab™.

Figure 6. 44 Individual value plots of frontal and temporal hBCATc protein levels with ACE genotype. The density of bands were measured using ImageJ™ software (Wayne Rasband, National Institute of Health, USA) and expressed relative to the density for GAPDH. Data was then analysed for significance using Kruskal-wallis test in Minitab™. Abbreviations: ACE – angiotensin converting enzyme, D – absent ACE allele insertion, I – present ACE allele insertion.

2003). The inheritance of one I allele results in a 2.43 increased observed risk of AD (reviewed by Kehoe, 2003). It was however not associated with the variables considered in this study (Figure 6.44, Figure 6.45, Figure 11.8).

The IRAP gene codes for the insulin responsive aminopeptidase enzyme which was first described as a Glut4 vesicle marker protein. The IRAP proteins proposed function is to decrease the degradation of Glut4 (Abel *et al.*, 2004). So far no genotype of IRAP has been associated with AD; however the enzyme has been associated with improved cognition so the genotype may still be associated with AD mechanisms in the future (Chai *et al.*, 2004). However, this variable did not correlate with alteration in hBCATc, hBCATm or S-glutathionylated protein levels (Figure 6.46, Figure 6.47, Figure 11.9).

The APOE genotype has the clearest association with AD. With an observed risk of 3.98, the ε4 has the largest positive association with AD and the ε2 allele is considered protective (Corder *et al.*, 1994; Sadigh-Eteghad *et al.*, 2012). In the human population the frequency of the ε2, ε3 and ε4 alleles are 8.4%, 77.9% and 13.7% respectively, but in AD they are 3.9%, 59.4% and 36.7%, representing a strong ε4 association in AD (ε4ε4 genotype results in an increased observed risk of 14.9) (Farrer *et al.*, 1997). No effect of APOE genotype was observed except for one instance where APOE ε4ε4 genotype was associated with a higher expression of the hBCATm protein in the temporal cortex (Figure 6.49 A, $p = 0.047$) with the frontal cortex (Figure 6.49 B, $p = 0.230$) similarly increased (Figure 6.48, Figure 6.49, Figure 11.10).
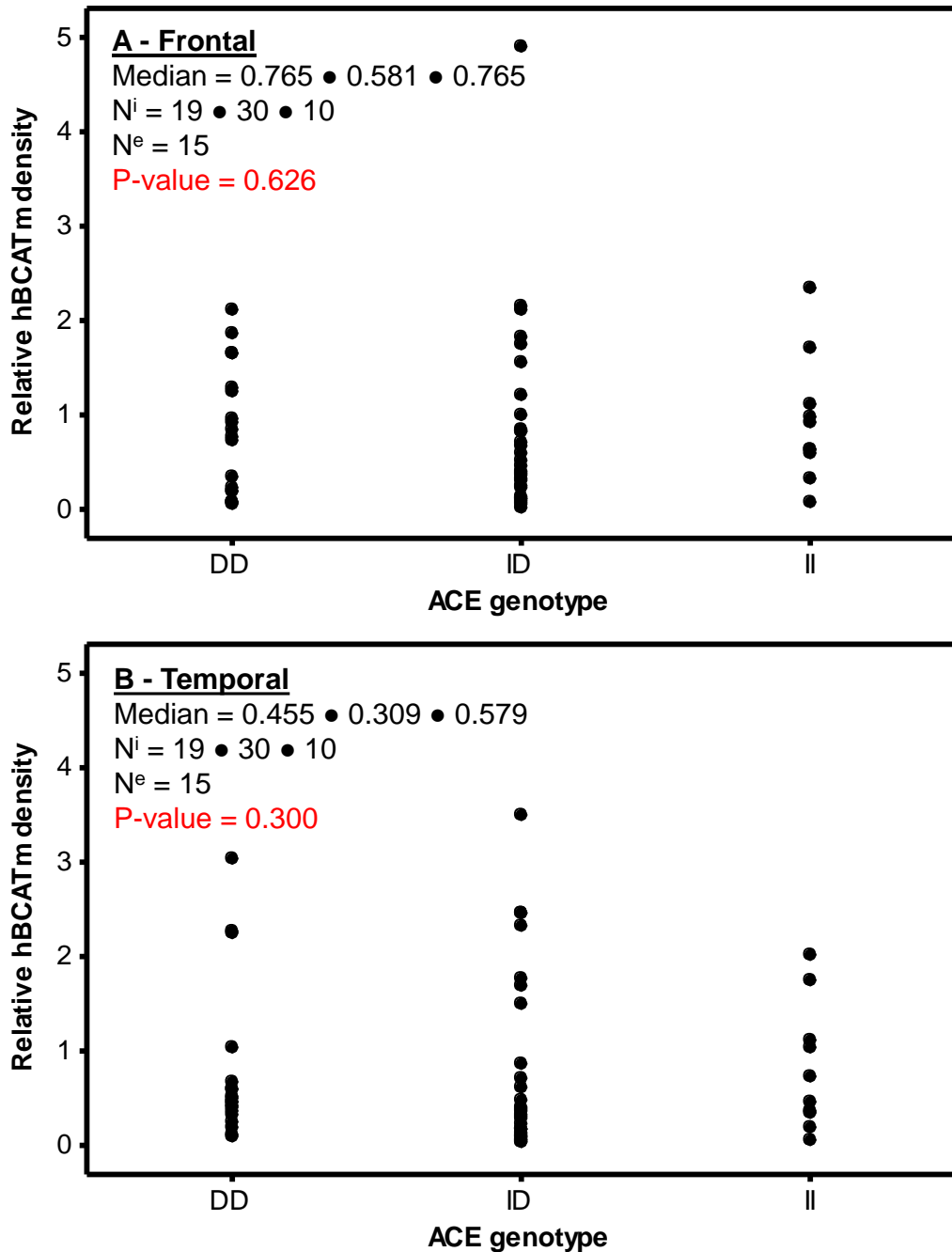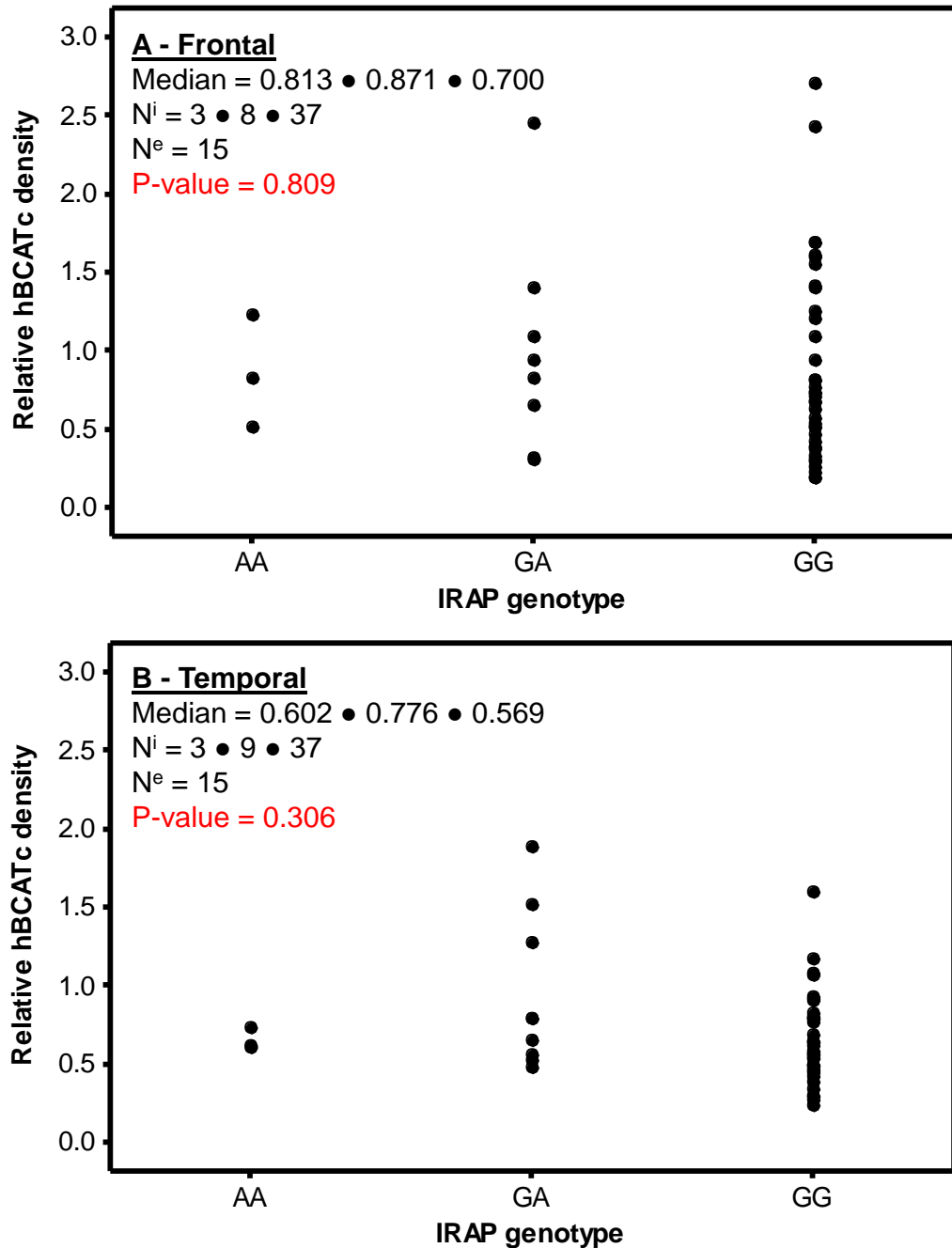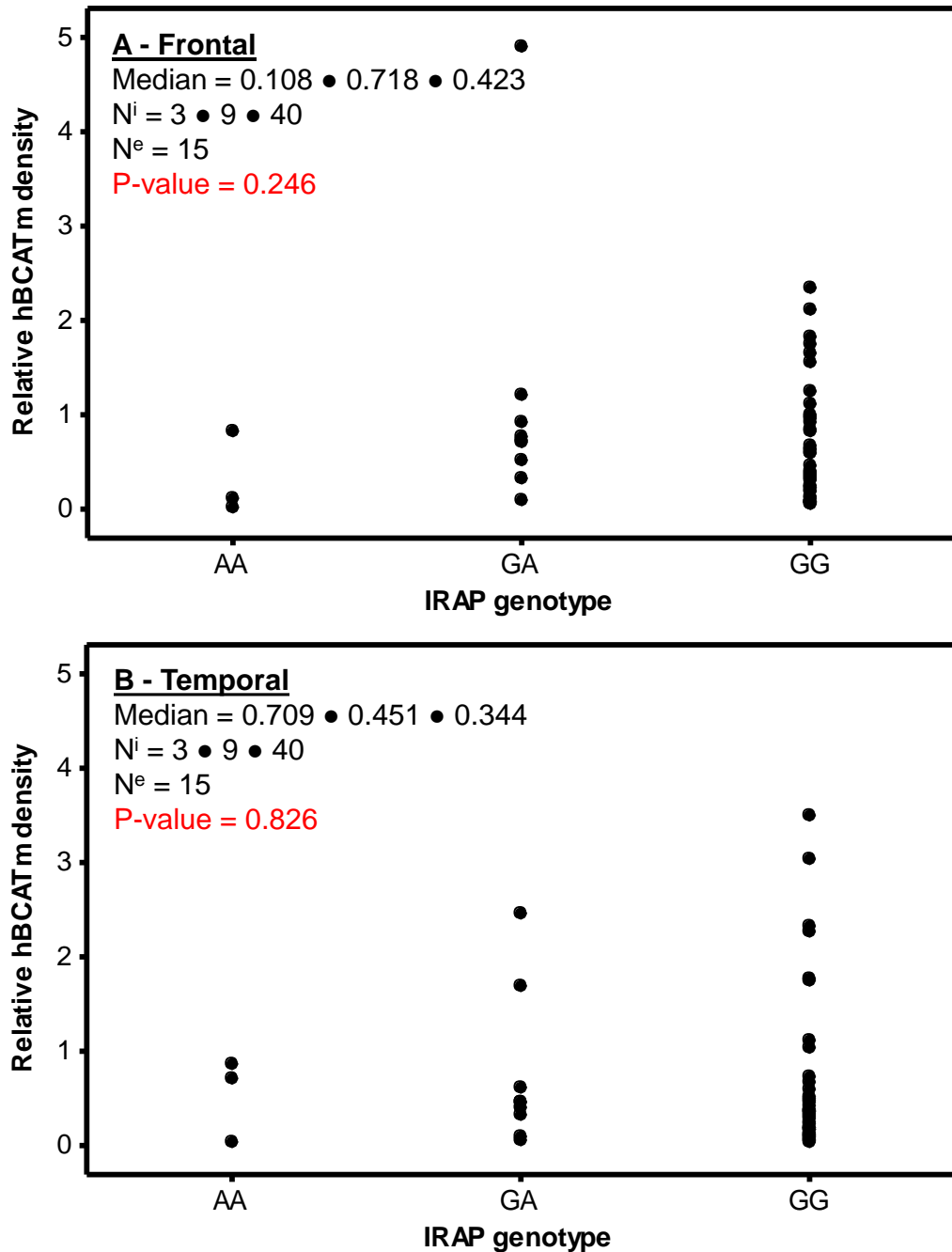
Figure 6. 45 Individual value plots of frontal and temporal hBCATm protein levels with ACE genotype. The density of bands were measured using ImageJ™ software (Wayne Rasband, National Institute of Health, USA) and expressed relative to the density for GAPDH. Data was then analysed for significance using Kruskal-wallis test in Minitab™. Abbreviations: ACE – angiotensin converting enzyme, D – absent ACE allele insertion, I – present ACE allele insertion.

Figure 6. 46 Individual value plots of frontal and temporal hBCATc protein levels with IRAP genotype. The density of bands were measured using ImageJ[TM] software (Wayne Rasband, National Institute of Health, USA) and expressed relative to the density for GAPDH. Data was then analysed for significance using Kruskal-wallis test in Minitab™. Abbreviations: A – A allele, G – G allele, IRAP – Insulin responsive aminopeptidase.
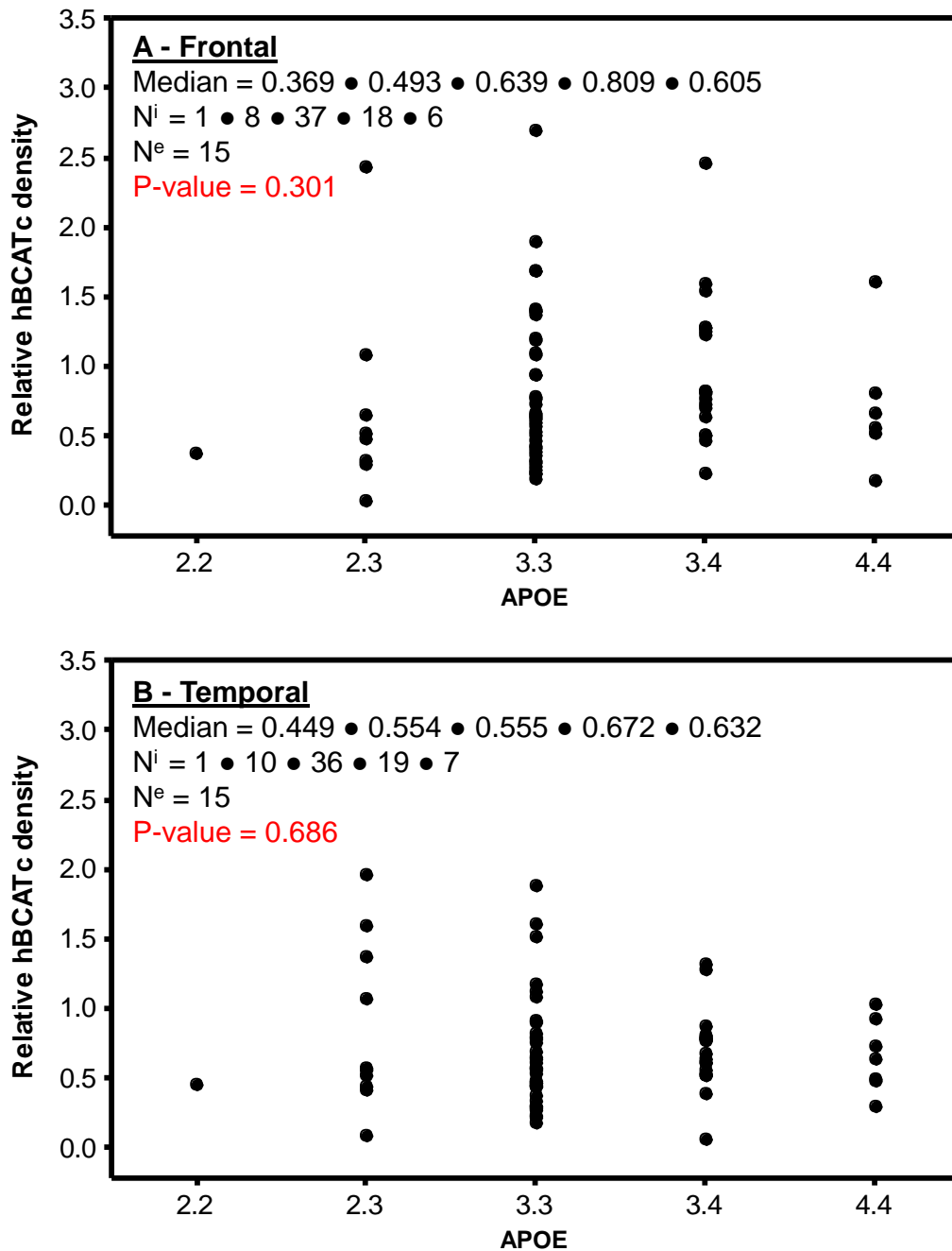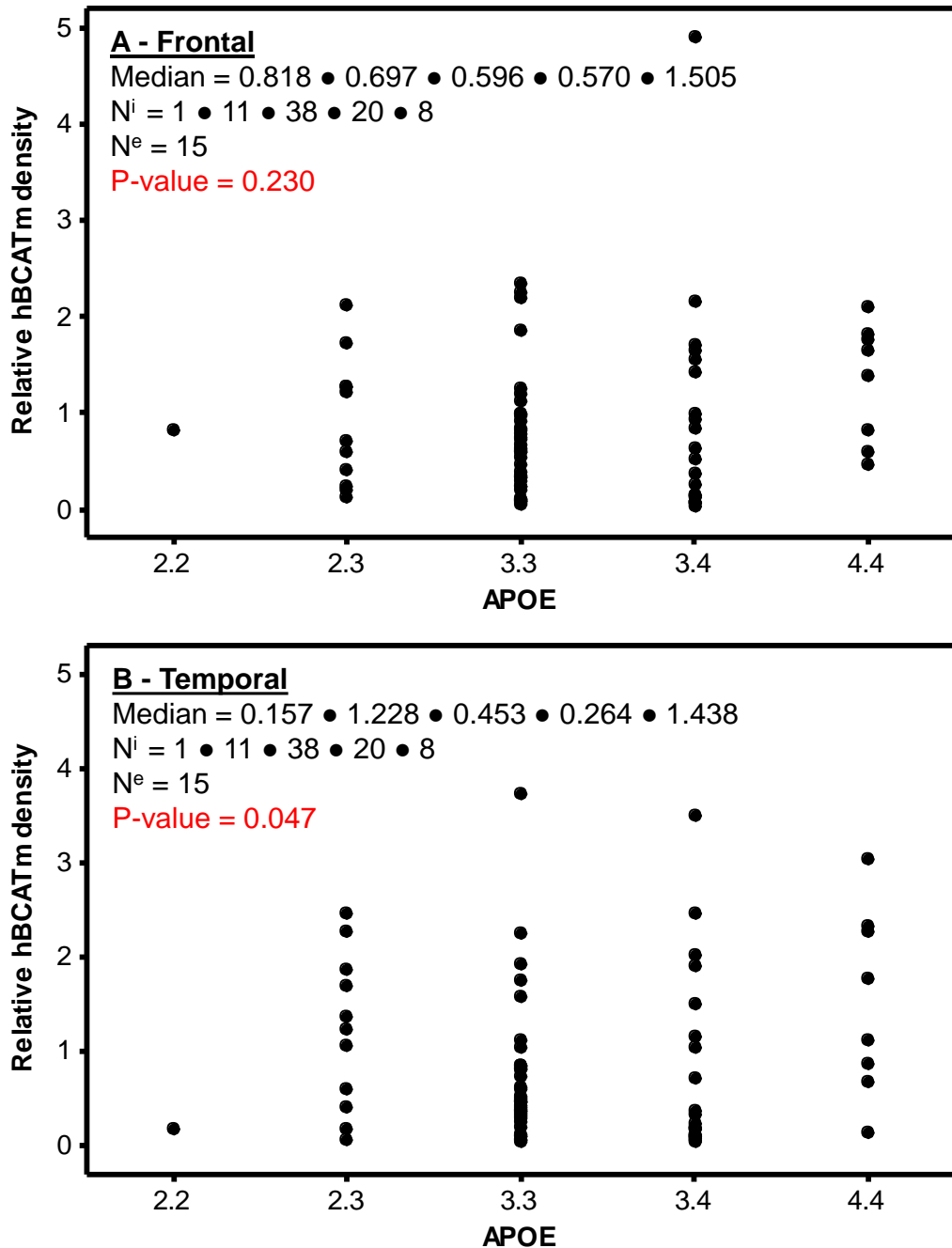
Figure 6. 47 Individual value plots of frontal and temporal hBCATm protein levels with IRAP genotype. The density of bands were measured using ImageJ™ software (Wayne Rasband, National Institute of Health, USA) and expressed relative to the density for GAPDH. Data was then analysed for significance using Kruskal-wallis test in Minitab™. Abbreviations: A – A allele, G – G allele, IRAP – Insulin responsive aminopeptidase.

Figure 6. 48 Individual value plots of frontal and temporal hBCATc protein levels with APOE genotype. The density of bands were measured using ImageJ™ software (Wayne Rasband, National Institute of Health, USA) and expressed relative to the density for GAPDH. Data was then analysed for significance using Kruskal-wallis test in Minitab™. Abbreviations: 2 – e2 allele, 3 – e3 allele, 4 – e4 allele, APOE – alipoprotein.

Figure 6. 49 Individual value plots of frontal and temporal hBCATm protein levels with APOE genotype. The density of bands were measured using ImageJ™ software (Wayne Rasband, National Institute of Health, USA) and expressed relative to the density for GAPDH. Data was then analysed for significance using Kruskal-wallis test in Minitab™. Abbreviations: 2 – e2 allele, 3 – e3 allele, 4 – e4 allele, APOE – alipoprotein.

Positive family history is another correlative factor of AD, with one first degree relative increasing the relative risk to 3.5 and two further increasing the relative risk to 7.5 (Van Duijn *et al.*, 1991). The role of family history was consistent, with frontal and temporal hBCATc protein levels non-significantly decreased by 25% and 11% respectively (Figure 11.11 A, p = 0.448 and Figure 11.11 B, p = 0.705 respectively) and hBCATm protein levels non-significantly decreased by 30% and 12% respectively (Figure 11.12 A, p = 0.133 and Figure 11.12 B, p = 0.372) in individuals without a family history of AD. These results suggest that the increased expression of hBCATm in AD is not predominantly caused by a genetic factor although some genetic characteristics appear to affect hBCATm.

6.2.6 Correlation of hBCATc, hBCATm and S-glutathionylated protein to key pathological features of AD

It was a sub-aim of specific aim 2 to correlate the hBCAT and S-glutathionylated protein levels with key features of AD. These features included Braak stage, disease duration, hyper phosphorylated tau average (%), soluble and insoluble Aβ, small vessel disease, perineuronal net and parvalbumin positive neurons. There was a small positive correlation between frontal hBCATc protein levels and Braak stage but this was not replicated within the temporal cortex and did not reach significance (Figure 6.50 A, p = 0.062, ρ +0.224 and Figure 6.50, p = 0.902, ρ +0.015 B respectively). However, there was a positive correlation of hBCATm concentration with increasing Braak stage in the frontal and temporal cortex (Figure 6.51 A, p = 1.2×10^{-5}, ρ +0.468 and Figure 6.51 B, p = 3.4×10^{-4},
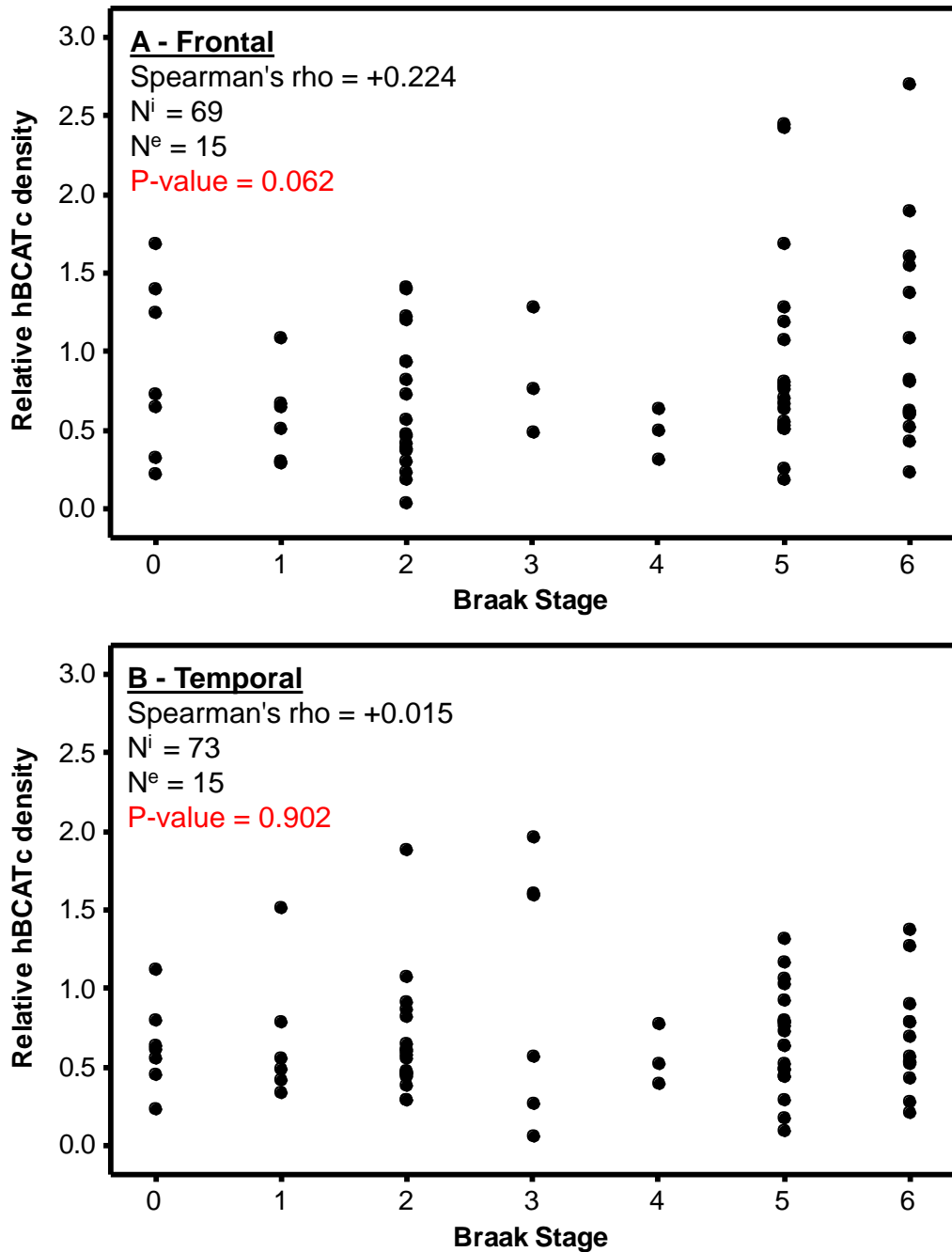
Figure 6. 50 Scatterplots of frontal and temporal hBCATc protein levels correlated with Braak stage. The density of bands were measured using ImageJ™ software (Wayne Rasband, National Institute of Health, USA) and expressed relative to the density for GAPDH. Data was then analysed for significance using Spearman's rho test in Minitab™.
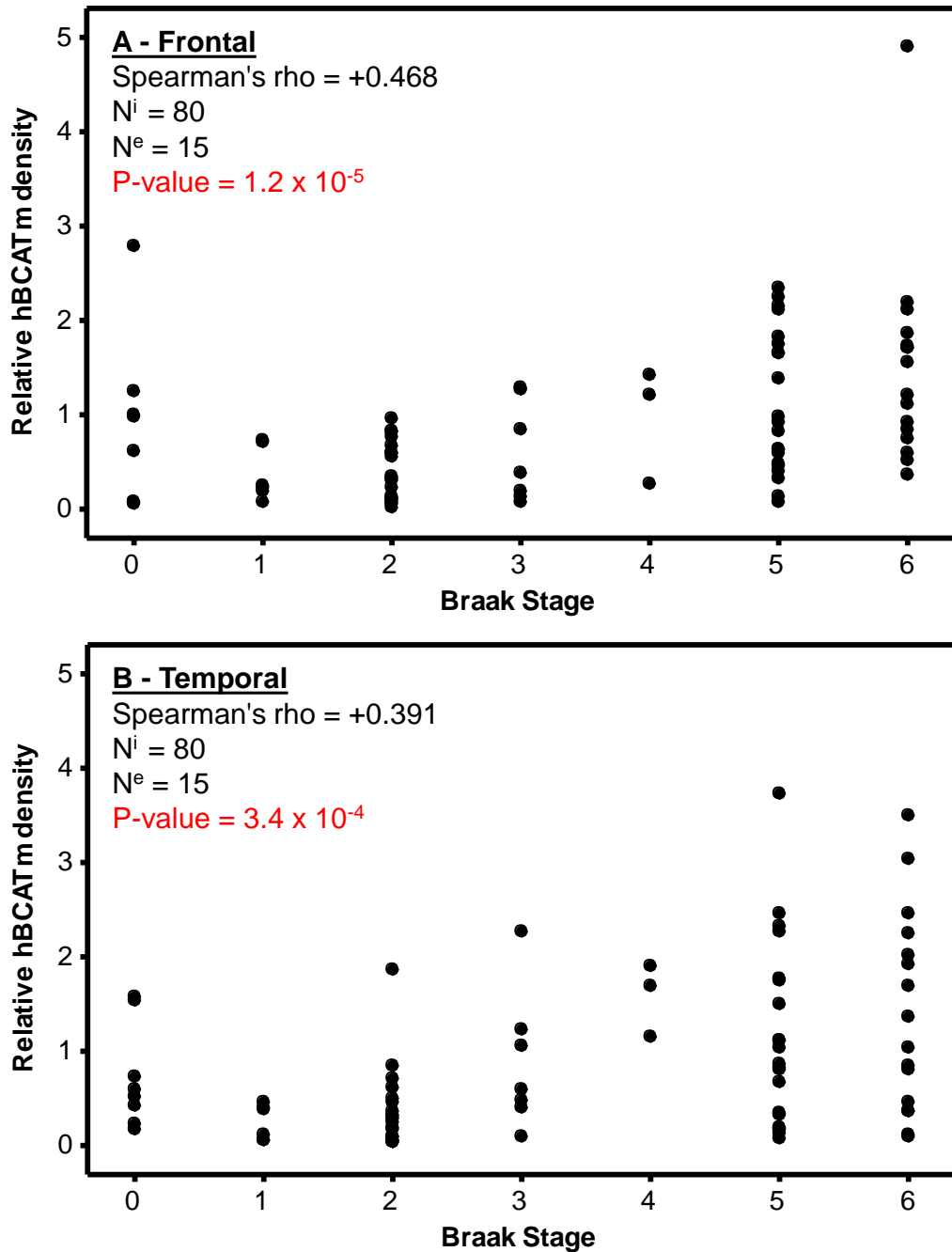
Figure 6. 51 Scatterplots of frontal and temporal hBCATm protein levels correlated with Braak stage. The density of bands were measured using ImageJ™ software (Wayne Rasband, National Institute of Health, USA) and expressed relative to the density for GAPDH. Data was then analysed for significance using Spearman's rho test in Minitab™.

ρ+0.391 respectively), and a decrease of S-glutathionylated protein (Figure 11.13 A, p = 0.038, ρ -0.351 and Figure 11.13 B, p = 0.147, ρ -0.237 respectively), rather than altered protein levels correlating with disease onset. However, no variable correlated to disease duration (Figure 11.14, Figure 11.15, Figure 11.16). Disease duration is difficult to account for due to the variable time of the diagnosis and the varied rate of progression of AD. It is therefore considered that Braak staging is a better estimation of disease progression.

Relating to AD pathology, it was observed that Tau (%) positively correlated with hBCATm in the frontal cortex (Figure 6.53 A, p = 0.029, ρ +0.405) but not with other variables (Figure 6.52, Figure 6.53, Figure 11.17). Other key pathological events in AD, such as the production of soluble and insoluble Aβ, also correlated (at least partially) with hBCATm expression but not hBCATc (except in one instance) or S-glutathionylated protein levels (Figure 6.54, Figure 6.55, Figure 11.18, Figure 6.56, Figure 6.57, Figure 11.19). Expression of hBCATm in the frontal and temporal cortex positively correlated with both soluble (Figure 6.55 A, p = 0.355, ρ +0.193 and Figure 6.55 B, p = 0.042, ρ+0.409 respectively) and insoluble amyloid (Figure 6.57 A, p = 0.0023, ρ +0.506 and Figure 6.57 B, p = 0.248, ρ +0.203 respectively). Expression of hBCATc was only observed to correlate in the frontal cortex with soluble Aβ (Figure 6.54 A, p = 0.024, ρ -0.434).

Small vessel disease score is (similar to Braak stage) a progressing system (0-III) to measure disease of the small vessels. This is not unique to AD and
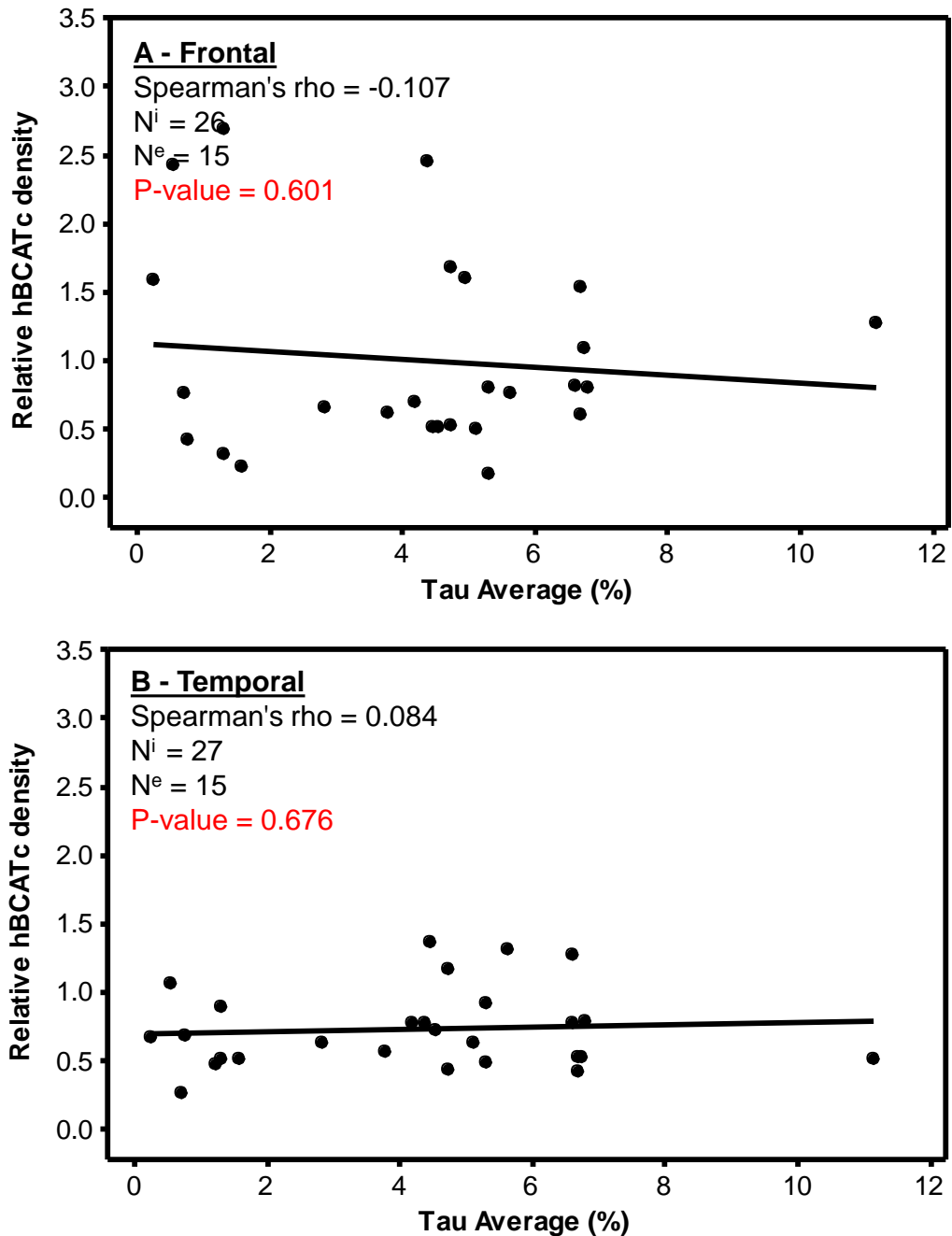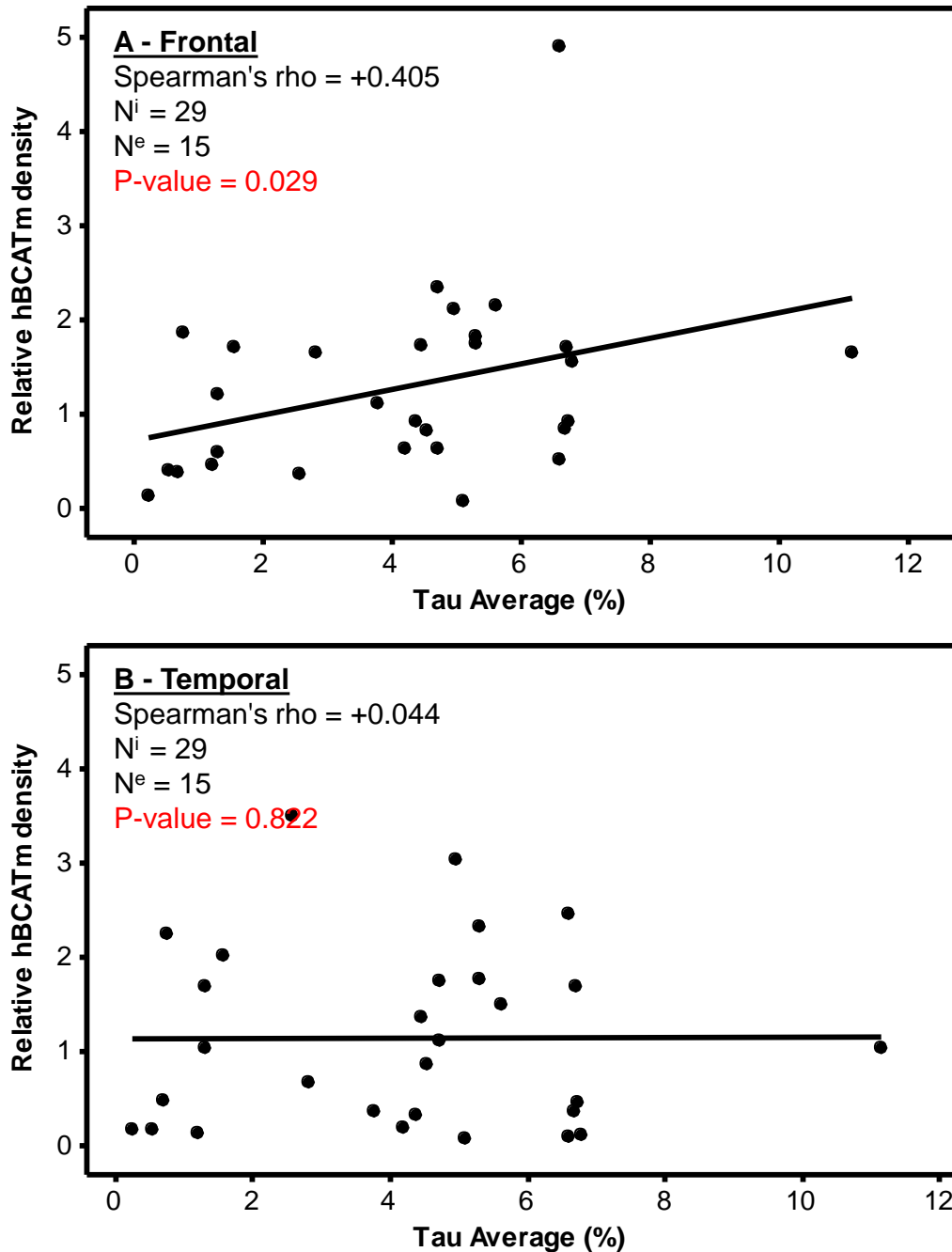
Figure 6. 52 Scatterplots of frontal and temporal hBCATc protein levels correlated with Tau average (%). The density of bands were measured using ImageJ[TM] software (Wayne Rasband, National Institute of Health, USA) and expressed relative to the density for GAPDH. Hyper phosphorylated tau average (%) was calculated using Histometrix software, driving a Leica microscope with a motorized stage, as the percentage area of cerebral cortex (measured in the temporal lobe) immunopositive for hyper phosphorylated tau (BR03, Autogen Bioclear). Data was then analysed for significance using Spearman's rho test in Minitab™.
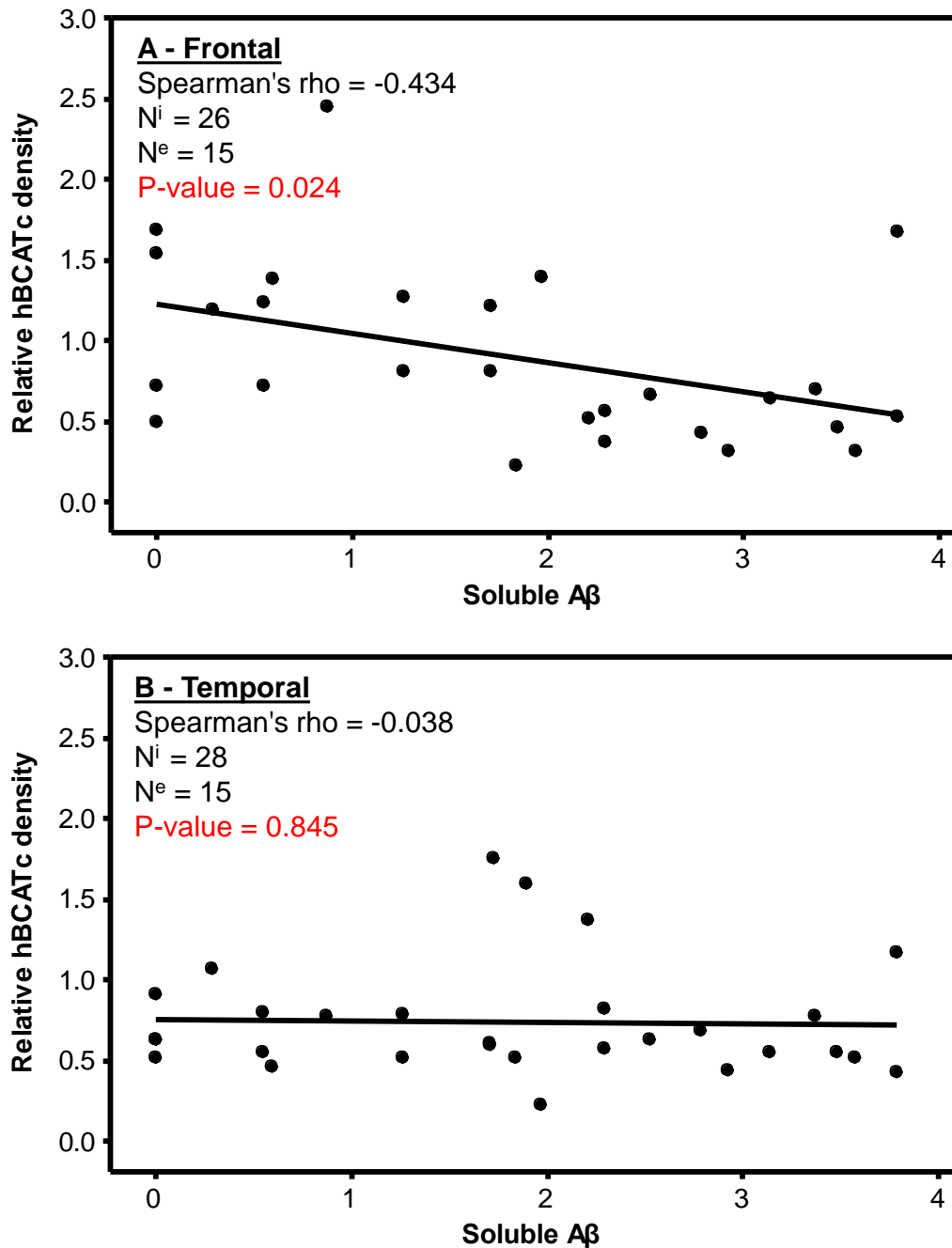
Figure 6. 53 Scatterplots of frontal and temporal hBCATm protein levels correlated with Tau average (%). The density of bands were measured using ImageJ[TM] software (Wayne Rasband, National Institute of Health, USA) and expressed relative to the density for GAPDH. Hyper phosphorylated tau average (%) was calculated using Histometrix software, driving a Leica microscope with a motorized stage, as the percentage area of cerebral cortex (measured in the temporal lobe) immunopositive for hyper phosphorylated tau (BR03, Autogen Bioclear). Data was then analysed for significance using Spearman's rho test in Minitab™.

Figure 6. 54 Scatterplots of frontal and temporal hBCATc protein levels correlated with soluble Aβ. The density of bands were measured using ImageJ™ software (Wayne Rasband, National Institute of Health, USA) and expressed relative to the density for GAPDH. Soluble Aβ was measured by sandwich ELISA on frontal homogenate extract that was soluble in detergent (1% NP-40). Data was then analysed for significance using Spearman's rho test in Minitab™.
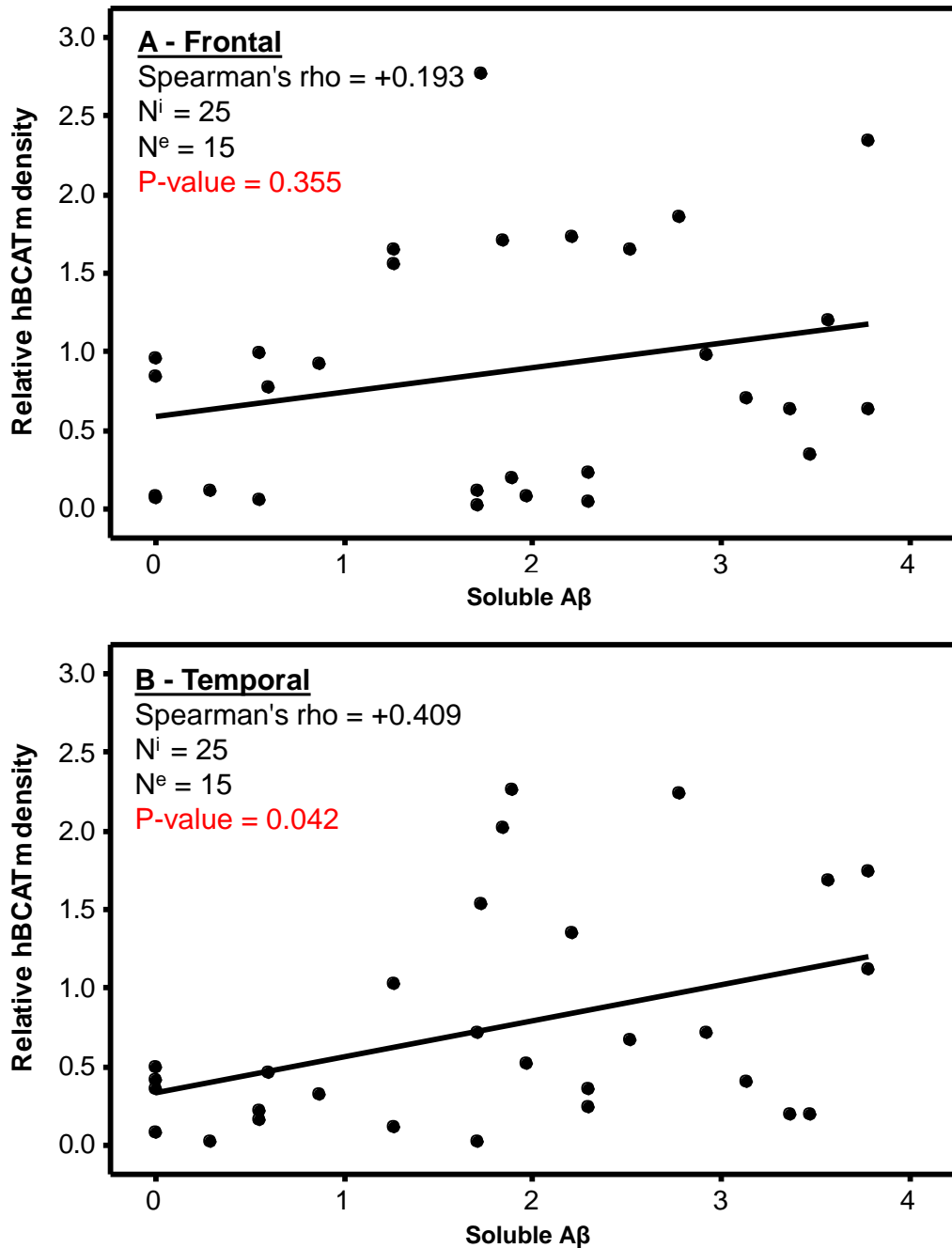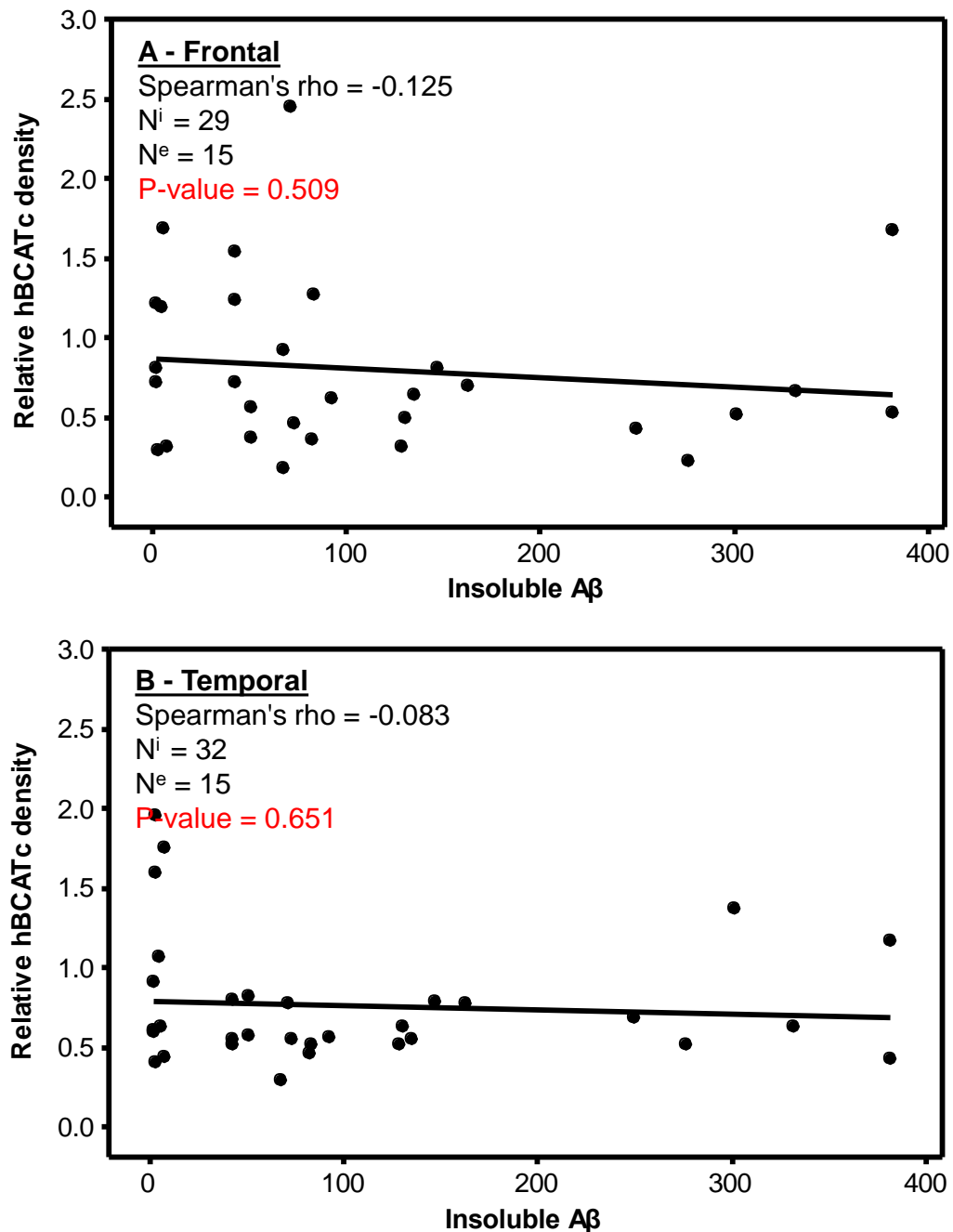
Figure 6. 55 Scatterplots of frontal and temporal hBCATm protein levels correlated with soluble Aβ. The density of bands were measured using ImageJ™ software (Wayne Rasband, National Institute of Health, USA) and expressed relative to the density for GAPDH. Soluble Aβ was measured by sandwich ELISA on frontal homogenate extract that was soluble in detergent (1% NP-40). Data was then analysed for significance using Spearman's rho test in Minitab™.

Figure 6. 56 Scatterplots of frontal and temporal hBCATc protein levels correlated with insoluble Aβ. The density of bands were measured using ImageJ™ software (Wayne Rasband, National Institute of Health, USA) and expressed relative to the density for GAPDH. Insoluble Aβ was measured by sandwich ELISA on frontal homogenate extract that was insoluble in detergent (1% NP-40), but was soluble upon guanidine HCl extraction. Data was then analysed for significance using Spearman's rho test in Minitab™.
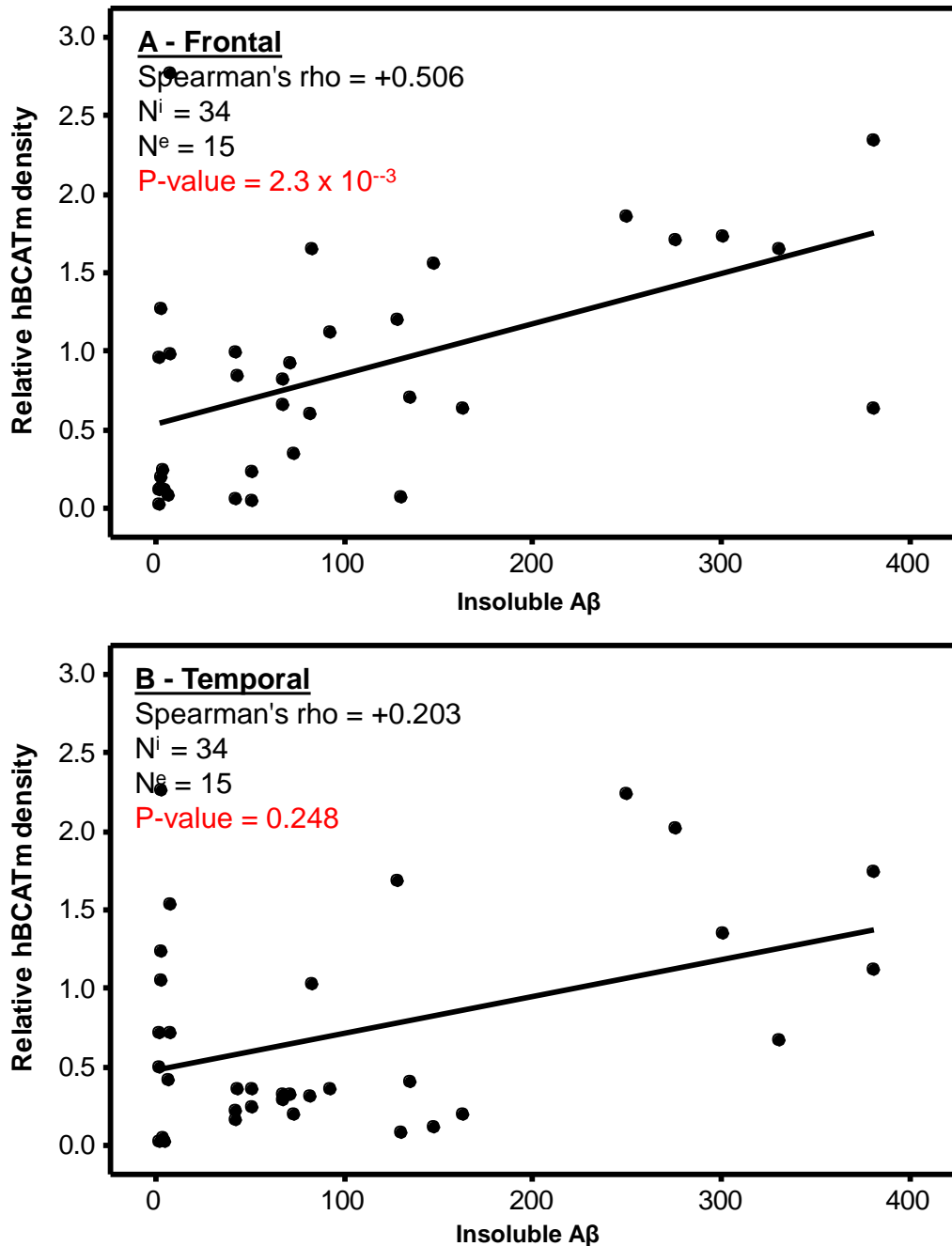
Figure 6. 57 Scatterplots of frontal and temporal hBCATm protein levels correlated with insoluble Aβ. The density of bands were measured using ImageJ™ software (Wayne Rasband, National Institute of Health, USA) and expressed relative to the density for GAPDH. Insoluble Aβ was measured by sandwich ELISA on frontal homogenate extract that was insoluble in detergent (1% NP-40), but was soluble upon guanidine HCl extraction. Data was then analysed for significance using Spearman's rho test in Minitab™.

occurs in other diseases such as vascular dementia. Small vessel disease score positively correlated with frontal and temporal hBCATm (Figure 6.59 A, p = 0.154, ρ +0.239 and Figure 6.59 B, p = 0.019, ρ +0.353 respectively) but no other variables (Figure 6.58, Figure 6.60), despite hBCATm not solely restricted to the smaller vessels. Finally, despite the fact that perineuronal net and parvalbumin positive neurons are decreased in AD no variable correlated with either (Baig *et al.*, 2005; Satoh *et al.*, 1991) (Figure 11.20, Figure 11.21, Figure 11.22).

In summary, this work demonstrates increased hBCATm expression in the frontal and temporal cortex of AD compared to matched controls. This increased expression was localised to the vasculature, with an additional increase in hBCATc in hippocampal neurons also observed. Levels of S-glutathionylated proteins were observed to be decreased in AD compared to matched controls. It is expected that this related to an increased oxidative stress and a decreased presence of free S-glutathione occurring in diseased tissue. The effect of genetics on variables studied demonstrated singular significance in the APOE genotype (increase hBCATm expression associated with ε4ε4 genotype). By far the strongest correlative factor for hBCATm expression was Braak staging, with soluble Aβ, insoluble Aβ, small vessel disease score and tau (%) also strongly correlating. These results suggest that hBCATm expression is correlating with the pathology of the disease, rather than the onset of the symptoms. It is already known that alterations to the vasculature are early events in dementia pathology but this

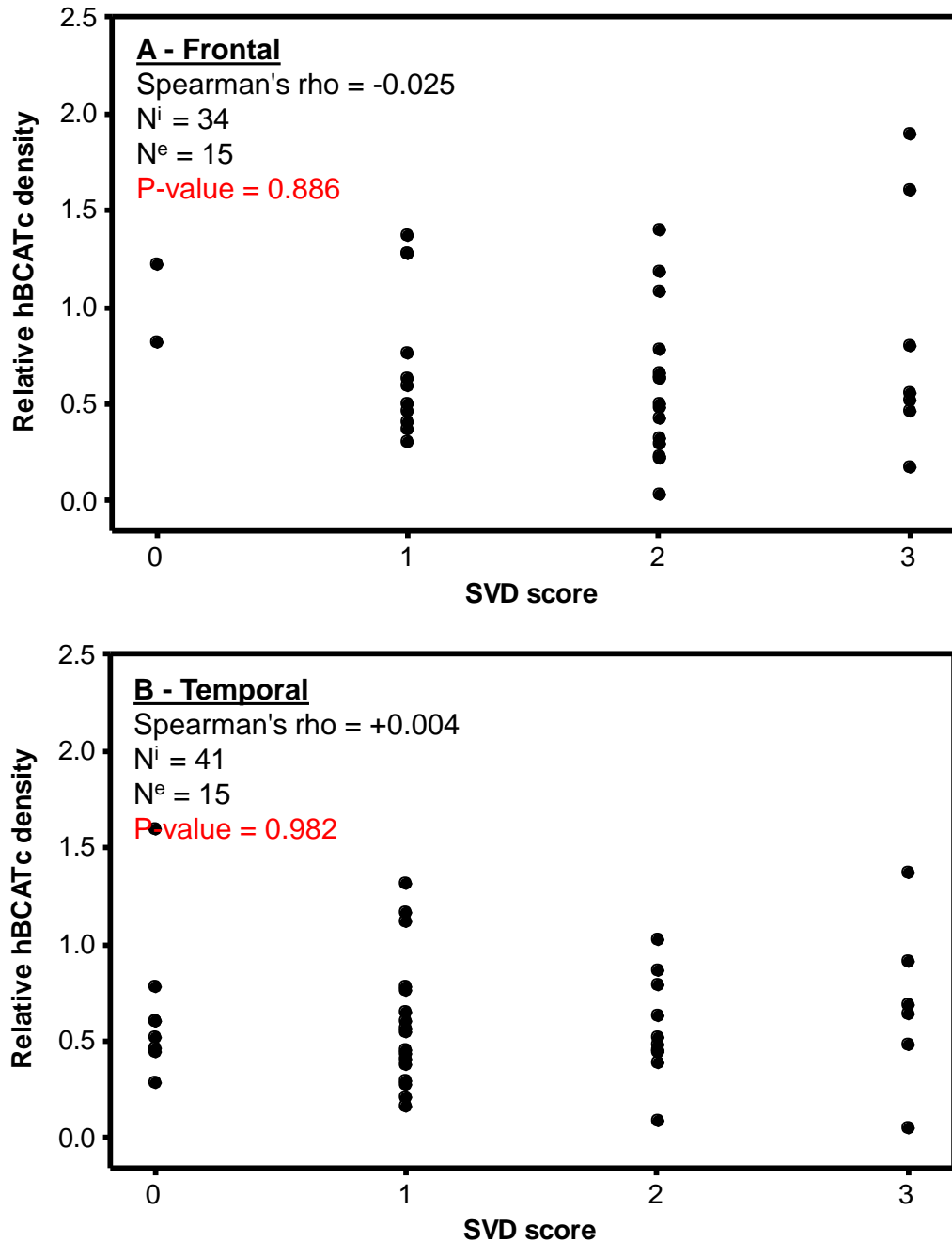work also suggests a possible role for BCAA and glutamate metabolism (reviewed by Torre, 2004).

Figure 6. 58 Scatterplots of frontal and temporal hBCATc protein levels correlated with small vessel disease (SVD) score. The density of bands were measured using ImageJ™ software (Wayne Rasband, National Institute of Health, USA) and expressed relative to the density for GAPDH. Data was then analysed for significance using Spearman's rho test in Minitab™. Abbreviations: SVD – small vessel disease.
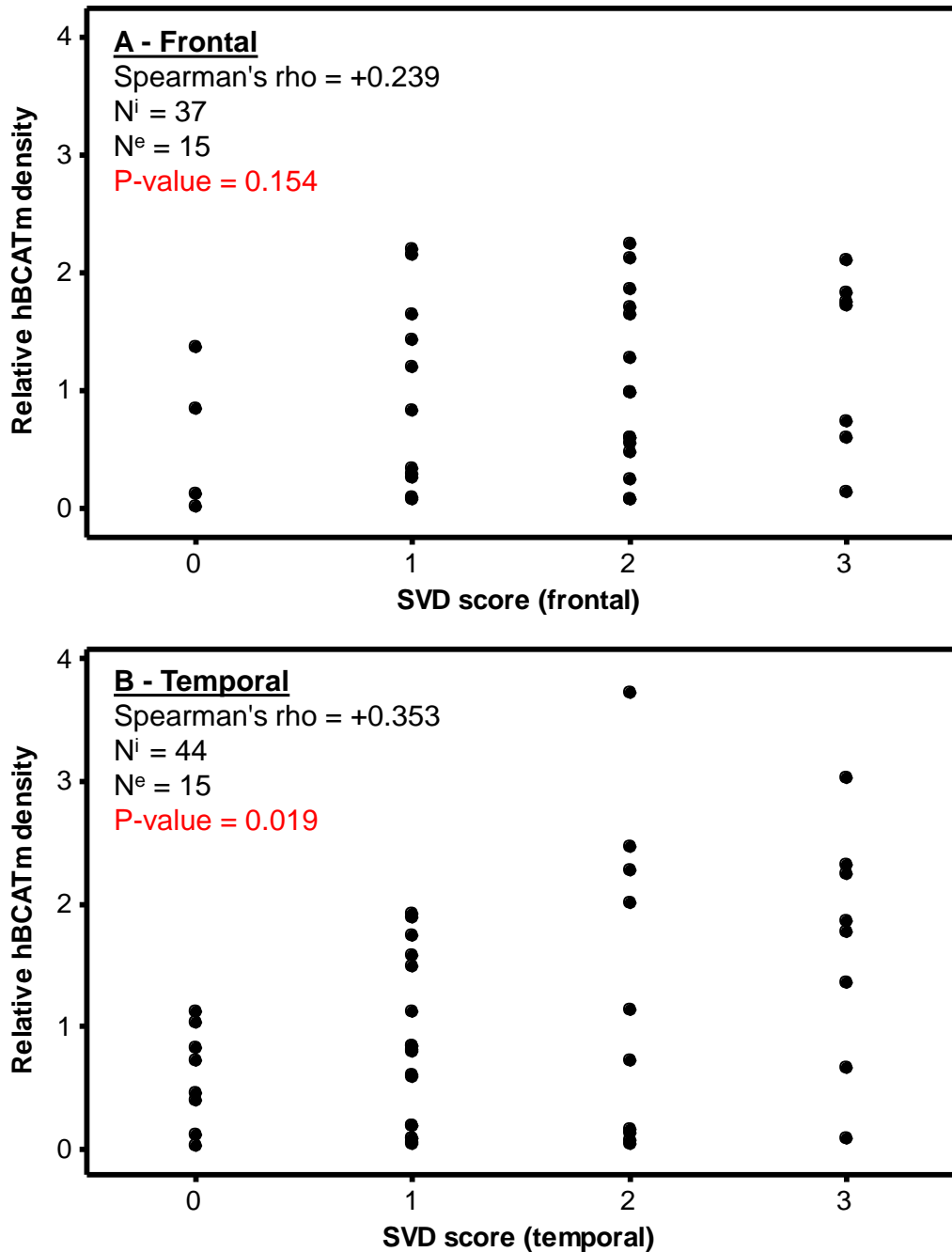
Figure 6. 59 Scatterplots of frontal and temporal hBCATm protein levels correlated with small vessel disease (SVD) score. The density of bands were measured using ImageJ™ software (Wayne Rasband, National Institute of Health, USA) and expressed relative to the density for GAPDH. Data was then analysed for significance using Spearman's rho test in Minitab™. Abbreviations: SVD – small vessel disease.
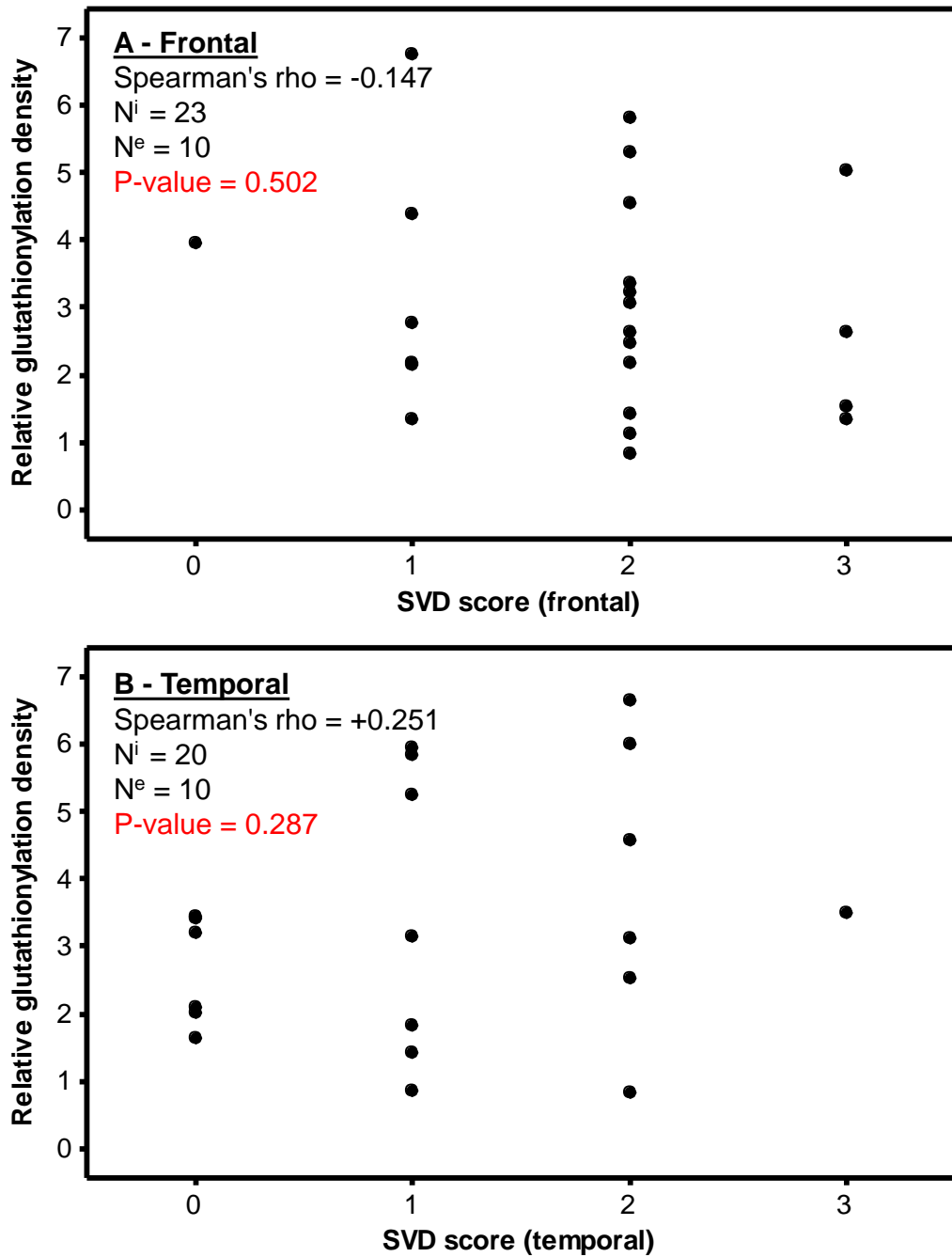
Figure 6. 60 Scatterplots of frontal and temporal glutathionylated protein levels correlated with small vessel disease (SVD) score. The density of lanes were measured using ImageJ™ software (Wayne Rasband, National Institute of Health, USA) and expressed relative to the density for GAPDH. Data was then analysed for significance using Spearman's rho test in Minitab™. Abbreviations: SVD – small vessel disease.

6.3 Functional analysis of hBCAT in the neuroblastoma cell line IMR32

Increased hBCAT expression could potentially lead to an increase in metabolites such as leucine, glutamate, or BCKAs. The human neuroblastoma cell line IMR32 were incubated in a time and concentration dependant manner to observe the effect of metabolites on cell morphology and viability. Previous work has demonstrated hBCATc association with a cell surface receptor protein (sodium channel type 10 α-subunit) therefore a method for flow cytometry analysis was developed and demonstrated cell surface expression of hBCATc (Coles *et al.*, 2009). This was further investigated with regards to receptor function. Finally, an hBCAT radioactivity assay was developed for cultured cells and this was compared with results obtained via Western blot analysis.

6.3.1 Neuroblastoma cell line IMR32 is sensitive to glutamate and KIC

Glutamate is the major excitatory neurotransmitter of the human brain and has a vital role in learning and memory. The concentration of glutamate within the human brain is 5-15 mM with the vast majority localised at nerve terminals inside synaptic vesicles. The extracellular concentration is much lower (3-4 μM) with signalling concentrations usually less than 1 mM (Danbolt, 2001). Ketoisocaproate is the keto acid of leucine when metabolised by BCAT. Concentrations of KIC are usually less than 1 mM, but capable of reaching 10 mM in MSUD (Tavares *et al.*, 2000; Zielke *et al.*, 1997). Cells were treated with toxic levels of both glutamate and KIC to determine the morphological effects of glutamate and KIC on the IMR32

cells, and phase-contrast microscopy was used to morphologically examine cell treatments.

It was examined if the toxicity of glutamate (at 12 mM) was impacted by the metabolic environment. Decreasing serum from 20% to 10% or 0% in the media had a detrimental effect on IMR32 cell number and morphology, as did the addition of 2 mM glutamine (Figure 6.61 A-D). However, the use of EMEM over RPMI demonstrated little effect on overall cell morphology with 12 mM glutamate insult (Figure 6.61 E). The effect of varying concentrations of KIC was measured over time on IMR32 cell morphology and at 4 mM KIC a growth inhibitory effect was observed at 24 and 72 hours (Figure 6.62 A+B), with 8 and 12 mM concentrations causing significant deleterious effects to cell morphology and number (Figure 6.62 C+D).

Even modestly uncontrolled MSUD can lead to increased BCKA concentration (similar to that observed in this work), long term neurological impairment and reduced IQ scores. Likewise, stroke and other neuronal cell death events can subject the surrounding tissue to large amounts of pooled glutamate (up to 12 mM). The fact that glutamate toxicity is ameliorated with serum concentrations of 10 and 20%, and exacerbated with the presence of 2 mM glutamine implies that glutamate is directly toxic but other factors define the full effect. For example, the detrimental effect of 2 mM glutamine can be attributed to the decreased capacity to convert glutamate to the (relatively) physiologically inert glutamine within the cell through enzymes
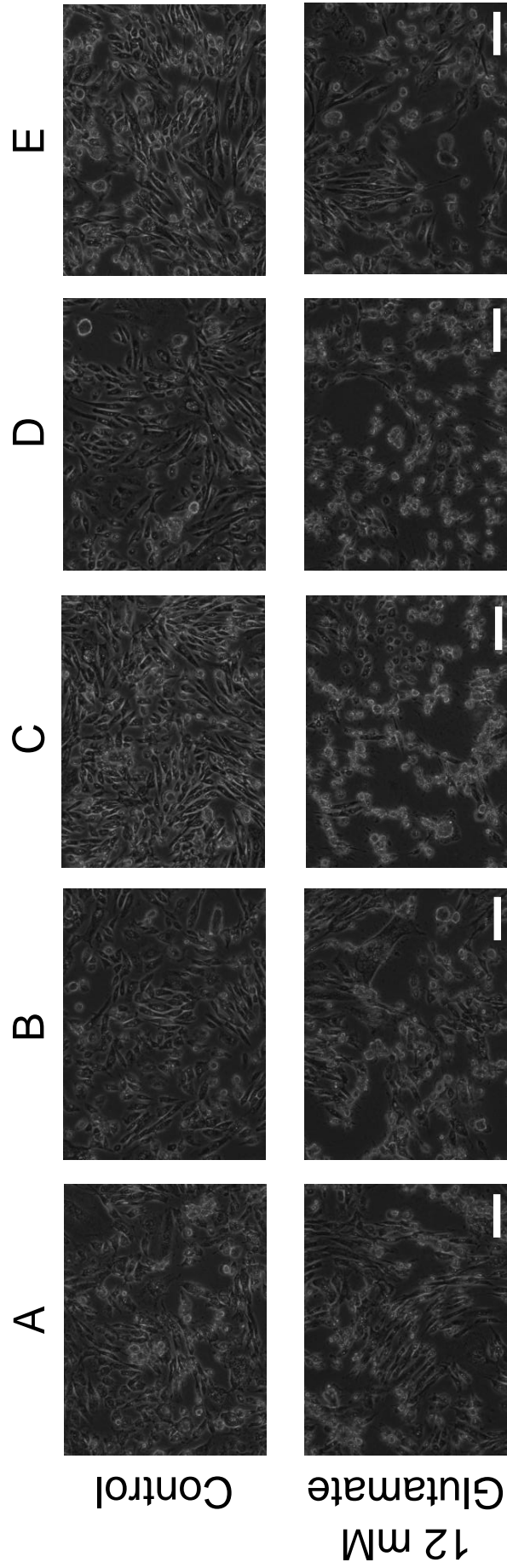
Figure 6. 61 The effect of 12 hour 12 mM glutamate treatment on cell morphology of the IMR32 cells in different media (n^e = 2). Treatment A: RPMI 1640 + 20% foetal calf serum + 1x RPMI amino acid solution + 1x pen/strep solution, Treatment B: RPMI 1640 + 10% foetal calf serum + 1x RPMI amino acid solution + 1x pen/strep solution, Treatment C: RPMI 1640 + 1x RPMI amino acid solution + 1x pen/strep, Treatment D: treatment C + 2 mM glutamine solution, Treatment E: EMEM + 10% foetal calf serum + 2 mM glutamine solution. Cells were equally loaded in each well of a 6 well plate. Images were acquired using a TE300 microscope. Images used are representative. Abbreviations: EMEM – Eagle's minimal essential medium, pen/strep – Penicillin/streptomycin, RPMI – Roswell park memorial institute. Magnifications: x10. Scale bars: 100 µm.
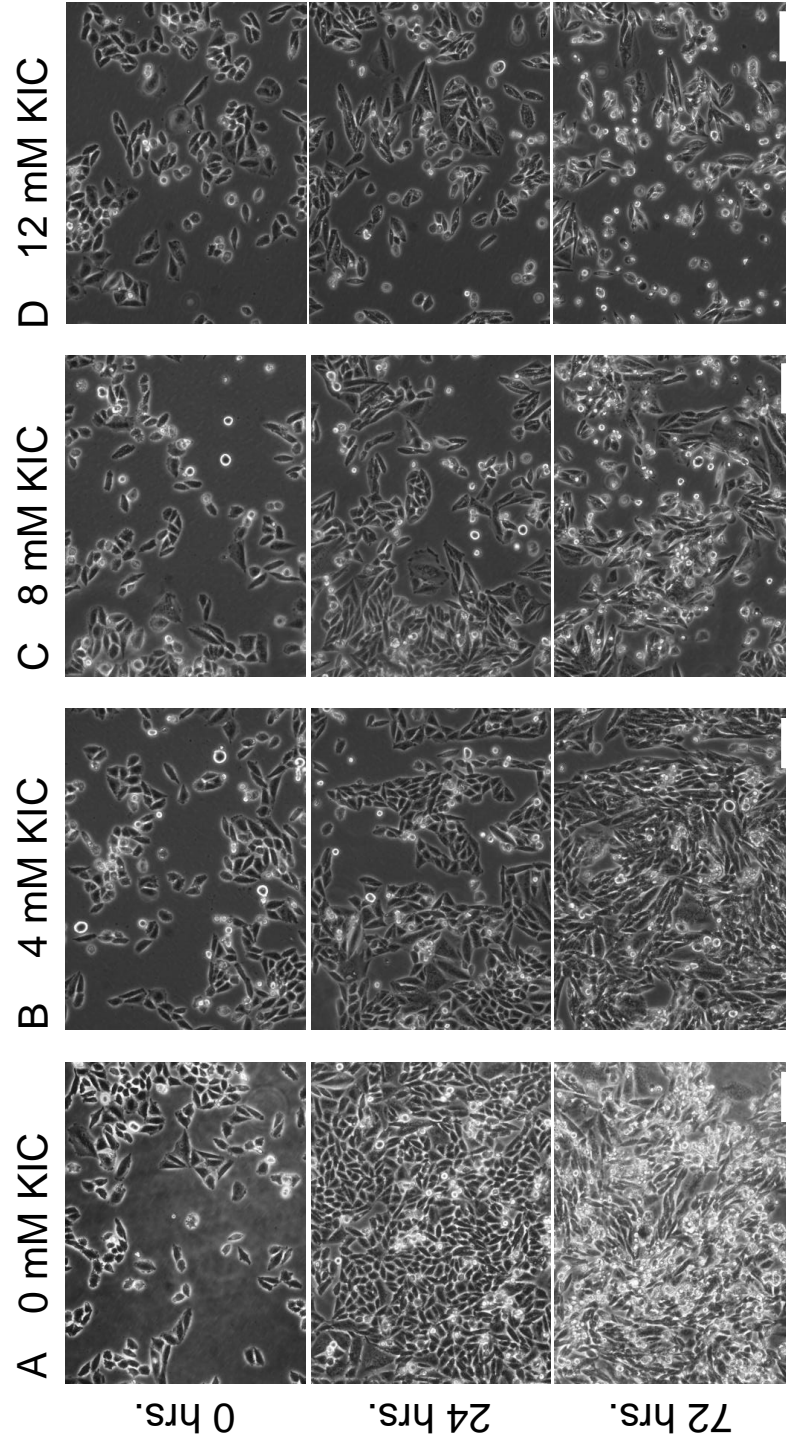
Figure 6. 62 The effect of KIC on IMR32 cell morphology and growth (n^e = 2). IMR32 cells were treated with increasing concentrations of KIC and imaged at increasing time points. Images were acquired using a TE300 microscope. Magnifications: x10. Scale bars: 100 μm. Abbreviations: KIC – Ketoisocaproate.

such as glutaminase. Serum likely protects cells by the sequestration of glutamate or promotes cell survival via growth factors.

6.3.2 Investigation of IMR32 cell line differentiation

Human IMR32 cells are adherent neuroblast cells derived from a 13 month old Caucasian neuroblastoma (Tumilowicz *et al.*, 1970). These cells are thus undifferentiated and not truly neuronal cells. Therefore, cellular differentiation of the IMR32 neuroblastoma cell line was investigated for the best morphological and expressional characteristic of the hBCATc protein. In the undifferentiated state IMR32 cells do not possess neuronal morphology; they also have an altered expression of hBCATc – with the presence of an additional undefined 35 kDa band likely the product of a splice variant. Phase-contrast microscopy was again used to determine the best morphological differentiation of five commonly used differentiation treatments and Western blot was used for expressional analysis.

Treatments such as 1 mM dibutyryl cAMP + 10 µg/mL Papaverine and 1 mM dibutyryl cAMP + 4 µM 5-bromo-2'-deoxyurisine (in the serum deprived medium) caused substantial neuronal loss (Figure 6.63 A+E1). The differentiation in media containing FCS had a larger cell number; however morphological characteristics were improved in the absence of FCS (Figure 6.63). The best morphological differentiation condition was considered to be 2 mM sodium butyrate in serum deprived medium, as IMR32 cells were morphologically similar to adult neurons, and neuronal clusters were
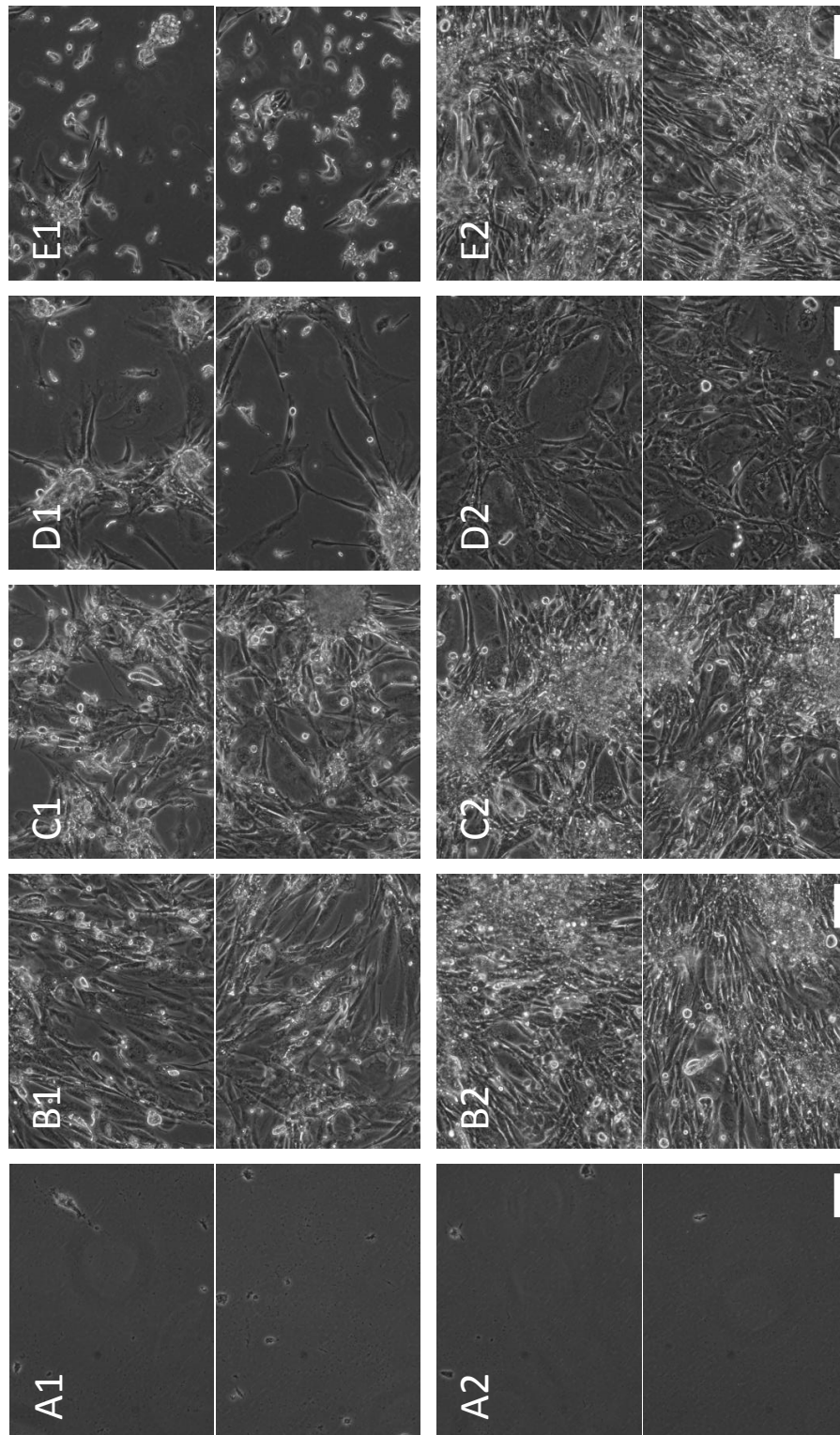
Figure 6. 63 Differentiation of IMR-32 cells in 0% (1) or 5% (2) FCS media at day 8 (n^e = 2). Treatment A: 1 mM dibutyryl cAMP + 10 µg/mL Papaverine, Treatment B: 10 µM retinoic acid, Treatment C: 10 µM retinoic acid + 1 mM dibutyryl cAMP, Treatment D: 2 mM sodium butyrate, Treatment E: 1 mM dibutyryl cAMP + 4 µM 5-bromo-2'-deoxyuridine. Images were acquired using a TE300 microscope. Abbreviations: cAMP – cyclic adenosine monophosphate, FCS – Fetal calf serum. Magnifications: x10. Scale bars: 100 µm.

numerous and interconnected (Figure 6.63 D1). Western blot analysis was also performed on these cell treatments and it was observed that in the presence of serum, two distinct bands for hBCATc were consistently observed (Figure 6.64 A). In the serum deprived state, despite the decrease in the overall level of hBCATc, 10 µM retinoic acid + 1 mM dibutyryl cAMP and 2 mM sodium butyrate in serum deprived medium treatment resulted in a loss of the 50 kDa band (Figure 6.64 B). This loss of the 50 kDa band makes the Western blot comparable between that observed at cell culture and that in human cortex homogenates. This indicates that, at least in the context of morphology and hBCATc protein expression, 2 mM sodium butyrate improves differentiation of neurons compared to other treatments used. Sodium butyrate is the sodium salt of butyric acid and promotes differentiation of cell cultures by the alteration of gene expression and histone hyper acylation (Candido *et al.*, 1978; Davie, 2003; Kruh, 1981). These experiments imply that nutrient signals, possibly even relating to nutrient deprivation, are necessary for the differentiation of these neurons.

6.3.3 Investigation of cell surface expression of hBCATc

Previous work by this group using confocal microscopy alluded to the presence of hBCATc close to or at the cell surface of IMR32 cells. Also, hBCATc has seven possible N-myristoylation sites (prosite.expasy.org). However, the functional relevance of these sites has so far not been investigated and the presence of hBCATc at the cell surface has yet to be considered in other work. These experiments were performed to confirm that hBCATc has cell surface expression and to investigate whether the
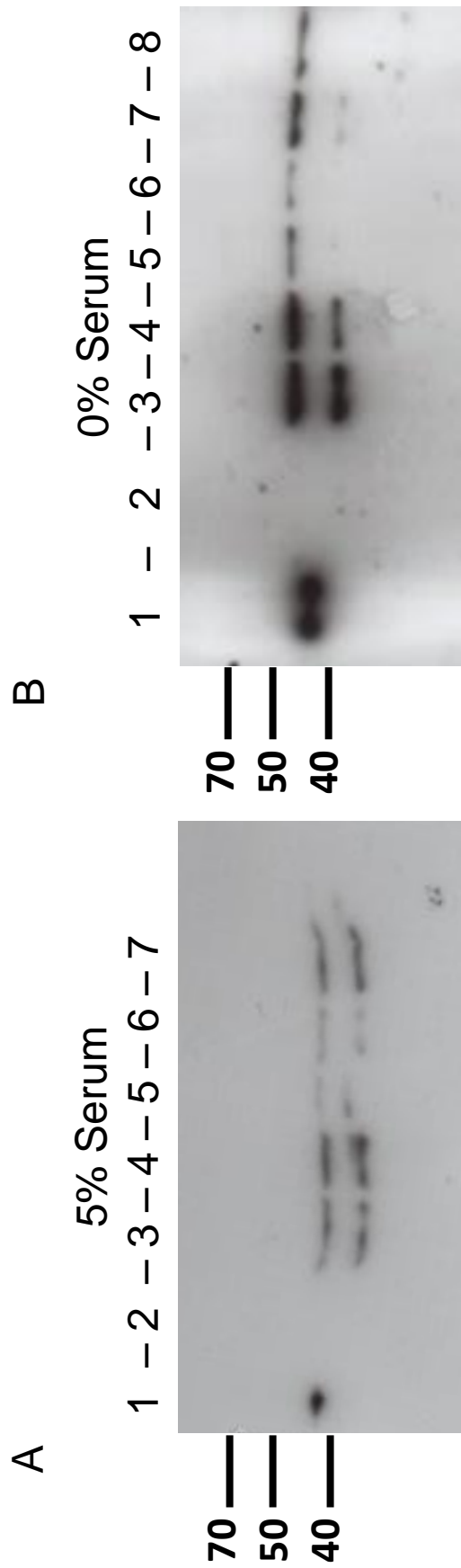
Figure 6. 64 Investigation of the expression of hBCATc in differentiated neurons (n^e = 2). Lane 1 – 10 ng of pure hBCATc protein; Lane 2 – 10 ng of pure hBCATm protein; Lane 3 – Treatment A (1 mM dibutyryl cAMP + 10 µg/mL Papaverine); Lane 4 – Treatment B (10 µM retinoic acid); Lane 5 – Treatment C (10 µM retinoic acid + 1 mM dibutyryl cAMP); Lane 6 – Treatment D (2 mM sodium butyrate); Lane 7 – Treatment E (1 mM dibutyryl cAMP + 4 µM 5-bromo-2'-deoxyuridine); Lane 8 – Control treatment of serum deprived medium (B only). Western blot analysis was carried out using rabbit polyclonal antibodies specific to hBCATc (PA 1/1000, SA 1/5000) (Insight biotechnologies, Wembley, UK) in 5% Marvel as described in Method 4.3. Equal amounts of protein was loaded into each lane (20 µg well) with a 10 ng pure protein control included on each gel. Abbreviations: cAMP – cyclic adenosine monophosphate, FCS – Fetal calf serum, hBCATc – human cytosolic branched chain aminotransferase.

metabolites glutamate and leucine affected this expression. Flow cytometry confirmed the presence of hBCATc at the cell surface membrane with both primary and secondary antibodies having a concentration dependant effect (Figure 6.65). Cell detachment methods were investigated to increase the live cell population compared to that of the cell scraping technique, in addition to see if detachment treatments improved the detectable levels of cell surface hBCATc expression.

The first experiment demonstrated that Trypsin increased the live cell population by 65% when compared to scraping. It was also observed that this moderately improved median fluorescence for cell surface hBCATc by 21% (Figure 6.66 A+D). Citrate and Dispase 2 detachment methods also improved cell survival by 51% and 19% respectively, and median fluorescence compared to scraping but to a lesser degree than Trypsin (Figure 6.66 B+C). Cell surface detachment methods were further investigated with a trial of the Split Kits from Sera Labs (Crawley Down, UK). The weak, medium and strong Split Kits all improved cell survival compared to scraping by 47%, 69% and 121% respectively. The weak Split Kit caused a decrease in median fluorescence observed by 35%, whereas the medium and strong Split Kits both improved median fluorescence significantly by 17% and 62% respectively (Figure 6.67). Although experiments demonstrated that the strong Split Kit improved cell survival in this technique, at the time of experimentation they were not available for continued purchase. For all future experiments Trypsin was used.
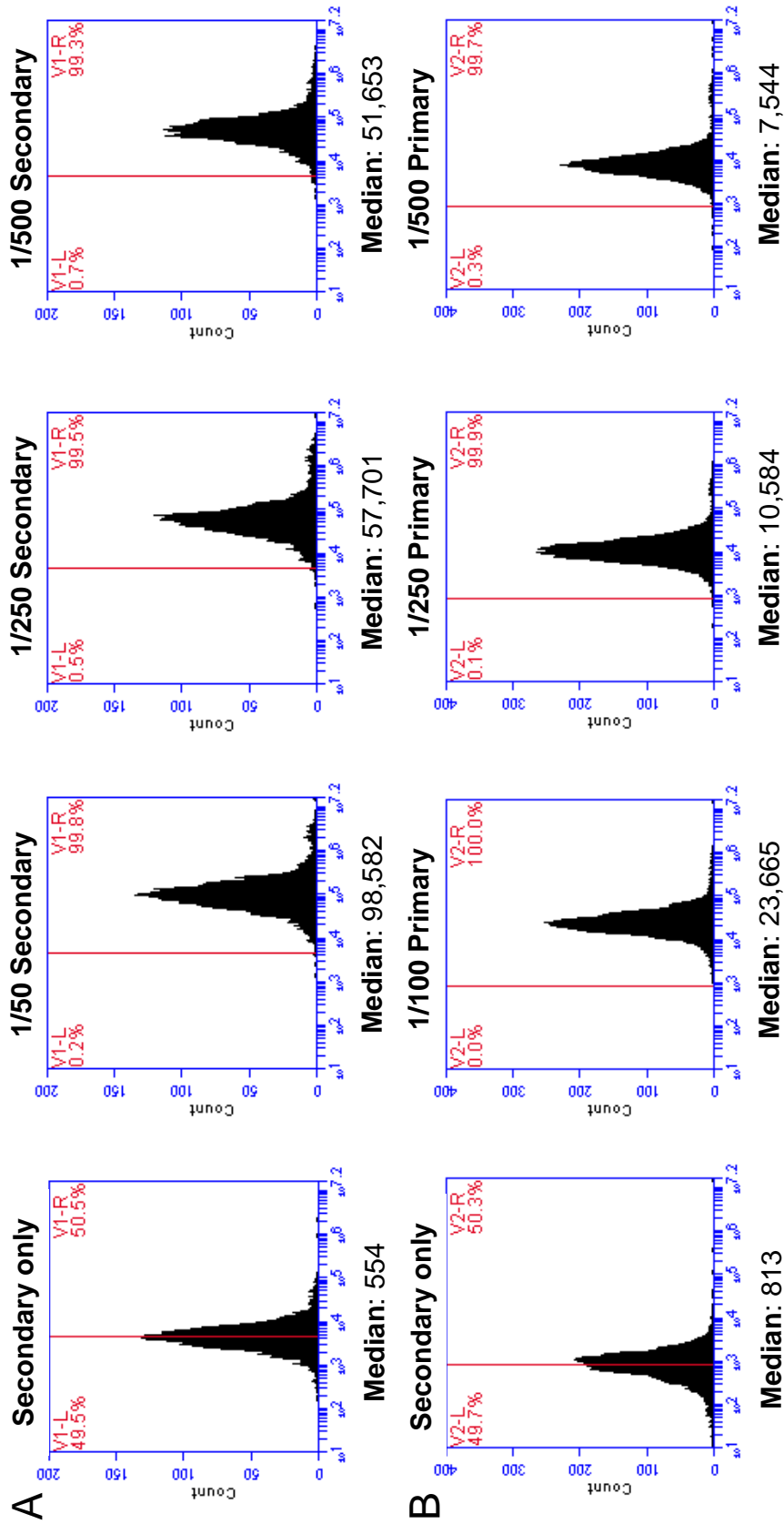
Figure 6. 65 Flow cytometry analysis of cell surface hBCATc on IMR-32 neuronal cells (n^e = 1). IMR32 cells were treated with a rabbit polyclonal antibody specific to hBCATc (A: 1/100, B: varying concentrations) (Insight biotechnologies, Wembley, UK) and a secondary Alexafluor 647 goat monoclonal antibody specific to rabbit IgG (A: varying concentrations, B: 1/500) (Invitrogen, Paisley, UK) as described in Method 4.5. Flow cytometry analysis was carried out using an accuri C6 flow cytometer and the live cell population was gated using PI and manual gating. Abbreviations: hBCATc – human cytosolic branched chain aminotransferase, PI – propidium iodide.
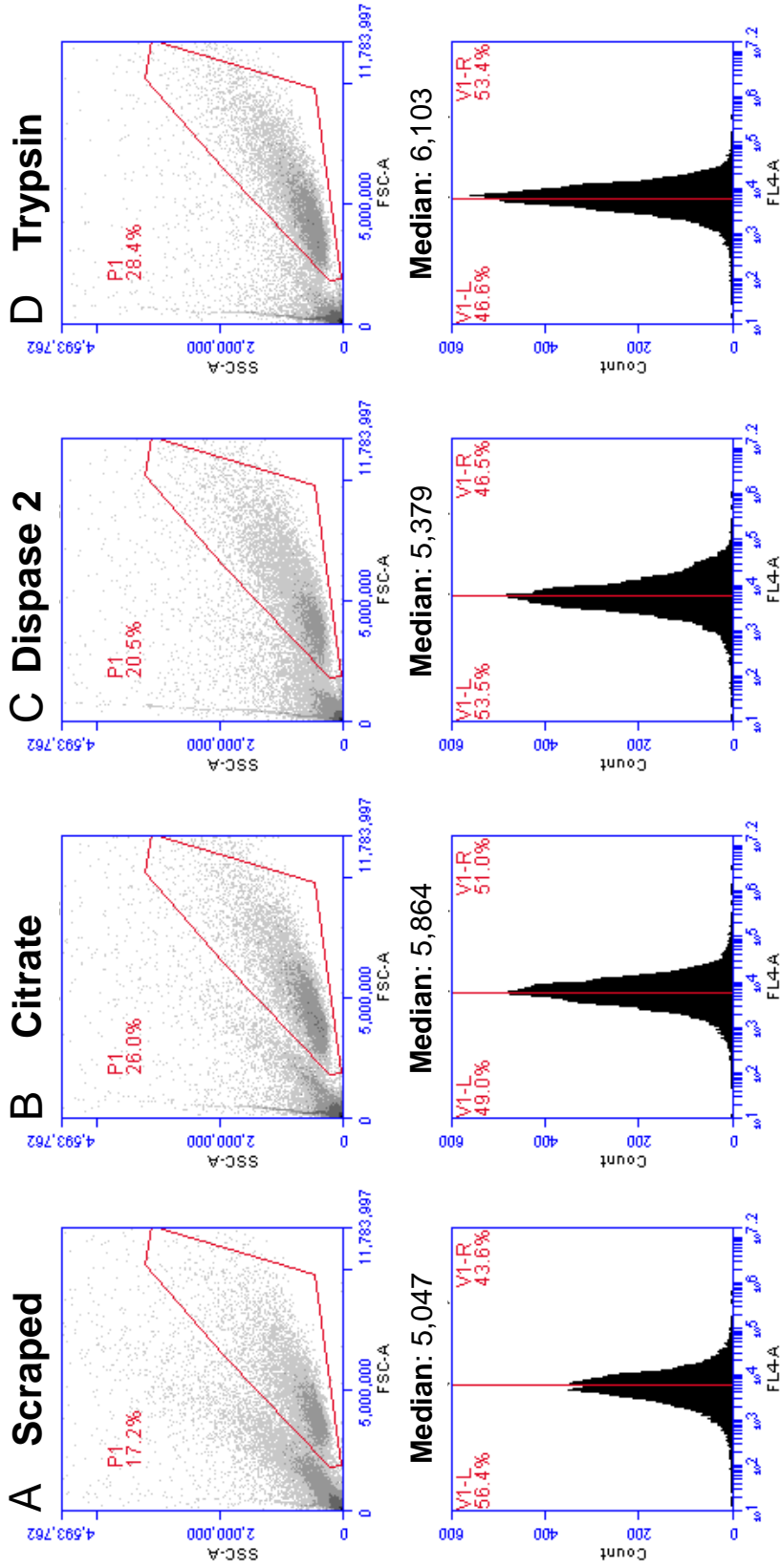
Figure 6. 66 Flow cytometry analysis of cell detachment methods for cell surface IMR32 hBCATc ($n^e = 2$). IMR32 cells were detached using a range of detachment methods. Cells were subsequently treated with a rabbit polyclonal antibody specific to hBCATc (1/500) (Insight biotechnologies, Wembley, UK) and a secondary Alexafluor 647 goat monoclonal antibody specific to rabbit IgG (1/500) (Invitrogen, Paisley, UK) as described in Method 4.5. Flow cytometry analysis was carried out using an accuri C6 flow cytometer and the live cell population was gated using PI and manual gating. Abbreviations: hBCATc – human cytosolic branched chain aminotransferase, PI – propidium iodide.
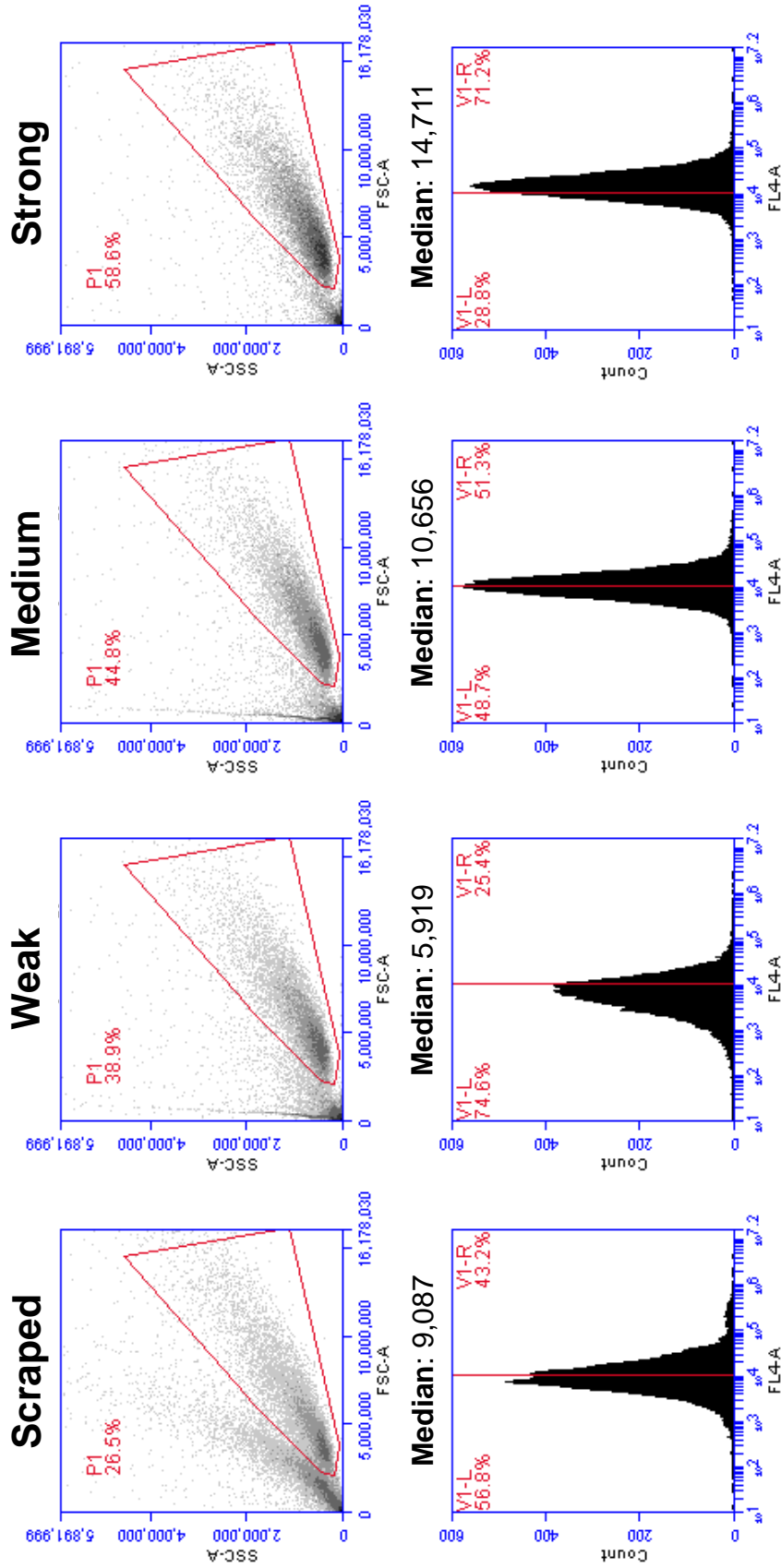
Figure 6. 67 Flow cytometry analysis of cell detachment methods for cell surface IMR32 hBCATc (n^e = 2). IMR32 cells were detached using an increasing strength of Split Kits (Sera Labs, Crawley Down, UK). Cells were subsequently treated with a rabbit polyclonal antibody specific to hBCATc (1/500) (Insight biotechnologies, Wembley, UK) and a secondary Alexafluor 647 goat monoclonal antibody specific to rabbit IgG (1/500) (Invitrogen, Paisley, UK) as described in Method 4.5. Flow cytometry analysis was carried out using an accuri C6 flow cytometer and the live cell population was gated using PI and manual gating. Abbreviations: hBCATc – human cytosolic branched chain aminotransferase, PI – propidium iodide.

Next it was investigated whether cell surface hBCATc expression was specific to IMR32 cells or whether this was a characteristic held by other cell types. Despite the neuronal specificity of hBCATc, the presence of hBCATc in immortal/ rapidly proliferating cells has been observed (Zhou *et al.*, 2013). For this the cell lines Jurkat (T cell leukaemia cell line), PC3 (prostate cancer cell line), U261 (myeloma cell line), RPMI (myeloma cell line) and Jim3 (myeloma cell line) were used. Flow cytometry data demonstrates that live cell surface hBCATc expression is unique to IMR32 cells when compared to these cell lines (Figure 6.68). However, when investigating PI positive cells hBCATc cell surface expression is indeed present in a subpopulation of U261, RPMI and Jim3 cells (Figure 6.69). This raises the possibility of cell surface hBCATc expression triggered by apoptosis processes in these cells.

Finally, it was investigated whether two key substrates of hBCATc (glutamate and leucine) altered cell surface expression of hBCATc and (in the case of glutamate) whether time had an effect on this altered expression. It was demonstrated that 10 and 20 mM glutamate caused a decrease in cell surface hBCATc expression after a 30 minute treatment, with a decrease in median fluorescence of 8% and 45% respectively (Figure 6.70). Contrary to this, 24 hour treatment (10 mM and 20 mM glutamate again) caused an overall increase in median fluorescence of 59% and 76% respectively (Figure 6.71). The effect of leucine was modest in comparison, with 24 hour treatments with 20 mM and 40 mM causing an increase in median fluorescence of 27% and 12% respectively (Figure 6.72). The immediate initial decrease of cell surface hBCATc upon 30 minute glutamate treatment
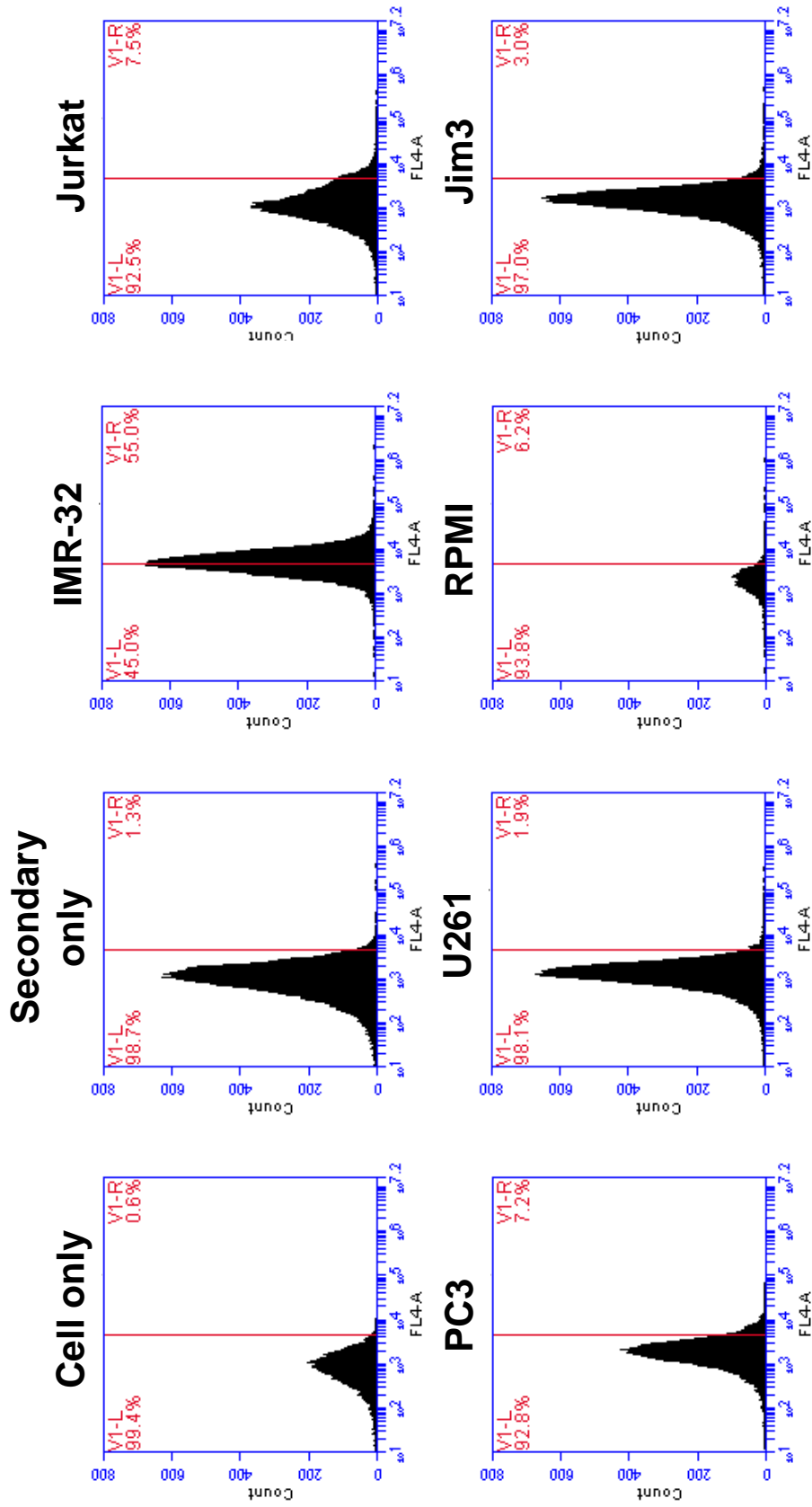
Figure 6. 68 Flow cytometry analysis of live cell surface expression of hBCATc on multiple cell lines (n^e = 1). IMR32 cells were detached (where appropriate) using Trypsin (Invitrogen, Paisley, UK). Cells were subsequently treated with a rabbit polyclonal antibody specific to hBCATc (1/500) (Insight biotechnologies, Wembley, UK) and a secondary Alexafluor 647 goat monoclonal antibody specific to rabbit IgG (1/500) (Invitrogen, Paisley, UK) as described in Method 4.5. Flow cytometry analysis was carried out using an accuri C6 flow cytometer and the live cell population was gated using PI and manual gating. Abbreviations: hBCATc – human cytosolic branched chain aminotransferase, PI – propidium iodide.
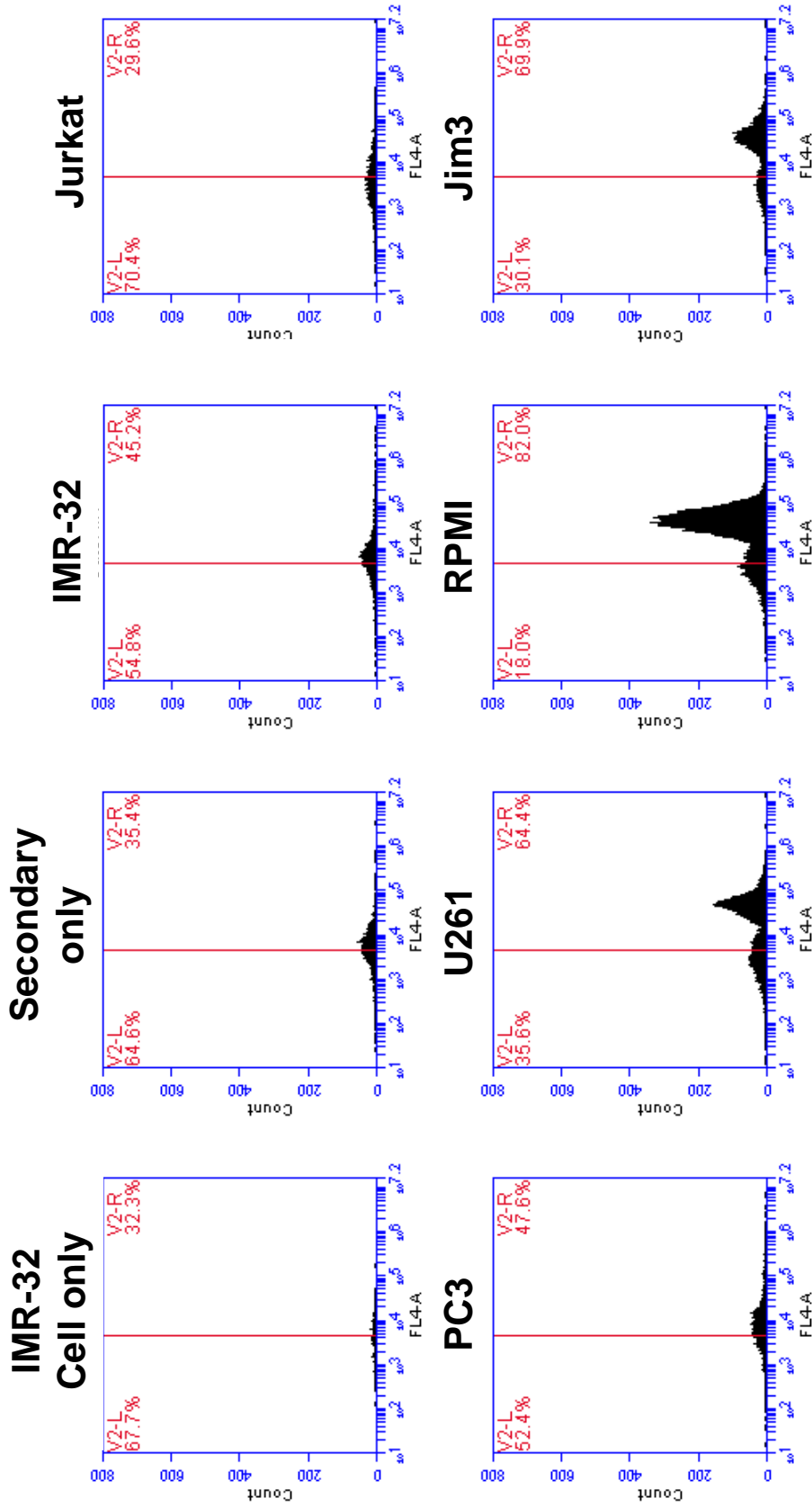
Figure 6. 69 Flow cytometry analysis of dead cell surface expression of hBCATc on multiple cell lines ($n^e = 1$). IMR32 cells were detached (where appropriate) using Trypsin (Invitrogen, Paisley, UK). Cells were subsequently treated with a rabbit polyclonal antibody specific to hBCATc (1/500) (Insight biotechnologies, Wembley, UK) and a secondary Alexafluor 647 goat monoclonal antibody specific to rabbit IgG (1/500) (Invitrogen, Paisley, UK) as described in Method 4.5. Flow cytometry analysis was carried out using an accuri C6 flow cytometer and the dead cell population was gated using PI and manual gating. Abbreviations: hBCATc – human cytosolic branched chain aminotransferase, PI – propidium iodide.
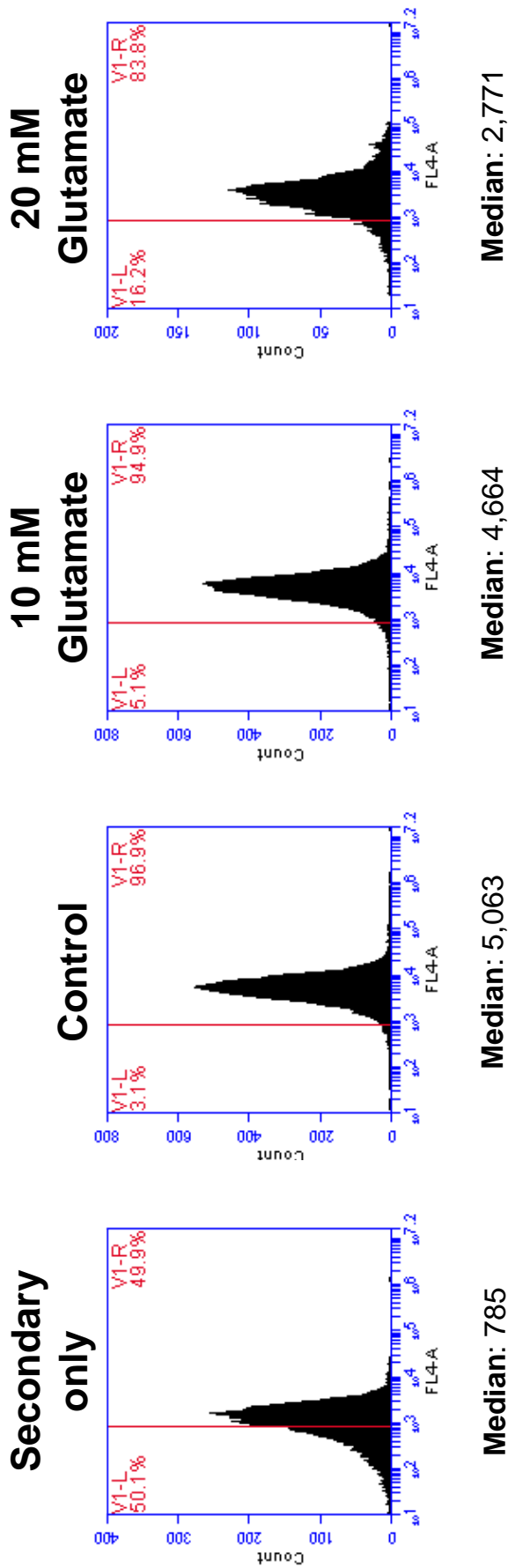
Secondary only — Median: 785

Control — Median: 5,063

10 mM Glutamate — Median: 4,664

20 mM Glutamate — Median: 2,771

Figure 6. 70 The effect of 30 minute glutamate treatment on cell surface expression of IMR32 hBCATc (n^e = 2). IMR32 cells were treated with a rabbit polyclonal antibody specific to hBCATc (1/500) (Insight biotechnologies, Wembley, UK) and a secondary Alexafluor 647 goat monoclonal antibody specific to rabbit IgG (1/500) (Invitrogen, Paisley, UK) as described in Method 4.5. Flow cytometry analysis was carried out using an accuri C6 flow cytometer and the live cell population was gated using PI and manual gating. Abbreviations: hBCATc – human cytosolic branched chain aminotransferase, PI – propidium iodide.
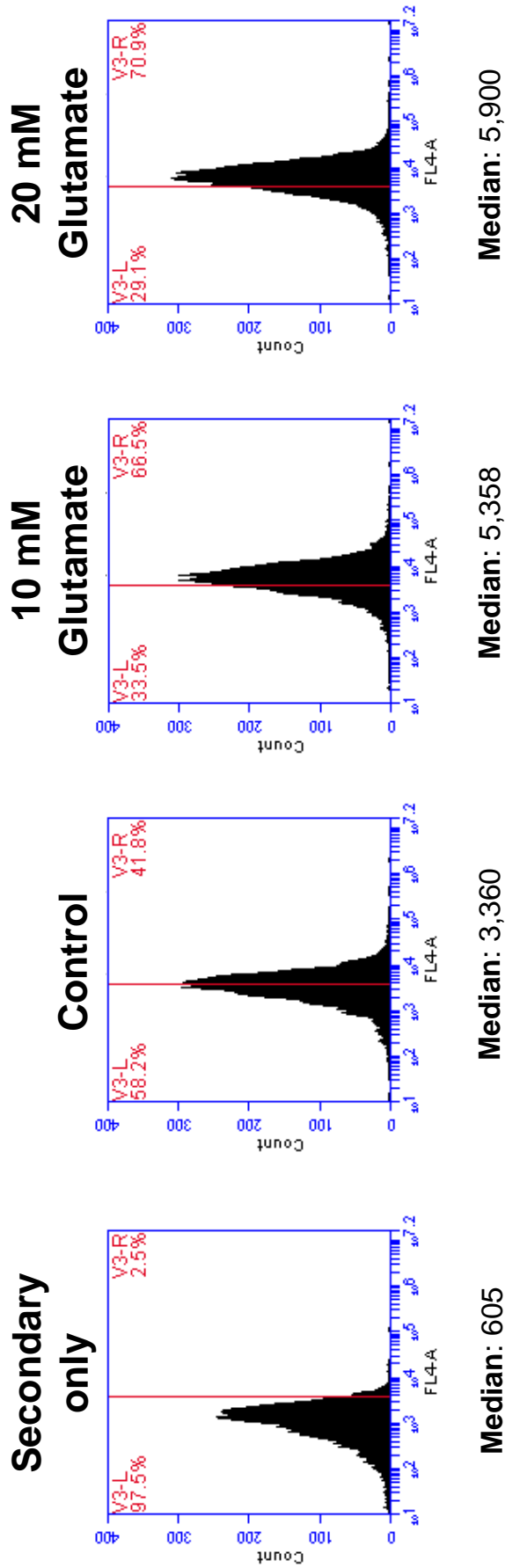
Figure 6. 71 The effect of 24 hour glutamate treatment on cell surface expression of IMR32 hBCATc (n^e = 2). IMR32 cells were treated with a rabbit polyclonal antibody specific to hBCATc (1/500) (Insight biotechnologies, Wembley, UK) and a secondary Alexafluor 647 goat monoclonal antibody specific to rabbit IgG (1/500) (Invitrogen, Paisley, UK) as described in Method 4.5. Flow cytometry analysis was carried out using an accuri C6 flow cytometer and the live cell population was gated using PI and manual gating. Abbreviations: hBCATc – human cytosolic branched chain aminotransferase, PI – propidium iodide.
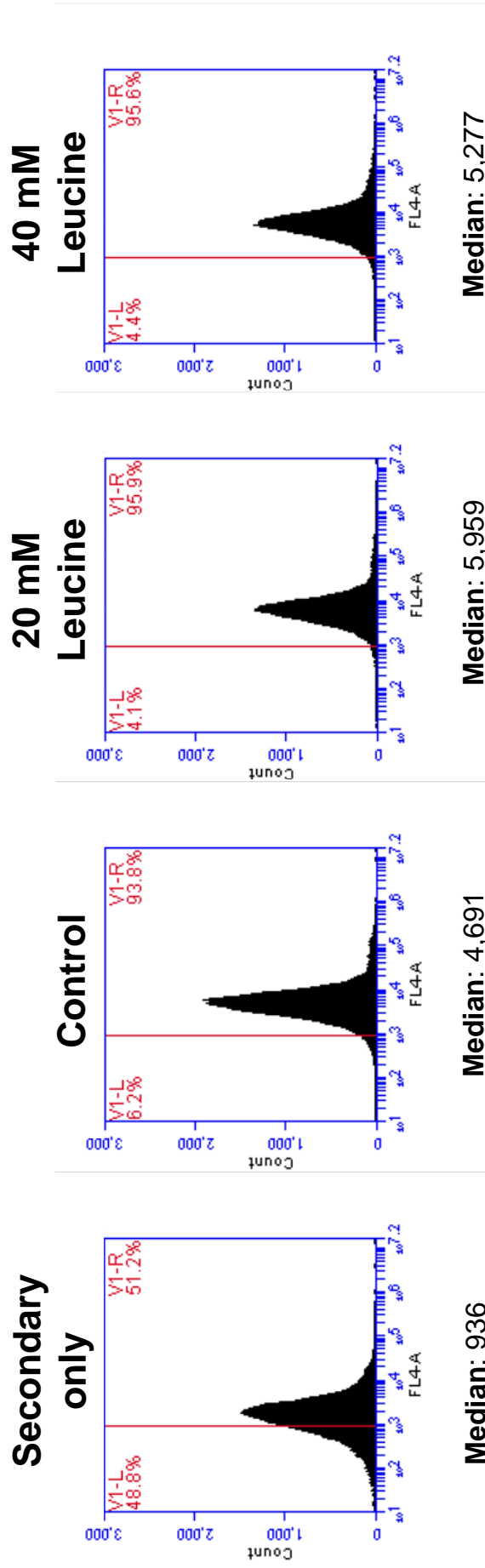
Figure 6. 72 The effect of 24 hour leucine treatment on cell surface expression of IMR32 hBCATc (n^e = 2). IMR32 cells were treated with a rabbit polyclonal antibody specific to hBCATc (1/500) (Insight biotechnologies, Wembley, UK) and a secondary Alexafluor 647 goat monoclonal antibody specific to rabbit IgG (1/500) (Invitrogen, Paisley, UK) as described in Method 4.5. Flow cytometry analysis was carried out using an accuri C6 flow cytometer and the live cell population was gated using PI and manual gating. Abbreviations: hBCATc – human cytosolic branched chain aminotransferase, PI – propidium iodide.

implies that the hBCATc is acting as a receptor, internalising upon glutamate binding. Longer treatments of 24-hours of both glutamate and leucine are likely the result of a self-propagating mechanism. In this context it is probable that the hBCATc is acting as a receptor sensing external concentrations of either the BCAAs or glutamate.

6.3.4 Expression and activity of hBCAT in the IMR32 cell line

The cytokines TNFα and IL1α are both involved in systemic inflammation and were investigated for an effect on hBCAT expression and activity due to their association with AD (Griffin & Mrak, 2002; Swardfager *et al.*, 2010). For example, IL1 overexpression in the brains of AD subjects has been observed to relate directly to the development and progression of neuropathological changes in AD (Griffin & Mrak, 2002). It has been further observed that TNFα levels are increased in AD and it is probable that these increased levels, along with increased IL1, represent a low level immune response occurring throughout the AD process (Swardfager *et al.*, 2010). Expressional analysis of human samples observed that hBCATm levels were 70% higher in the frontal cortex in females compared to males; therefore a key gender related hormone, 17β oestradiol, was used to see if this mediated change in hBCAT expression. A radioactivity assay was developed to measure the activity of hBCAT within IMR32 cell lysates. Intermediates of hBCAT, along with insulin and TNFα were used to observe the effect on hBCAT activity. This experiment was performed to compliment expression analysis to determine whether the alterations in expression correlate with activity.

The radioactivity assay was developed by utilising variations of previous buffers that have been used to extract BCAT or other proteins whilst maintaining enzyme activity. Buffer 2 (25 mM HEPES; 1% Triton X; 20 mM EDTA; 20 mM EGTA; 1x protease inhibitor; 5 mM DTT; 0.5 mM PLP, (pH 7.5)) was the appropriate buffer to extract hBCAT whilst maintaining optimum activity (Figure 6.73). Also noted was the complete loss of activity with buffer 4 (20 mM Tris-HCl (pH 8.0); 50 mM ammonium acetate; 2 mM EDTA; 1x protease inhibitor; 20 mM DTT; 0.5 mM PLP) (Figure 6.73). This relates to previous work demonstrating that Tris inhibits the hBCAT proteins (Yennewar *et al.*, 2001). Buffer 2 was further improved by the relatively acidic pH of 6.5, rather than 7.5 that was used by Suryawan *et al.* (Figure 6.74).

This established method was subsequently used to assess the activity of hBCAT after treatment with hBCAT substrates (glutamate and leucine) or immune components (TNFα). Glutamate treatment produced a decrease in hBCAT activity at both 2 mM ($p = 0.031$) and 20 mM ($p = 0.062$) by 8% and 11% respectively (Figure 6.75). This is contrary to what was observed on Western blots where glutamate caused an increase in hBCATc expression by 260% (Figure 6.78 B+C). A decrease in hBCAT activity was also observed with TNFα, with a decrease observed at 1 ng/mL ($p = 0.008$) and 5 ng/mL ($p = 0.065$) of 17 and 20% respectively (Figure 6.76). This was a smaller decrease than the decrease in expression observed at Western blot of 80% (Figure 6.78 D+F).

| Buffer	Contents
Buffer 1 – from Suryawan et al. (1998)	25 mM HEPES (pH 7.5); 0.4% CHAPS; 20 mM EDTA; 20 mM EGTA; 1x protease inhibitor; 5 mM DTT; 0.5 mM PLP
Buffer 2 – an altered version of that used by Suryawan et al. (1998)	25 mM HEPES (pH 7.5); 1% Triton X; 20 mM EDTA; 20 mM EGTA; 1x protease inhibitor; 5 mM DTT; 0.5 mM PLP
Buffer 3 – an accumulation of various published buffers used for hBCAT	20 mM potassium phosphate (pH 7.5); 1 mM EDTA; 1 mM EGTA; 1x protease inhibitor, 20 mM DTT; 0.5 mM PLP
Buffer 4 – TCA buffer	20 mM Tris-HCl (pH 8.0); 50 mM ammonium acetate; 2 mM EDTA; 1x protease inhibitor; 20 mM DTT; 0.5 mM PLP
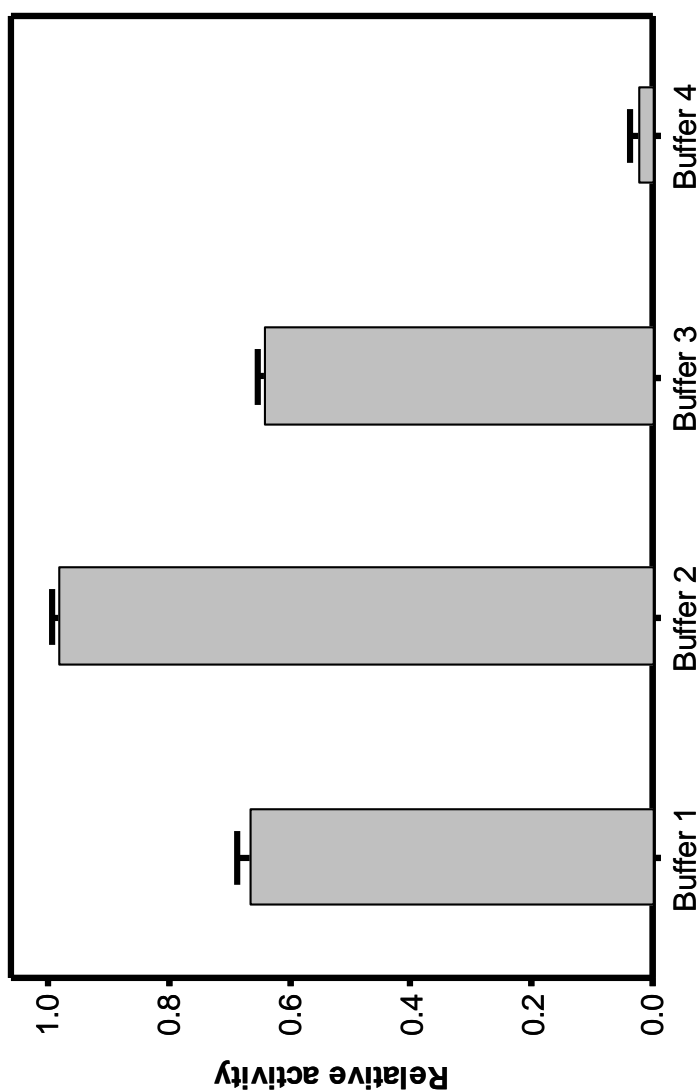
Figure 6. 73 The effect of protein extraction buffer on IMR32 hBCAT activity (n^e = 2). IMR-32 cells were extracted using 4 varying buffers. C^{14} radioactivity assay was carried out using C^{14}-KIV (American Radiolabelled Chemicals Inc. MO, USA) as described in Method 4.7. Equal volumes of extraction lysate were used in each reaction and a negative (water instead of lysate) and positive control (pure KIV in scintillation fluid) were also counted in the scintillation counter (PerkinElmer life sciences Winspectral 1414 liquid scintillation counter). Activities were subsequently calculated to give nmol/min/mL valine produced and made relative to the highest numerical value. Error bars displayed are standard errors of the mean. The bar chart displayed is the result of two separate experiments ran in duplicate.
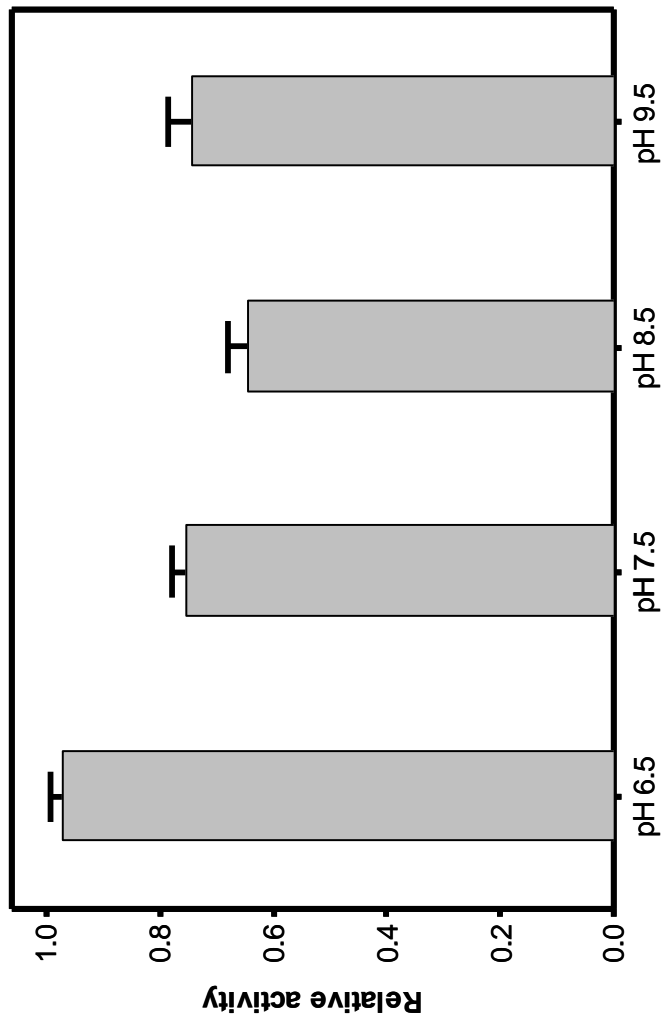
Figure 6. 74 The effect of protein extraction buffer 2 pH on IMR32 hBCAT activity (n^e = 2). IMR-32 cells were extracted using buffer 2 with increasing pH. C^{14} radioactivity assay was carried out using C^{14}-KIV (American Radiolabelled Chemicals Inc. MO, USA) as described in Method 4.7. Equal volumes of extraction lysate were used in each reaction and a negative (water instead of lysate) and positive control (pure KIV in scintillation fluid) were also counted in the scintillation counter (PerkinElmer life sciences Winspectral 1414 liquid scintillation counter). Activities were subsequently calculated to give nmol/min/mL valine produced and made relative to the highest numerical value. Error bars displayed are standard errors of the mean. The bar chart displayed is the result of two separate experiments ran in duplicate.
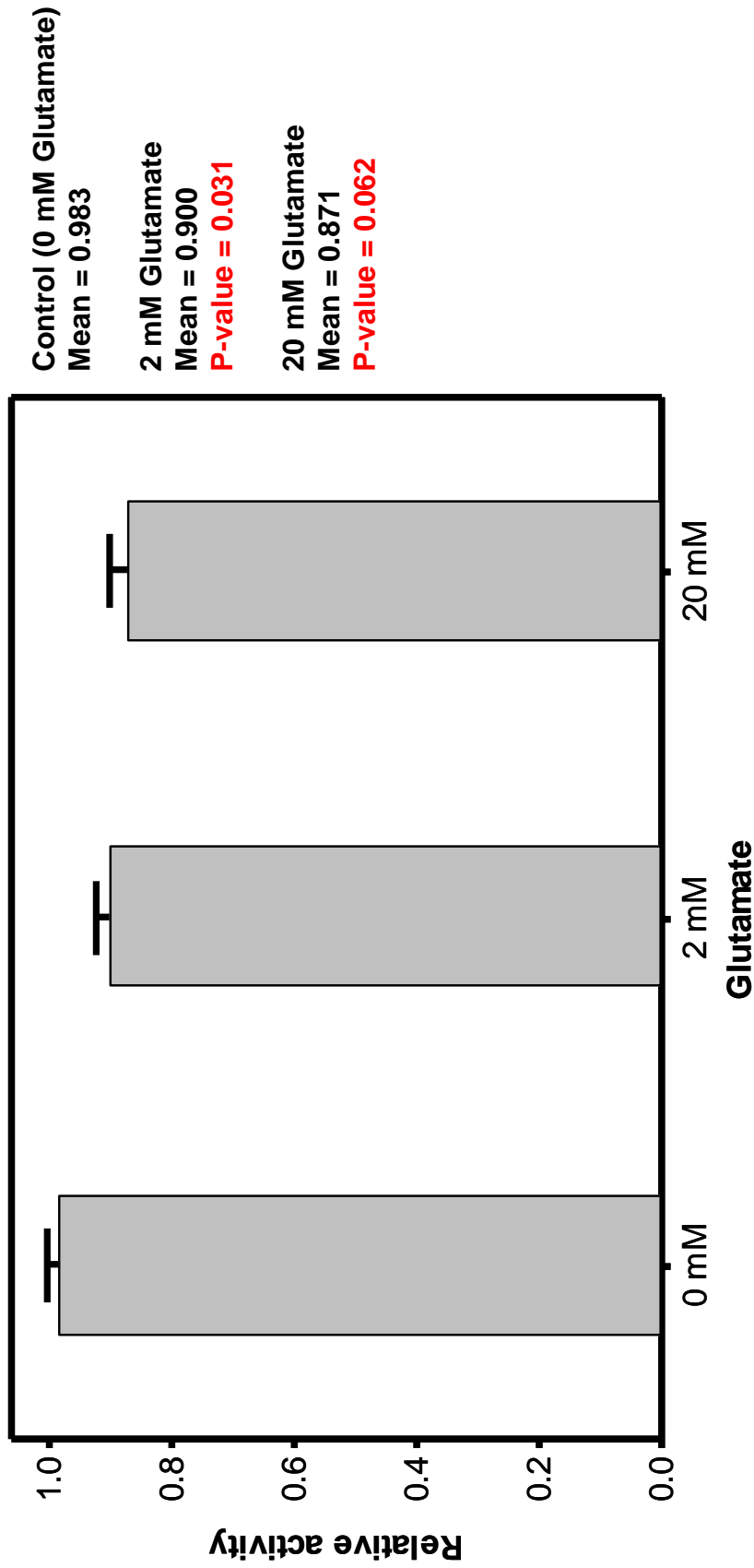
Figure 6. 75 The effect of glutamate treatments on IMR32 hBCAT activity (n^e = 2). IMR-32 cells were extracted using buffer 2 after 24 hour treatment with increasing glutamate concentrations. C^{14}-KIV (American Radiolabelled Chemicals Inc. MO, USA) as described in Method 4.7. Equal volumes of extraction lysate were used in each reaction and a negative (water instead of lysate) and positive (pure KIV in scintillation fluid) control were also counted in the scintillation counter (PerkinElmer life sciences Winspectral 1414 liquid scintillation counter). Activities were subsequently calculated to give nmol/min/mL valine produced and made relative to the highest numerical value of the control treatment. The bar chart displayed is the result of a single experiment ran in duplicate. Error bars displayed are standard errors of the mean.
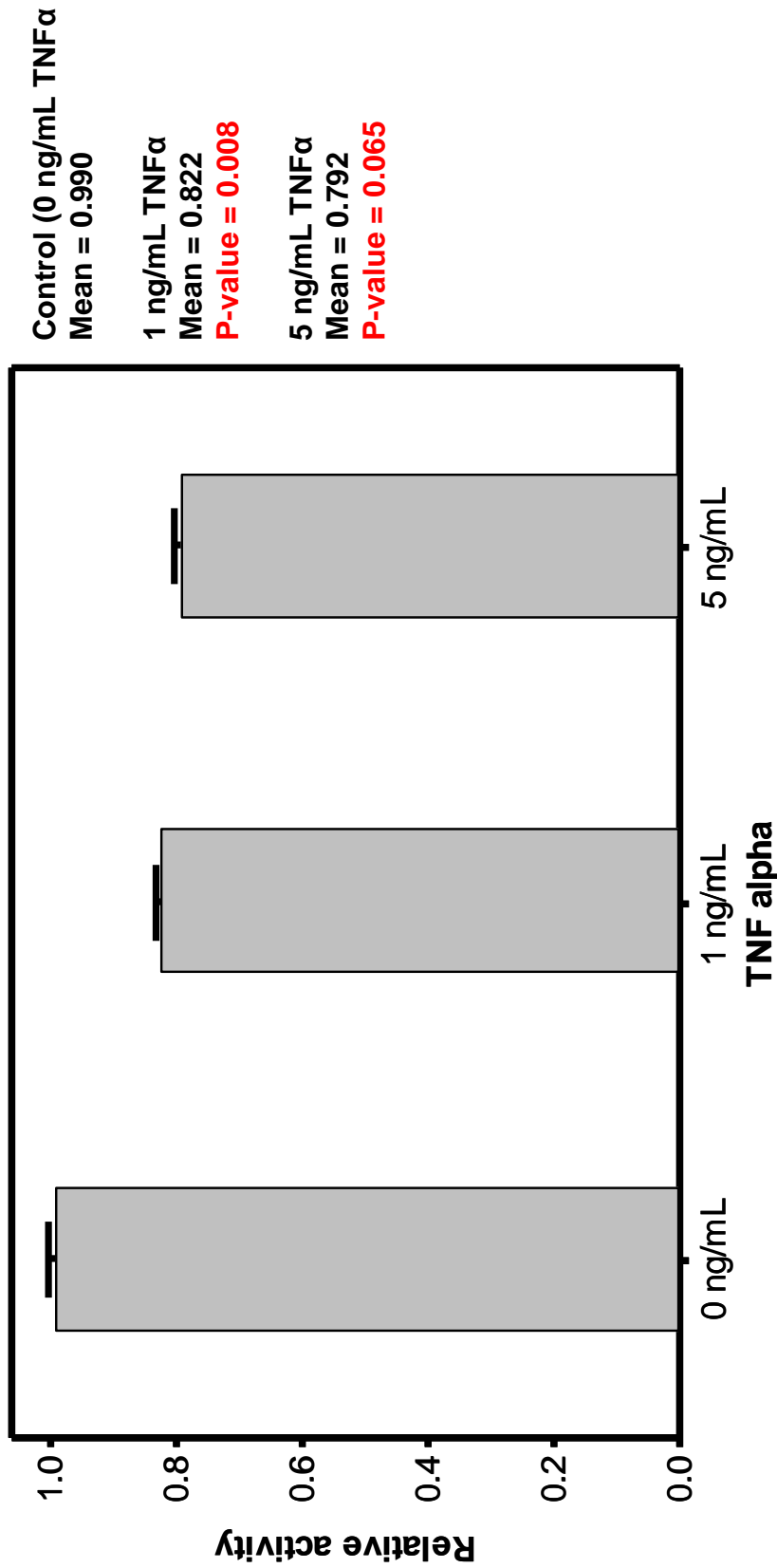
Figure 6. 76 The effect of TNFα treatment on IMR32 hBCAT activity (n^e = 2). IMR-32 cells were extracted using buffer 2 after 24 hour treatment with increasing TNFα concentrations. C^{14} radioactivity assay was carried out using C^{14}-KIV (American Radiolabelled Chemicals Inc. MO, USA) as described in Method 4.7. Equal volumes of extraction lysate were used in each reaction and a negative (water instead of lysate) and positive (pure KIV in scintillation fluid) control were also counted in the scintillation counter (PerkinElmer life sciences Winspectral 1414 liquid scintillation counter). Activities were subsequently calculated to give nmol/min/mL valine produced and made relative to the highest numerical value of the control treatment. Error bars displayed are standard errors of the mean. The bar chart displayed is the result of a single experiment ran in duplicate.
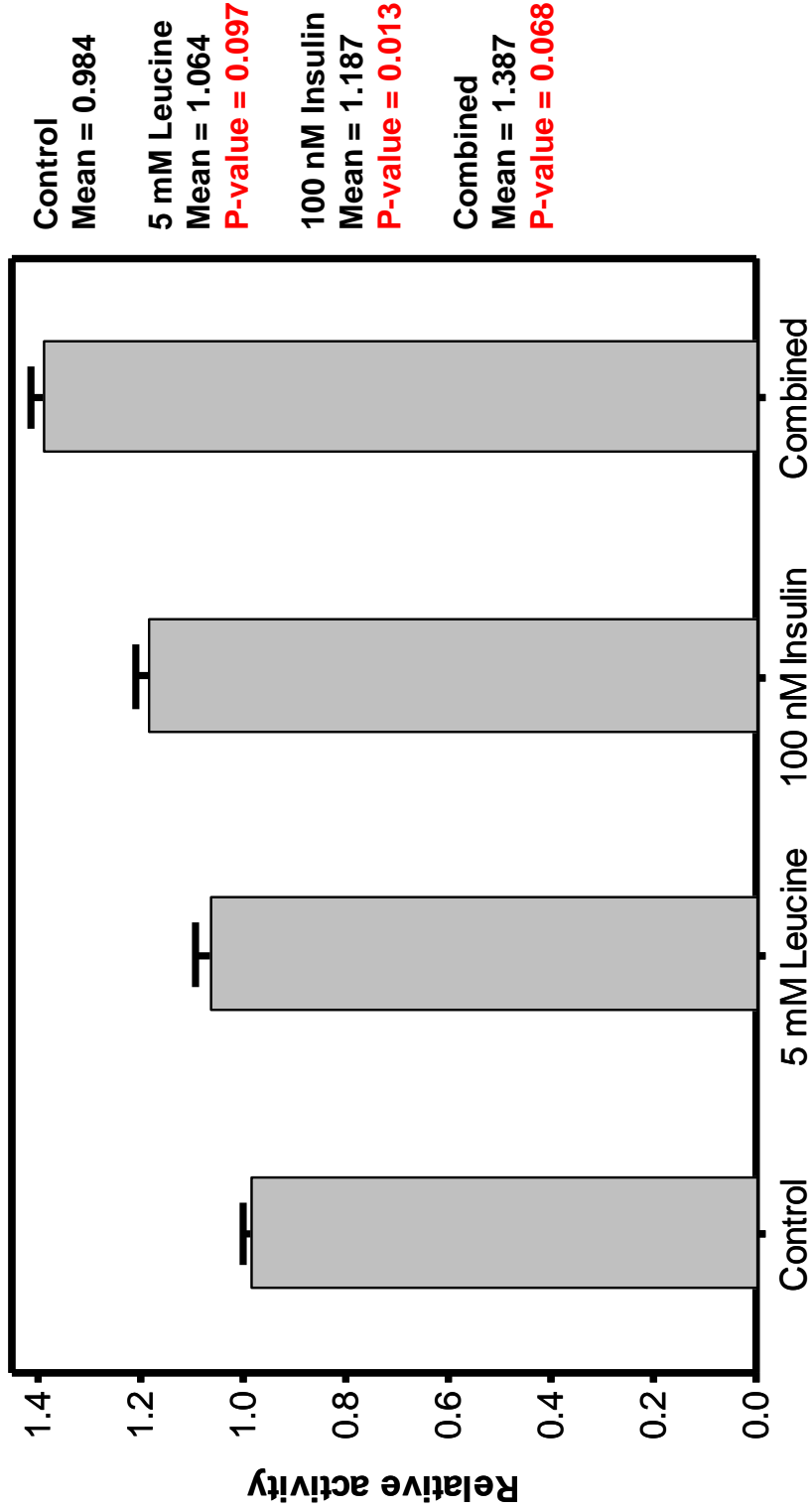
Figure 6. 77 The effect of leucine, insulin and combination treatment on IMR32 hBCAT activity ($n^e = 2$). IMR-32 cells were extracted using buffer 2 after 24 hour treatment with either leucine, insulin or a combination of both. C^{14} radioactivity assay was carried out using C^{14}-KIV (American Radiolabelled Chemicals Inc. MO, USA) as described in Method 4.7. Equal volumes of extraction lysate were used in each reaction and a negative (water instead of lysate) and positive (pure KIV in scintillation fluid) control were also counted in the scintillation counter (PerkinElmer life sciences Winspectral 1414 liquid scintillation counter). Activities were subsequently calculated to give nmol/min/mL valine produced and made relative to the highest numerical value of the control treatment. Error bars displayed are standard errors of the mean. The bar chart displayed is the result of a single experiment ran in duplicate.
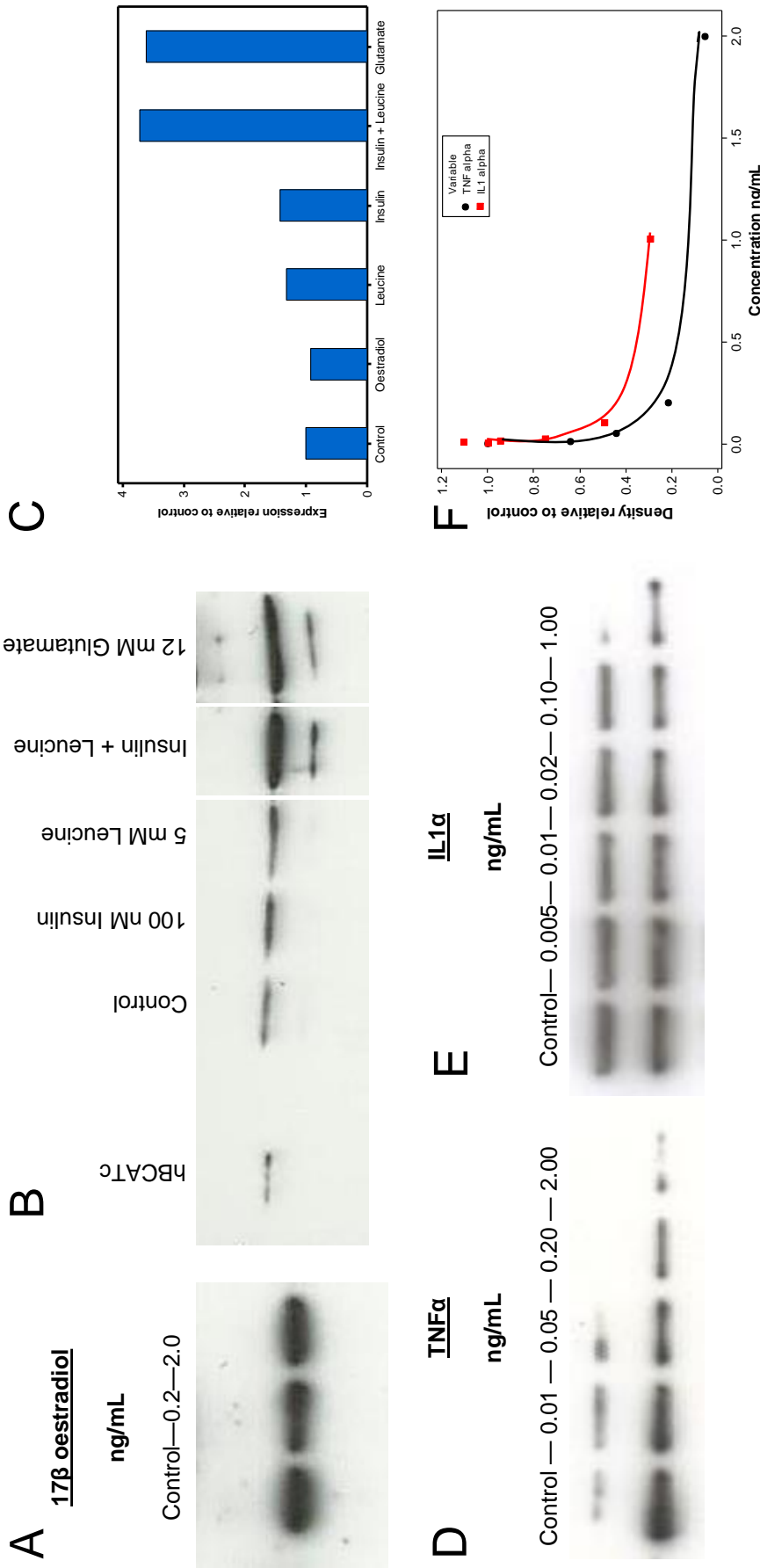
Figure 6. 78 The effect of Immune factors (TNFα and IL1α), hormones (oestradiol and insulin) and substrates (glutamate and leucine) on hBCATc protein levels ($n^e = 2$). Protein from IMR-32 cells were extracted using RIPA buffer after 24 hour treatment. Western blot analysis was carried out using rabbit polyclonal antibodies specific to hBCATc (PA 1/1000, SA 1/5000) (Insight biotechnologies, Wembley, UK) in 5% Marvel as described in Method 4.3. Equal amounts of protein was loaded into each lane (20 μg well) with a 10 ng pure protein control included on each gel. Abbreviations: hBCATc – human cytosolic branched chain aminotransferase, IL1α – Interleukin 1α, TNFα – Tumour necrosis factor α.

The effect of leucine and insulin (either individually or in combination) was complex. Individually their effect on hBCAT expression and activity was seemingly lower than in combination. For activity, leucine ($p = 0.097$), insulin ($p = 0.013$) and the combination of both ($p = 0.068$) resulted in an increase in hBCAT activity by 8, 21 and 41% respectively (Figure 6.77). This was mirrored in the Western blot where leucine and insulin treatment alone resulted in a minimal increase in expression and the combination demonstrating a much larger increase of 270% (Figure 6.77 B+C). This indicates that the effect of leucine and insulin operates synergistically for both expression and activity. Additionally, Western blot analysis observed that 17β oestradiol had no effect on hBCATc expression (Figure 6.78 A) but the immune factor IL1α produced a dose dependant decrease in hBCATc expression similar to that observed with TNFα (Figure 6.78 E+F). This implies that immune factors can significantly down regulate hBCATc expression, although it is not entirely apparent what role this would have in the nervous system. This will likely allow immune cells to alter neuronal function but will also allow neurons to alter immune cell function in turn.

In summary, hBCAT substrates tested (glutamate and KIC) have a detrimental effect on cellular morphology. Cell surface expression of hBCATc was confirmed and this expression was sensitive to substrates of hBCATc with glutamate differentially altering cell surface expression depending of the treatment time used. Activity of IMR32 hBCAT was also altered by hBCAT substrates although these were not always directly

comparable with the expressional studies. Aspects of the immune system (TNFα and IL1α) altered the expression (as measure by Western blot) and (in the case of TNFα) hBCAT activity however the mechanism and function of this is unclear.